General Disclaimer

One or more of the Following Statements may affect this Document

- This document has been reproduced from the best copy furnished by the organizational source. It is being released in the interest of making available as much information as possible.

- This document may contain data, which exceeds the sheet parameters. It was furnished in this condition by the organizational source and is the best copy available.

- This document may contain tone-on-tone or color graphs, charts and/or pictures, which have been reproduced in black and white.

- This document is paginated as submitted by the original source.

- Portions of this document are not fully legible due to the historical nature of some of the material. However, it is the best reproduction available from the original submission.

1

HETEROEPITAXY OF III-V COMPOUND SEMICONDUCTORS ON INSULATING SUBSTRATES
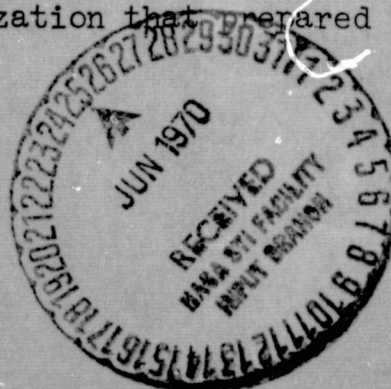
Final Report

by Harold M. Manasevit and Arthur C. Thorsen

January 1970

Distribution of this report is provided in the interest
of information exchange. Responsibility for the contents
resides in the author or organization that prepared it.

HETEROEPITAXY OF III-V COMPOUND SEMICONDUCTORS ON INSULATING SUBSTRATES

Final Report

by Harold M. Manasevit and Arthur C. Thorsen

January 1970

CONTENTS

ILLUSTRATIONS

iv

ILLUSTRATIONS (Cont)

ILLUSTRATIONS (Cont)

ILLUSTRATIONS (Cont)

TABLES

HETEROEPITAXY OF III-V COMPOUND SEMICONDUCTORS ON INSULATING SUBSTRATES

By H. M. Manasevit and A. C. Thorsen

Autonetics Division of North American Rockwell Corporation
Anaheim, California

SUMMARY

Thick (>15 μm) undoped GaAs films with room temperature mobilities between 5000 and 6000 cm^2/V-sec for carrier concentrations in the range from ~10^{15} to ~10^{17} cm^{-3} have grown on (0001) Aℓ_2O_3 by the trimethylgallium (TMG)-arsine (AsH$_3$) process in the temperature range 650-700 C.

The carrier concentrations of the resulting films are found to depend primarily on the purity of the starting materials and the carrier gases used in growing the films. Depending on the source of AsH$_3$ and TMG, net impurity concentrations in the films may range from ~10^{15} to over 10^{17} cm^{-3}. It has also been demonstrated that good quality films can be obtained by using either H$_2$ or He as a carrier gas.

The quality of the films was also shown to be quite dependent on the relative AsH$_3$-TMG concentrations. By manipulation of this ratio it is possible to control to some extent the carrier concentration, resistivity, and even conductivity type of the resultant films.

The first few microns of growth of an intentionally undoped GaAs film have in general been p-type. The thickness of the p-type layer has been shown to be related to the donor impurities of the reactant gases; for gases high in donor impurities the thickness of the p-layer may be less than 1μm, while for gases with low impurity content the thickness may be 5μm or greater. With subsequent growth beyond the p-type layer, the sample converts to n-type with a continuing improvement in film quality. The average mobilities of $\geq$5000 cm^2/V-sec measured in thick films can therefore be considered quite reasonable for such a graded structure.

Nucleation studies of the growth of very thin (i.e., $\leq$1μm) films of GaAs have shown that the early states of growth appear to involve formation of small islands with pyramidal structure. A smoothing of the surface evidently occurs shortly after complete coverage is obtained. Reflection electron diffraction studies indicate some improvement in the crystal structure in thin layers with heat treatment.

GaAs/Aℓ_2O_3 orientation relationships have been extensively investigated. The studies to date, which encompass several orientations on six major crystallographic zones in Aℓ_2O_3, indicate a preferential growth of (111) GaAs, with pronounced twinning being the rule rather than the exception. The (0001) Aℓ_2O_3 plane has been the best plane for deposition; twin-free deposits of GaAs have been grown on this orientation.

Techniques for producing layered structures of alternating conductivity type or doping level have been developed and simple device structures have been fabricated and characterized. Excellent quality vertical-junction tunnel diodes have been fabricated in heavily Zn-doped GaAs/$A\ell_2O_3$ and operated in a 100 MHz oscillator.

Preliminary studies using stoichiometric spinel as substrates have shown that nearly equivalent quality films can be grown on this material; however, the growth of good quality GaAs films is more sensitive to the surface preparation of spinel than of $A\ell_2O_3$.

2

INTRODUCTION

Some of the highest purity Ga-Group V compounds prepared today are made by epitaxial growth on GaAs employing chemical vapor deposition (CVD) techniques (Ref 1, 2). Most of the various reported CVD methods were tested in Autonetics laboratories to attempt the growth of GaAs on insulating substrates.

In the early stages of the investigation, the $HC\ell$-transport open-tube process was used. Using a geometry involving close spacing between the substrate and a polycrystalline GaAs source, epitaxial films of GaAs were achieved on GaAs and/or Ge, but no continuous-film growth was formed on $A\ell_2O_3$. When growth did occur, it was traced to the presence of Ge (Ref 3) used as a companion substrate for simultaneous deposition in the same experiment.

Failure to achieve epitaxial growth of GaAs directly on insulating substrates by the $HC\ell$ transport method without the intermediate Ge nucleating film was at first attributed only to the presence of $HC\ell$ in the environment, in concentrations greater than that necessary for it to function as a transport agent. A few attempts were made in the close-spaced system to control the $HC\ell$ concentration by using $AsC\ell_3$ as the transport agent, but the results were not encouraging.

The results suggested that the process used for promoting growth on insulators should be free from halides and any other transport agents that might contact and change the insulator surface in some way. However, the existing CVD processes all relied upon such transporting agents, so a new method for compound-semiconductor film formation was needed.

A process for epitaxial film growth was sought which would have at least the following attributes:

1. Low temperature film growth, to minimize decomposition of the resultant film.

2. Formation of the compound at the heated substrate.

3. A single temperature zone, for simplicity in film formation and apparatus.

4. No gaseous etchants, to minimize possible substrate surface problems and remove complications due to autodoping.

5. Compatibility with gas-phase dopants, for in situ doping during film formation.

These attributes were realized when Autonetics demonstrated (Ref 4) that Ga-Group V semiconductor films could be produced on GaAs, Ge, and insulating substrates by decomposing organo-gallium compounds and Group V hydrides. This deposition process appeared to offer the best means for achieving epitaxial films with reproducible properties. Although the growth of single-crystal films of GaAs on $A\ell_2O_3$

and other substrates had been demonstrated (Ref 4, 5), optimization of the process to produce films with properties approximating those of bulk material was necessary. A thorough study of interdependent deposition parameters was indicated.

This report summarizes the work accomplished under NASA Contract No. NAS 12-2010 during the period July 1, 1968 - December 31, 1969.

4

EXPERIMENTAL STUDIES

Work on the contract program was begun early in July 1968. The company-supported effort carried out prior to that time provided a good base for pursuit of the proposed contract program. The principal activities from July 1, 1968, through December, 1969, were in the following important areas: deposition parameters, material purity, crystal perfection, film homogeneity, orientation relationships, early-stage growth studies, and device studies.

Apparatus

The apparatus originally in use consisted principally of a vertical 60-mm-O.D. quartz tube 38 cm long, containing a SiC-covered C pedestal which could be inductively heated; stainless-steel bubblers containing the liquid organo-metallic compounds; appropriate flowmeters for monitoring the carrier gas, AsH_3, and dopant gas flows; a H_2 burn-off area; and a manifold made from 1/4-in. stainless-steel tubing. Provisions were made for bypassing the quartz reactor and keeping the reactants separate until the gases were equilibrated and ready to be mixed for film formation. A schematic of the apparatus is shown in Figure 1.

During the course of the study several modifications have been made in the reactor portion of the system in order to assure a more uniform temperature control of the SiC-covered pedestal. By modifying the induction coil and minimizing the physical contact between the pedestal and the support rod, temperatures could be regulated to ±5 deg C from the center of the 1-1/2-in.-diameter pedestal to within 1/4 in. of the pedestal edge. Provision has also been made to provide rotation of the pedestal during the deposition process. Film thickness control within ±10 percent across a 1 1/2 in.-diameter pedestal is being achieved routinely.

The reactor shape was also modified to a narrower design (45mm O.D.) which expands to 60mm O.D. at about the pedestal height. This new design also contains a sight window for temperature measurements.

Temperatures reported are those of the SiC-coated pedestal, as measured with an infrared radiation thermometer through the quartz reactor tube. The readings of the thermometer were compared with those of an optical pyrometer for pedestal temperatures greater than 750C. This provided a means for establishing an average emissivity value for the system in this temperature range. With this value, the infrared thermometer readings were then extrapolated to still lower temperatures. All "deposition temperatures" reported here have been measured in this way.

Materials

Arsine (AsH_3). - The AsH_3 used in these studies has been obtained from five different suppliers. It has been found necessary to use in-stream purification of the AsH_3, nominally 10 percent in H_2 or He, to remove major impurities which probably are residuals from the process used to clean the cylinders prior to filling with the gas mixtures. In-house studies using pure AsH_3 were also explored in an attempt to alleviate the impurity problem. The suppliers of the AsH_3-and-gas mixtures are also attempting to correct this problem.

H$_2$ BURN OFF

VACUUM

AIR

DEWAR

DEWAR

SUBSTRATE

SiC

PEDESTAL

TMG BUBBLER

DEZ BUBBLER

H$_2$

H$_2$ PURIFIER

AsH$_3$ IN H$_2$

H$_2$S$_e$ IN H$_2$

H$_2$S IN H$_2$

R. F. SOURCE

VACUUM

FLOW METERS

VERTICAL REACTOR
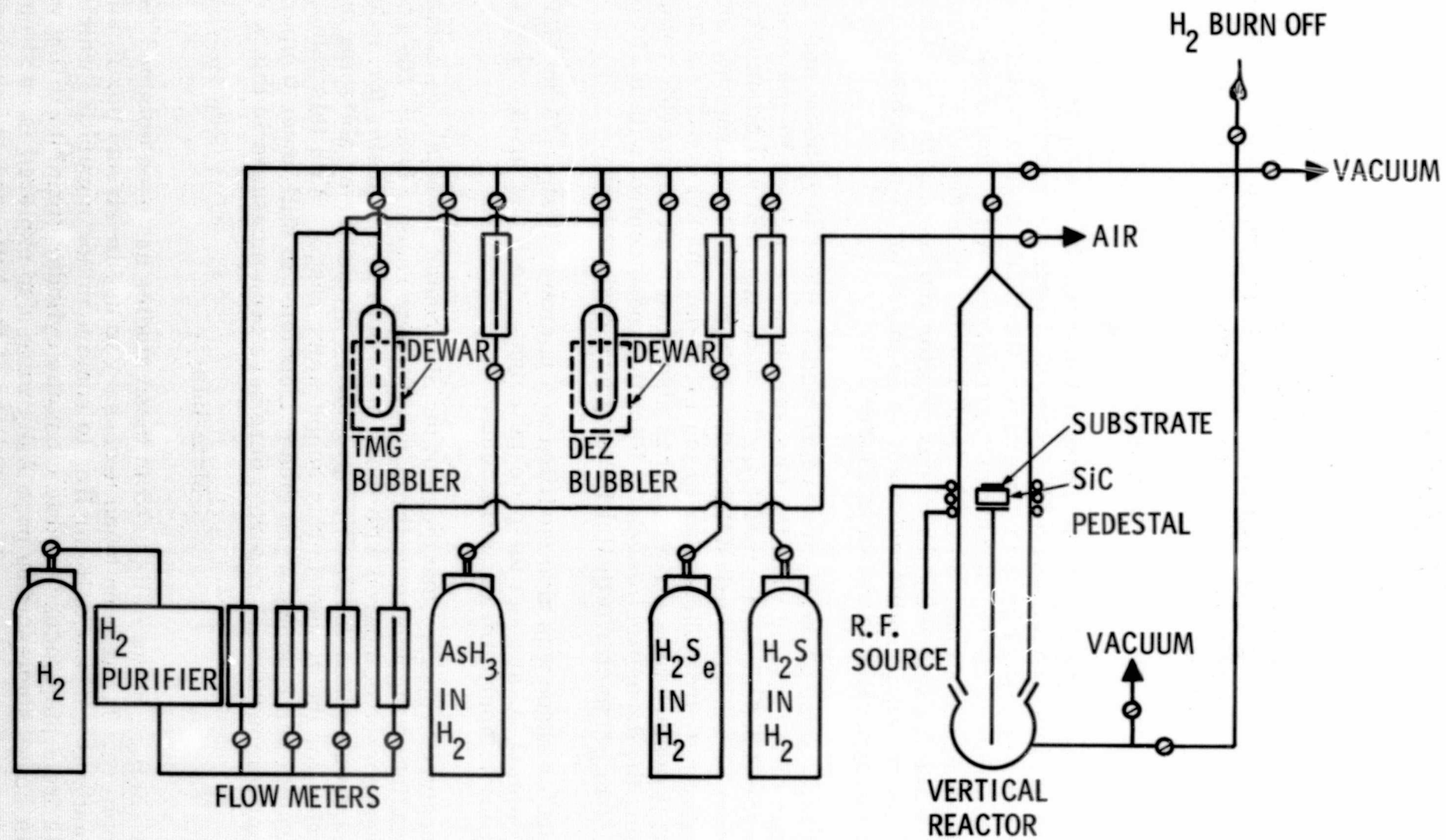
Figure 1. Chemical Vapor Deposition Apparatus

Trimethylgallium (TMG). - The TMG has been obtained from several commercial sources but made to order in each case for our specific investigations. The study has included TMG made from three-9s Ga, four-9s Ga halide, and six-9s Ga halide. The material made from three-9s Ga was obtained in an "unpurified" state and subsequently purified in our laboratory after evaluation in the "unpurified" form. The TMG made from four-9s Ga and from Ga halide was purchased already prepurified by the vendor. These materials were used initially as received, by transferring the liquid directly into the bubbler, freezing and pumping on the TMG while it was under vacuum, admitting an atmosphere of the carrier gas, and equilibrating at 0 C. The TMG was carried into the reactor for film growth by a carrier gas of H_2 or He passing through the liquid. The appearance of the grown layer indicated whether or not the TMG was adequate for growth studies.

Dopants. - Both n- and p-type dopant impurities have been introduced into the GaAs layers in these investigations:

N-type - Both H_2Se in H_2 and H_2S in H_2 had been evaluated prior to this contract as to their compatibility with the metal-organic system and as dopants for the GaAs films being grown. The nominal tank concentrations were 500 and 200 ppm, respectively, in the carrier gas. However, these mixtures also required in-line purification to remove residual impurities, which were found to be reactive with the TMG.

P-type. - Diethylizinc (DEZ) has been used as the p-type dopant for the GaAs films. The DEZ is normally purged with the carrier gas at -23 C for about 30 minutes in order to remove the more volatile impurities, and then stored at 0 C under the carrier gas until used for doping experiments. During doping, the "bubbling" tube is kept above the liquid surface.

Carrier gases. - Both H_2 and He have been used successfully as carrier gases in preparing GaAs from TMG and AsH_3. It was observed in the studies with He that if 99.995 percent He was used as the carrier gas, then special repurification of the TMG was occasionally necessary and beneficial in order to provide high quality reflective films. Such handling was not required when six-9s He or Pd-purified H_2 was used. However, the lower purity He was often adequate if the He was passed through a liquid-N_2 trap placed near the gas source. A condensate, presumably H_2O, was obtained. A condensate was also obtained at -196 C from six-9s He, and standard practice in our laboratories now involves this purification step for He. The major advantage of using six-9s material with a -196 C in-line purification lies presumably in the lower hydrocarbon and O_2 impurity levels.

Substrates. - Most of the $A\ell_2O_3$ and spinel substrates used in these investigations have been polished commercially by vendors specializing in such work. Although the standard specification to the vendor requires "no polishing scratches visible at 400X", it has generally been difficult to obtain consistently good polished surfaces on the $A\ell_2O_3$ substrates. The ease of obtaining a good polish is dependent upon the crystallographic orientation of the surface; some orientations are sensitive to the differences in the polishing procedures used by various vendors (these same observations held true when substrates were being obtained for the Si-on-$A\ell_2O_3$ investigations). In some instances, substrates polished by one vendor had to be repolished by another before GaAs epitaxy could be successfully achieved on the $A\ell_2O_3$ surfaces. GaAs epitaxy is found to be much more sensitive to the $A\ell_2O_3$ substrate surface conditions than is Si epitaxy.

Since the polishing procedures of the vendors are generally proprietary, it was determined that the necessary polishing methods for Al_2O_3 and spinel should be developed at Autonetics in the Semiconductor Materials Group. Considerable progress has been made toward this end, and substrates now final-polished in-house have been found to be superior to those prepared by outside sources.

Deposition Procedures

The deposition procedures most often used involve the growth of GaAs films in an atmosphere containing As produced by decomposing AsH_3 at the hot pedestal for two or three minutes prior to the introduction of the TMG into the reactor. When the substrate is GaAs, As is formed from AsH_3 at about 600 C in order to prevent decomposition of the substrate at the higher growth temperature. AsH_3 flow is also continued after the deposition is completed until the temperature has dropped to about 600 C. An alternative approach sometimes employed is to premix the AsH_3 and TMG before they enter the reactor chamber.

Dopant gases are normally added to the TMG gas stream but are also found to be compatible with the AsH_3. Some success has also been achieved by introducing the AsH_3-TMG mixture into the reactor after the dopant gas flow has been established.

Evaluation Procedures

Much of the effort of this program has been directed to evaluating the characteristics of the GaAs layers by a variety of metallurgical, optical, and electrical techniques.

Metallurgical. - Following deposition, the epitaxial layers are routinely examined by optical microscopy. It is usually possible to identify good epitaxy by visual inspection. Beyond inspection of the epitaxial layers by optical microscopy, extensive investigation of the thickness, surface characteristics, and crystallographic perfection of the deposited semiconductor is carried out. The film thicknesses are measured by observation of the interference fringe pattern in the reflectance spectrum in the infrared region, as obtained with a Beckman IR-5A double-beam spectrophotometer, or by a tracing made with a Talysurf surface-roughness gauge with stripchart recorder.

Considerable knowledge of the nature of the epitaxial films has been gained by x-ray diffraction techniques. These are used for evaluating both the substrate defect structure and that of the deposited overgrowth. Laue back-reflection x-ray patterns are used to select composites for full-circle goniometer determination of the orientation relationships and twin structures.

Lang-type topography cameras can provide displays of the defect structure throughout the crystal being examined. This technique has been applied to several of the substrates used in this program. Replica electron microscopy and reflection electron diffraction (RED) are used as required to screen the epitaxial composites prior to x-ray evaluation, to examine the substrate and surface of the GaAs deposit for inhomogeneities, and to reveal changes which occur during the nucleation and annealing studies.

8

Electrical. - Measurement of fundamental electrical properties to characterize the semiconductor films prepared in this program has constituted an extremely valuable part of the investigations. The electrical measurements may range from routine determination of conductivity type with a thermoelectric probe to detailed studies of carrier-scattering mechanisms and impurity or defect energy levels by means of low temperature Hall-effect measurements, employing a double-dewar cryostat. Measurement of the carrier mobility and concentration in the epitaxial semiconductor films being grown at any given time provides valuable information about the nature of the epitaxial growth mechanisms on the insulating substrates, the degree of control over the deposition processes, and the directions to be taken next by the materials studies.

Electrical characterization of the GaAs/Aℓ_2O$_3$ or GaAs/spinel systems is usually carried out on a "bridge sample" etched in the epitaxial layer by standard photolithographic techniques. Attempts to use the van der Pauw technique on the same layers have been found to be unsatisfactory. A group of twenty samples, grown by both the H$_2$ and the He process, was measured by the two techniques. The resistivity measured by the van der Pauw method appeared to be within ~5 percent of the values obtained by the bridge measurements; however, the measured carrier concentrations were found to be consistently 25-40 percent high. Since this leads to errors in mobility on the order of 40 percent, the van der Pauw measurement technique was discontinued, except for the measurement of GaAs films grown on semi-insulating GaAs.

The reasons for the discrepancy are not fully understood, since the contacts were placed in a symmetrical fashion on the edges of a sample whose dimensions were typically much larger than the size of the contacts. Although inhomogeneities in film properties, particularly near the edges, could be a possible cause for variation between the two techniques, such a consistent difference for a large group of samples would not be expected.

Ohmic contact was made to the bridge samples by vacuum evaporation of a suitable metal or alloy, after which the sample was heated to ~400 C for ~1 min to form a low-resistance contact. During part of the contract program, Zn was used as the contacting metal for thin undoped (p-type) samples. It was later established that these samples became contaminated with Zn during the heating cycle, leading to erroneous measurements of electrical parameters. Most recently, Au has been used for the contacting metal to these thin p-type layers, eliminating this source of contamination.

RESULTS AND DISCUSSION

Significant progress has been made in a number of areas related to the growth of GaAs on insulating substrates. In other areas only preliminary studies have been undertaken, but considerable insight into the understanding of the nucleation and growth of GaAs has been obtained. The sections below describe in detail the primary areas of study during the contract period and the progress that has been made.

Film Properties

Effects of deposition parameters. — Emphasis was placed during the first part of the contract on the growth of undoped GaAs/Al_2O_3 samples in order to determine the optimum growth rates and optimum flow rates of the various constituent gases. Films were grown on (0001) Al_2O_3 at various temperatures between 650 and 700 C with a wide variety of AsH_3 and TMG concentrations. Experimentally, it is convenient to express the concentrations of AsH_3, TMG, and dopant gases by flowmeter readings, given in cubic centimeters per minute (cc/min). As an example, in the data to be presented below, the notation 45–22–0 refers to an experiment in which the carrier gases were mixed with 45 cc/min of 10 percent AsH_3-in-H_2 and 22 cc/min of H_2 which was bubbled through TMG (equilibrated at 0 C). The last number, in this case 0, refers to the amount of dopant gas added, if any. The AsH_3:TMG mole ratio in this case is 3.5 (0.2 mmole of AsH_3 to 0.058 mmole TMG). For the initial experiments the flow rate of pure H_2 (or He) gas was fixed at 1.5 liters/min; in later studies this flow was increased to 3 liters/min.

As discussed in the contract proposal and demonstrated again during the course of the contract program, undoped GaAs films grown on Al_2O_3 by the CVD method used here have always appeared to be p-type for the first few microns of growth. During subsequent growth the films become n-type and higher in quality as the thickness of the film increases. (This behavior will be discussed in more detail in a later section.) Since the electrical properties of the films are changing with thickness, the measured electrical parameters are necessarily "averages" over the thickness of the film. In general, the outermost layers of the film will, therefore, have properties superior to the "average" value, and the layers nearer the interface will have inferior properties.

The growth of a high quality film was found to depend on the flow rates of the constituent gases through the reactor. The electrical measurements made on a number of films for various growth conditions are shown in Tables I through IV.

The effects of changing the AsH_3 flow at constant TMG flow rates (at 650-660 C) for various thicknesses are shown in Table I. The carrier concentration has been found to be dependent on the AsH_3 flow rate for a given temperature and a fixed rate of H_2 flow through TMG. For the higher AsH_3 flow rates the carrier concentration saturates at some value characteristic of the gases used. (See section below on effects of starting materials.) As the AsH_3 flow is reduced, the net carrier concentration also tends to decrease. With continued decrease in AsH_3, the films eventually become p-type, and the quality of the films appears visually to deteriorate at very low AsH_3 concentrations. This behavior was examined for a variety of growth conditions, and it was found that p-type films could be produced in this manner with net hole concentrations ranging from $\sim10^{15}$ to $\sim10^{19} cm^{-3}$.

10

TABLE I

ELECTRICAL PROPERTIES OF EPITAXIAL (111) GaAs/(0001) Aℓ_2 O_3
AS A FUNCTION OF AsH$_3$ CONCENTRATION AND
FILM THICKNESS AT 650-660C

Deposition Conditions* (AsH$_3$-TMG-Dopant)	Thickness (μm)	Resistivity (ohm-cm)	Carrier Concentration (cm^{-3})	Mobility (cm^2/V-sec)
10-10-0	13.9	-	-	(p-type)
20-10-0	10.9	-	-	(p-type)
45-10-0	7.9	20.6	~3 x 10^{15}	100 (n-type)
90-10-0	12.0	0.345	6.4 x 10^{15}	2840 (n-type)
90-10-0	29.5	0.169	8.4 x 10^{15}	4400 (n-type)
20-22-0	4.0	-	-	(p-type)
45-22-0	7.0	-	-	(p-type)
90-22-0	8.2	0.42	8.5 x 10^{15}	1750 (n-type)
90-22-0	10.5	0.10	2.3 x 10^{16}	2940 (n-type)
90-22-0	18.3	0.28	6.8 x 10^{15}	3280 (n-type)
180-22-0	21.8	0.15	1.2 x 10^{16}	3740 (n-type)
180-45-0	10.9	0.15	1.1 x 10^{16}	4050 (n-type)
180-45-0	11.5	0.10	1.5 x 10^{16}	4150 (n-type)
180-45-0	15.6	0.15	1.1 x 10^{16}	3890 (n-type)
250-45-0	16.4	0.27	7.2 x 10^{15}	3200 (n-type)
180-60-0	18.5	-	-	(p-type)
250-60-0	16.4	0.27	7.2 x 10^{15}	3200 (n-type)

*See text, p. 10, for significance of numbers.

11

Table II illustrates the effect of lowered AsH_3 flow at 675 C for a group of thicker films grown later in the program using different reactant gases. Note that reasonably good hole mobilities can be obtained in thick films by this technique.

TABLE II
ELECTRICAL PROPERTIES OF EPITAXIAL (111) GaAs/(0001) $A\ell_2O_3$
FILMS GROWN AT 675 C AS AFFECTED BY CHANGES
IN AsH_3-in-H_2 FLOW RATES

Growth Conditions* (AsH_3-TMG-Dopant)	Thickness (μm)	Carrier Concentration (cm^{-3})	Mobility (cm^2/V-sec)	Conductivity Type
125-45-0	20.6	1.5×10^{15}	1400	N
100-45-0	29.2	–	High Resistivity	–
75-45-0	29.2	1.2×10^{15}	160	P
50-45-0	20.4	1.8×10^{16}	157	P

*See text, p. 10, for significance of numbers.

The effects of changing TMG flow rate at constant AsH_3 rate (at~650-660 C) for films of various thickness are shown in Table III. In general it is found that the higher flow rates of TMG, and hence faster deposit growth rates, produce superior quality films. Increasing the concentration ratio of Ga to As by increasing the TMG rate to a very high value (for constant AsH_3 rate) again leads to a p-type film as evidenced by the last sample in the table.

Further examination of even faster growth rates later in the contract has shown that equivalent quality films (in terms of the electrical properties) may be grown with rates of from ~0.6 to 1.5 μm/min (Table IV). However, the AsH_3 flow necessary for a reflective film at the higher growth rates is found to be more critical than at the lower rates. Even a "gray" film produced at high AsH_3 flow rates possessed good electrical properties; the surface structure of such a film is shown in Figure 2.

As the growth temperature is increased it is found that higher AsH_3 rates are needed to produce a more reflective film. The properties of several films grown at 675 and 700 C are shown in Tables V and VI. The necessary flow rates of AsH_3 range from ~180 cc/min at 650 C to ~325 cc/min at 700 C. A flow rate of 35-45 cc/min of H_2 passing over TMG usually yields good quality films over the whole temperature range from 650 to 700 C for films >10 μm thick.

TABLE III

ELECTRICAL PROPERTIES OF EPITAXIAL (111) GaAs/(0001) Al_2O_3
AS A FUNCTION OF TMG CONCENTRATION AND
FILM THICKNESS AT 650–660 C

Deposition Conditions* (AsH_3–TMG–Dopant)	Thickness (μm)	Resistivity (ohm-cm)	Carrier Concentration (cm^{-3})	Electron Mobility (cm^2/V-sec)
90-5-0	15.5	0.189	1×10^{16}	3300
90-10-0	29.5	0.169	8.4×10^{15}	4400
90-22-0	18.3	0.28	6.8×10^{15}	3280
90-30-0	20.3	0.43	5.8×10^{15}	2520
180-22-0	21.8	0.15	1.2×10^{16}	3740
180-35-0	15.4	0.11	1.2×10^{16}	4650
180-35-0	23.9	0.1	1.5×10^{16}	4430
180-45-0	10.9	0.15	1.1×10^{16}	4050
180-45-0	11.5	0.1	1.5×10^{16}	4150
180-45-0	15.6	0.15	1.1×10^{16}	3890
180-60-0	18.5	--	--	(p-type)

*See text, p. 10, for significance of numbers.

Experimental investigations using a "premixing" procedure for the TMG-AsH_3-dopant gases were carried out during this contract program. With this technique, a stabilized flow of the reactants at a desired concentration ratio was established in the system prior to introduction of the reactant mixture into the reactor chamber in the region of the heated substrate. The reactant mixture was formed either in the stainless-steel tubing lines or in a special premixing chamber (volume ~4 liters) just prior to introduction into the reactor chamber. The electrical properties of films grown at two different deposition temperatures on (0001)-oriented Al_2O_3 substrates by these two premixing procedures are given in Tables VII and VIII.

It was observed that either mixing process can be used to grow thick, undoped GaAs/Al_2O_3 films which possess mobilities comparable with those of films grown with the "pre-AsH_3" treatment, that is, where excess AsH_3 in introduced into the reactor chamber prior to introduction of the TMG. Similarly, thin (~1 μm) films grown by the premixing technique exhibited electrical characteristics comparable with those grown by the pre-AsH_3 treatment.

TABLE IV

ELECTRICAL PROPERTIES OF EPITAXIAL (111) GaAs'/(0001) Aℓ_2 O$_3$ GROWN AT 675 TO 680 C AT VARIOUS GROWTH RATES

Growth Conditions* ("Tank Z" AsH$_3$-"Tank R" TMG)	Thickness (μm)	Growth Rate (μm/min)	Resistivity (ohm-cm)	Carrier Concentration (cm^{-3})	Electron Mobility (cm^2/V-sec)	Surface Condition
275-45	27.2	0.8	0.096	1.3×10^{16}	5000	reflective
325-45	21.6	0.6	0.081	1.5×10^{16}	5300	reflective
350-45	21.5	0.6	0.080	1.5×10^{16}	5100	reflective
250-90	23.1	1.2	0.060	2.0×10^{16}	5300	reflective
275-90	20.3	1.0	0.041	2.8×10^{16}	5400	reflective
400-90	28.2	1.3	0.073	1.6×10^{16}	5200	gray
250-120	23.1	1.5	0.047	2.5×10^{16}	5300	reflective

*See text, p. 10, for significance of numbers

TABLE V

ELECTRICAL PROPERTIES OF EPITAXIAL (111) GaAs/(0001) $A\ell_2O_3$
AS A FUNCTION OF AsH_3 AND TMG CONCENTRATIONS AT 675 C

Deposition Conditions* (AsH_3-TMG-Dopant)	Thickness (μm)	Resistivity (ohm-cm)	Carrier Concentration (cm^{-3})	Electron Mobility (cm^2/V-sec)
45-22-0	~39	--	--	(p-type)
90-22-0	25.4	0.21	7.9×10^{15}	3720
180-22-0	17.4	0.35	7.0×10^{15}	2530
250-22-0	22.9	0.12	1.1×10^{16}	4560
150-35-0	11.2	1.11	3.8×10^{15}	1500
180-35-0	11.7	0.65	5.1×10^{15}	1900
250-35-0	8.6	0.14	1.2×10^{16}	3610
250-22-0	22.9	0.12	1.1×10^{16}	4560
250-35-0	24.4	0.11	1.3×10^{16}	4400
250-45-0	20.5	0.08	1.6×10^{16}	4530
250-60-0	18.9	0.12	1.3×10^{16}	4000

*See text, p. 10, for significance of numbers.

TABLE VI

ELECTRICAL PROPERTIES OF EPITAXIAL (111) GaAs/(0001) $A\ell_2O_3$
AS A FUNCTION OF TMG AND AsH_3 CONCENTRATIONS AT 700 C

Deposition Conditions* (AsH_3-TMG-Dopant)	Thickness (μm)	Resistivity (ohm-cm)	Carrier Concentration (cm^{-3})	Electron Mobility (cm^2/V-sec)
250-35-0	19.2	0.24	7.4×10^{15}	1940
325-35-0	13.7	0.21	8.8×10^{15}	3470
325-45-0	13.7	0.11	1.3×10^{16}	4290
325-60-0	10.0	0.21	1.1×10^{16}	2800
250-60-0	12.5	0.19	1.0×10^{16}	3210

*See text, p. 10, for significance of numbers.
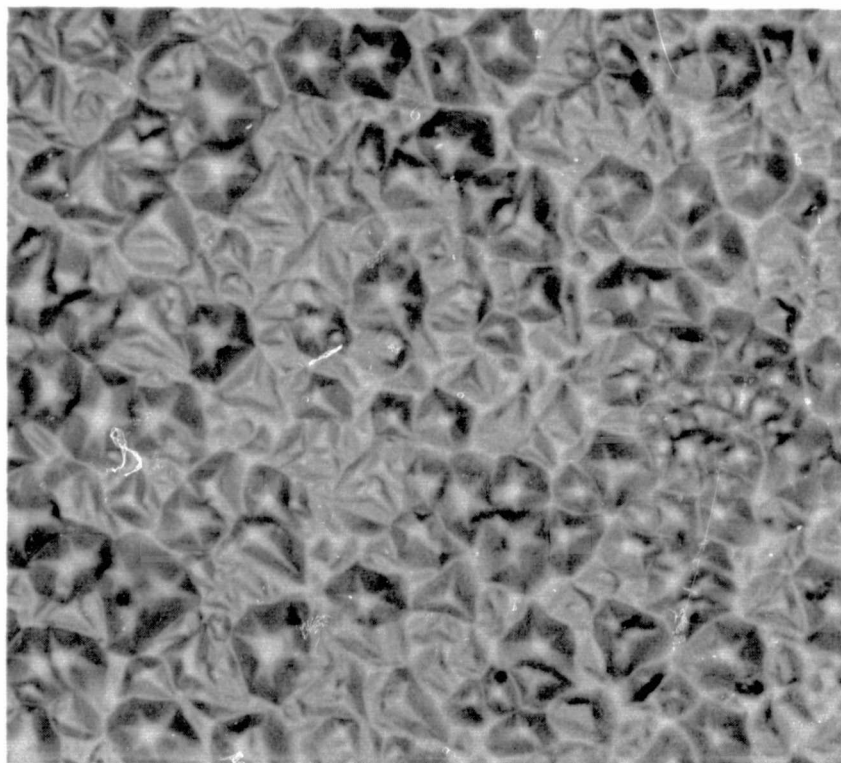
Figure 2. Surface Structure of a Gray GaAs/Al$_2$O$_3$ Film

Although the data in Table VII could suggest that a lowering in carrier concentration results from increased AsH$_3$ flow, it is believed that such changes are due instead to impurities in the tank being slowly removed through use and to surface passivation of the tank walls.

A new reactor of smaller cross-section was installed in the H$_2$ carrier gas system during these investigations to explore the effects of reactor geometry on GaAs/Al$_2$O$_3$ film properties. The new reactor was used initially in conjunction with gas supplies which had previously yielded thick undoped films in the low-10^{15}cm^{-3} carrier concentration range. Electrical measurements on a series of thick (>20 μm) films grown in this system indicated a considerable improvement in film quality. Room temperature electron mobilities in a number of n-type films were found to be ~5200-5900 cm^2/V-sec for carrier concentrations of 1.6-3.2 x 10^{15}cm^{-3}. The high quality of these films is further evidenced by mobilities at liquid-N$_2$ temperature of 20,000-25,000 cm^2/V-sec. A summary of the electrical data on several of these films is given in Table IX.

TABLE VII

ELECTRICAL PROPERTIES OF EXPITAXIAL GaAs/Aℓ_2O$_3$ FILMS
PRODUCED AT 700 C BY PREMIXING AND EQUILIBRATING
THE AsH$_3$ AND TMG IN A 4-LITER CHAMBER

Growth Conditions (AsH$_3$-TMG)*	Thickness (μm)	Resistivity (ohm-cm)	Carrier Concentration (cm^{-3})	Electron Mobility (cm^2/V-sec)
125-65	22.9	0.018	9.0×10^{16}	4000
175-65	22.9	0.016	8.9×10^{16}	4400
175-65**	23.9	0.019	7.1×10^{16}	4700
225-65	23.1	0.034	4.5×10^{16}	4100
275-65	24.1	0.037	3.7×10^{16}	4500
425-65	26.7	0.10	1.5×10^{16}	4200
475-65	22.9	0.14	1.1×10^{16}	4000
425-100	34.7	0.075	1.8×10^{16}	4800

*See text, p.10, for significance of numbers
**Premixed in lines

TABLE VIII

ELECTRICAL PROPERTIES OF EPITAXIAL GaAs/Aℓ_2O$_3$ FILMS
PRODUCED AT 680C BY PREMIXING AsH$_3$
WITH TMG IN THE LINES ONLY

Growth Conditions (AsH$_3$-TMG)*	Thickness (μm)	Resistivity (ohm-cm)	Carrier Concentration (cm^{-3})	Electron Mobility (cm^2/V-sec)
200-45	18.3	0.08	1.8×10^{16}	4400
200-65	16.5	0.10	1.5×10^{16}	4000
200-85	12.7	0.11	1.6×10^{16}	3590

*See text, p. 10, for significance of numbers

TABLE IX

ELECTRICAL PROPERTIES OF EPITAXIAL (111) GaAs/(0001) $A\ell_2O_3$ FILMS PREPARED IN THE NARROW-NECK REACTOR

Thickness (μm)	Resistivity (ohm-cm)	Carrier Concentration (cm^{-3})	Electron Mobility (cm^2/V-sec)	
			300 K	77 K
26.5	0.37	3.2×10^{15}	5250	20,000
34	0.45	2.6×10^{15}	5320	22,000
32	0.69	1.6×10^{15}	5580	25,200
29	0.40	2.7×10^{15}	5850	21,900

These samples represented a significant improvement in that high mobilities were achieved in samples having comparatively low carrier concentrations.

Effects of starting materials. — Considerable attention has been given to the question of the effects of the impurity content of the reactants upon the properties of the GaAs layers.

Carrier gases. — Hydrogen gas has been primarily used as the carrier gas throughout the contract program and was used to produce the films described in the previous section. Helium was investigated as an alternative to H_2 in order to determine the feasibility of using inert gases and to help distinguish between the various possible reaction mechanisms for the formation of GaAs by the metal-organic process. Initial experiments involved first the use of five-9s-purity He with 10 percent AsH_3-H_2 mixtures and then five-9s-He with 10 percent AsH_3-He mixtures. These experiments indicated that excellent quality GaAs could be grown with these gases; however, there was evidence to suggest that the He was contaminating the supply of TMG after continuous use. A short distillation at 0 C returned the TMG to a purity which yielded good quality films. With the substitution of six-9s-purity He gas, excellent films were consistently produced. The six-9s-purity He did not apparently contaminate the TMG source, and no further purification steps were necessary. The electrical data on a number of films grown with the higher purity He are shown in Table X.

Reactant materials. — It has been demonstrated throughout the contract work that the materials from which GaAs films are grown are of considerable importance in determining the quality and impurity levels in the films. As a result, investigation of the effect of the purity and source of starting materials on the electrical properties of the GaAs films has been a continuing effort.

18

TABLE X

ELECTRICAL PROPERTIES OF EPITAXIAL (111) GaAs/(0001) Al_2O_3
GROWN UNDER DIFFERENT CONDITIONS, USING SIX-9s He AS
CARRIER GAS AND TEN PERCENT AsH_3-IN-He

Growth Conditions* (AsH_3-TMG-Dopant)	Temp (C)	Thickness (μm)	Resistivity (ohm-cm)	Carrier Concentration (cm^{-3})	Electron Mobility (cm^2/V-sec)
400–45–0 (5 min) 225–45–0 (55 min)	675	26.4	0.15	7.9×10^{15}	5230
600–45–0 (6 min) 400–45–0 (27 min)	700	18.6	0.12	1.1×10^{16}	4330
600–45–0 (2 min) 400–45–0 (4 min) 275–45–0 (54 min)	700	52.0	0.15	6.2×10^{15}	6230 19,300 (77 K)
400–45–0 (30 min)	700	14.3	0.11	1.2×10^{16}	4560
400–45–0 (30 min)	725	19.5	0.14	1.1×10^{16}	4360
400–45–0 (30 min)	750	23.8	0.18	9.6×10^{15}	3527

*See text, p. 10 for significance of numbers.

It has been found that n-type impurity concentrations from $\sim 10^{15}$ to $\sim 10^{17}$ cm^{-3} are obtained in films in which no dopant was intentionally added during growth. The impurity concentration is measured by growing thick films under optimum growth conditions. Since there is little variation in film properties for films greater than 15-20 μm, the measured impurity concentration can be a good indication of the quality of the starting materials.

Unfortunately, it is still not possible to predict what impurity concentrations will result from a given set of starting materials. It has been determined that the dominant source of impurity can be either the TMG or the AsH_3 and, to a lesser extent, the carrier gas. In addition, the purity of the starting material may vary considerably from tank to tank even though the vendor's purity specifications are the same.

Table XI illustrates the carrier concentrations measured in thick (nominally undoped) films produced with various combinations of AsH_3 and TMG using H_2 as a carrier gas. From the measurements of films grown from different combinations of the same gases, it is usually possible to determine the number of donor impurities (per cm^3) each gas contributes to the GaAs. The gases may then be used in appropriate combinations to produce "undoped" GaAs films with desired carrier concentrations from $\sim 10^{15}$ to $\sim 10^{17} cm^{-3}$.

19

TABLE XI

VARIATION IN CARRIER CONCENTRATION IN EPITAXIAL (111) GaAs/(0001)
$A\ell_2O_3$ FILMS FOR VARIOUS COMBINATIONS OF REACTANT GASES

AsH$_3$* (Tank Designation)	AsH$_3$ Source	TMG (Tank Designation)	TMG Source	Approximate Carrier Concentration in GaAs Films (cm^{-3})
J	Airco	UM	Orgmet	$2\text{-}3 \times 10^{15}$
P	Scientific Gas Products	UM	Orgmet	2×10^{15}
Z	Airco	UM	Orgmet	10^{15}
P	Scientific Gas Products	Q	Alfa Inorganic	3×10^{16}
V	Matheson	Q	Alfa Inorganic	10^{17}
P	Scientific Gas Products	X	Alfa Inorganic	10^{16}
V	Matheson	X	Alfa Inorganic	10^{17}
V	Matheson	R	Orgmet	$6\text{-}8 \times 10^{16}$
P	Scientific Gas Products	R	Orgmet	10^{16}
C	Air Products	R	Orgmet	10^{17}
U	Matheson	R	Orgmet	$2\text{-}3 \times 10^{16}$
V"	Matheson	R	Orgmet	10^{16}
V'	Matheson	R	Orgmet	10^{17}
Z	Airco	R	Orgmet	$1\text{-}2 \times 10^{16}$
AA	Scientific Gas Products	UM	Orgmet	10^{15}
AA	Scientific Gas Products	AC	Alfa Inorganic	2×10^{16}
AA	Scientific Gas Products	AD	Orgmet	4×10^{15}
AE	Air Products	AD	Orgmet	$4\text{-}6 \times 10^{16}$
AO	Precision Gas	AK	Orgmet	2×10^{15}
Z	Airco	AK	Orgmet	2×10^{15}

* The AsH$_3$ sources are 10% AsH$_3$ in H$_2$ except for V, V', V", which are 100% AsH$_3$, and J and Z, which are 10% AsH$_3$ in He.

These studies have clearly demonstrated that there are definite differences in the quality of the purchased 10 percent AsH_3-in-carrier gas mixtures. Mass spectrographic analyses of the mixtures by the vendors have not revealed the copious quantities of water removed from the gases by the in-line purification steps in use in the laboratory, nor has the source of the donor impurity yet been established.

A quantity of 100 percent AsH_3 was obtained in order to examine this material in the condition in which it is secured by vendors prior to their preparation of gas mixtures. It was established by electrical measurements that an n-type impurity was associated with the 100 percent AsH_3, producing carrier concentrations of $\sim 10^{17} cm^{-3}$ in GaAs films grown on $A\ell_2O_3$.

Attempts to purify the AsH_3 by passing it over NaOH pellets or through an NaOH-water solution were not sufficient to lower the film carrier concentration significantly, so additional purification procedures were undertaken. Distillation of about 1 lb of AsH_3 at -78 C separated at least 0.5 ml of liquid and a volatile yellow solid, which slowly turned orange and then became a brown nonvolatile residue as it warmed to room temperature in the liquid environment.

These products were analyzed by an outside laboratory. The liquid condensate was determined by mass spectrographic analysis to be predominantly water, with a trace of ethanol. The vapor in the bulb containing the brown nonvolatile residue was found to consist of toluene, xylene, trichloroethylene, and AsH_3. On heating the solid to 300 C, sublimination and decomposition took place, producing As, AsH_3, H_2, and a compound which appeared to be diarsine (As_2H_4). The laboratory observations and chemical analyses of the brown solid residue are consistent with the results of Jolly et al (Ref 6).

The stainless-steel cylinder from which the AsH_3 was distilled was found to contain magnetic and metallic particles, presumably due to improper cleaning of the tank by the vendor before filling. After "pickling," the tank was reinstalled into the apparatus. The AsH_3 was redistilled at -78 C from a second tank into the cleaned tank. A -78 C condensate was also found in the second tank, with properties similar to the solid condensate described above; magnetic particles were also found in the second tank.

Distillation of a portion of the 100 percent AsH_3, which had previously provided n-type films with $n \sim 10^{17} cm^{-3}$, left behind a fraction which yielded n-type thick GaAs films with $n \sim 2 \times 10^{16} cm^{-3}$ on $A\ell_2O_3$ and spinel, but the distilled portion produced films with $n \sim 10^{17} cm^{-3}$. This fractionation step indicated the n-type impurity was slightly more volatile than the AsH_3 itself. These experiments represented the first encouraging progress in attempting to purify the 100 percent AsH_3 in-house.

Mobility variation with carrier concentration. — During the early months of the contract, primary emphasis was placed on determining the proper conditions for the growth of GaAs/(0001)$A\ell_2O_3$ films with the H_2 process. The criterion used for good growth was the Hall mobility, which is plotted versus carrier concentration for a group of these early samples in Figure 3.

Figure 3. Mobility vs Carrier Concentration for GaAs/Aℓ2O3, Undoped Samples
(Thickness Range: 4 – 30 μm)
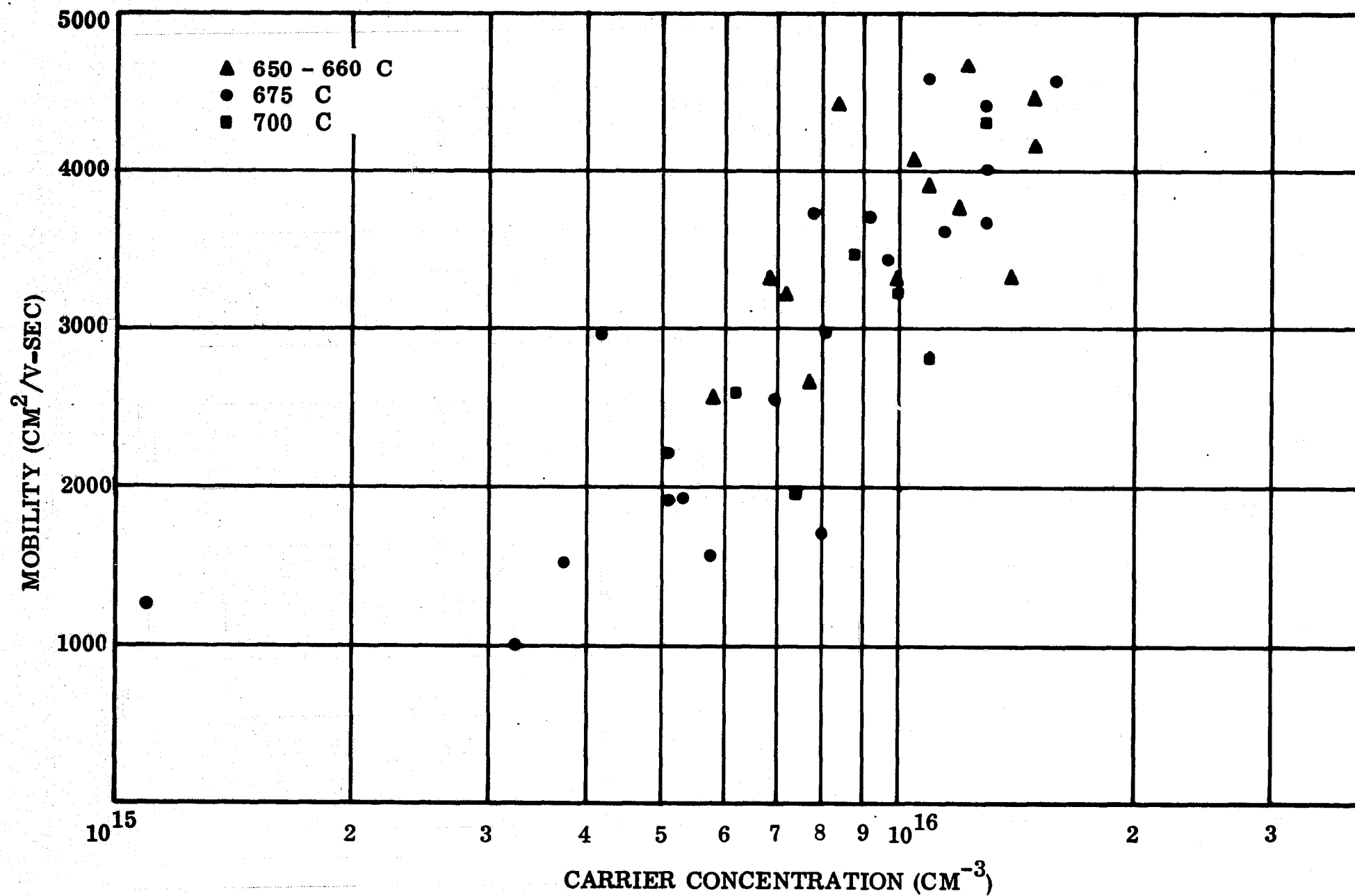
The films represented by the data points were grown at different temperatures, as indicated in the figure, and under a variety of gas flow conditions, not necessarily optimum. These results suggested that there is no definite correlation between carrier mobility and growth temperature in the range from 650 to 700 C.

The importance of the quality of the starting materials in determining the electrical characteristics of the films was soon realized; accordingly, mobility data on a number of films grown in H_2 subsequent to the above were separated according to differences in starting materials, and are shown plotted in Figure 4. Basically the same quality TMG has been used for all, and the different data points correspond to different tanks of AsH_3. It should be noted that the carrier concentration is these undoped samples varies by nearly two orders of magnitude.

Mobility-versus-carrier concentration data on the films grown by the He process are shown in Figure 5. These data are similarly divided according to starting materials; however, in this case, the variation of carrier concentration reflects primarily the quality of the TMG. Changing the available AsH_3-in-He tanks appeared to make little difference, and changing the He carrier gas from six-9s to four-9s purity resulted in the small differences between the solid circles and open squares in the figure. The carrier concentration is again found to vary over two orders of magnitude, illustrating the importance of high quality TMG as well as AsH_3 in producing films of low carrier concentration. That there are considerable impurities or defects in the films is suggested by the depression of mobility for carrier concentrations approaching $10^{15} cm^{-3}$.

A summary of electrical data on more recent undoped films grown by the H_2 process (and a number of different reactant gas sources) is shown in Figure 6. The high average mobilities are indicative of consistently good quality GaAs/$A\ell_2O_3$ and represent a significant improvement over those films grown early in the program, particularly for the lower carrier concentration samples. The high quality of the material is further attested to by mobilities in a number of these low carrier-concentration samples of over 20,000 cm^2/V-sec at 77 K.

The reduction in mobility at low carrier concentrations in thick samples suggests that the films are partially compensated. Although the origin of any acceptors is unknown, such impurities could very likely occur in the gases. The role of defects in GaAs is not well understood, but the formation of defects or defect-impurity complexes could conceivably provide another compensating mechanism. In addition to the above, GaAs is known to exhibit anomalous mobility effects which can be associated with inhomogeneous distributions of impurities. Such distributions, by creating space-charge regions in the semiconductor, lead to scattering centers quite effective in reducing the mobility in GaAs.

Impurity concentration. — It is evident from the electrical data on undoped GaAs films grown by the CVD process that the limitations in mobility are strongly related to unwanted impurities present in the films. That a considerable portion of these limitations results from impurities in the gases used to grow the films has been demonstrated. It is probable that in addition there are impurities present on the $A\ell_2O_3$ surface which can influence the interface layer. Also the defect structure near the interface may contribute electrically-active species deleterious to the quality of the GaAs.
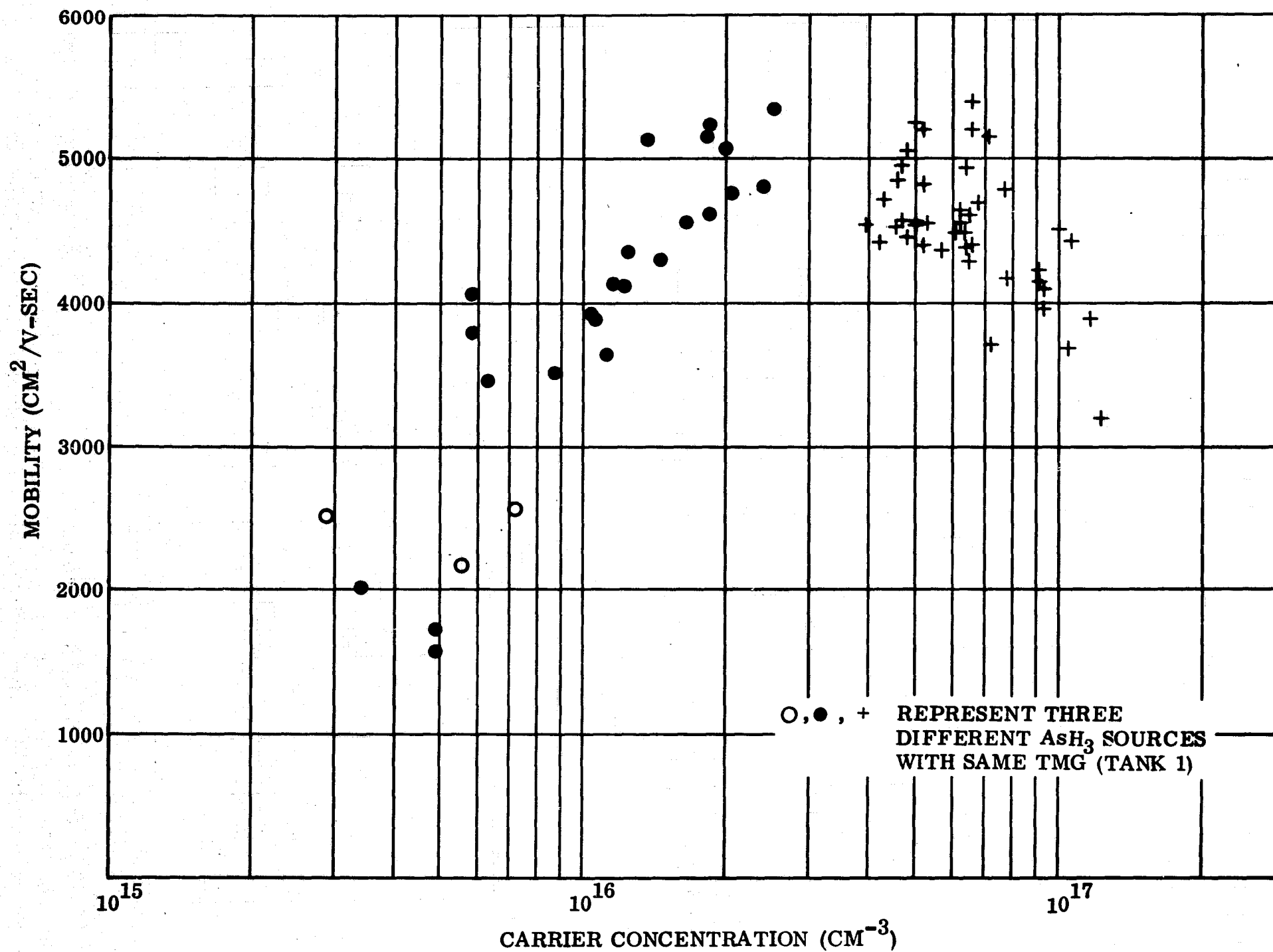
Figure 4. Mobility vs Carrier Concentration for GaAs/Aℓ_2O$_3$, Undoped Samples
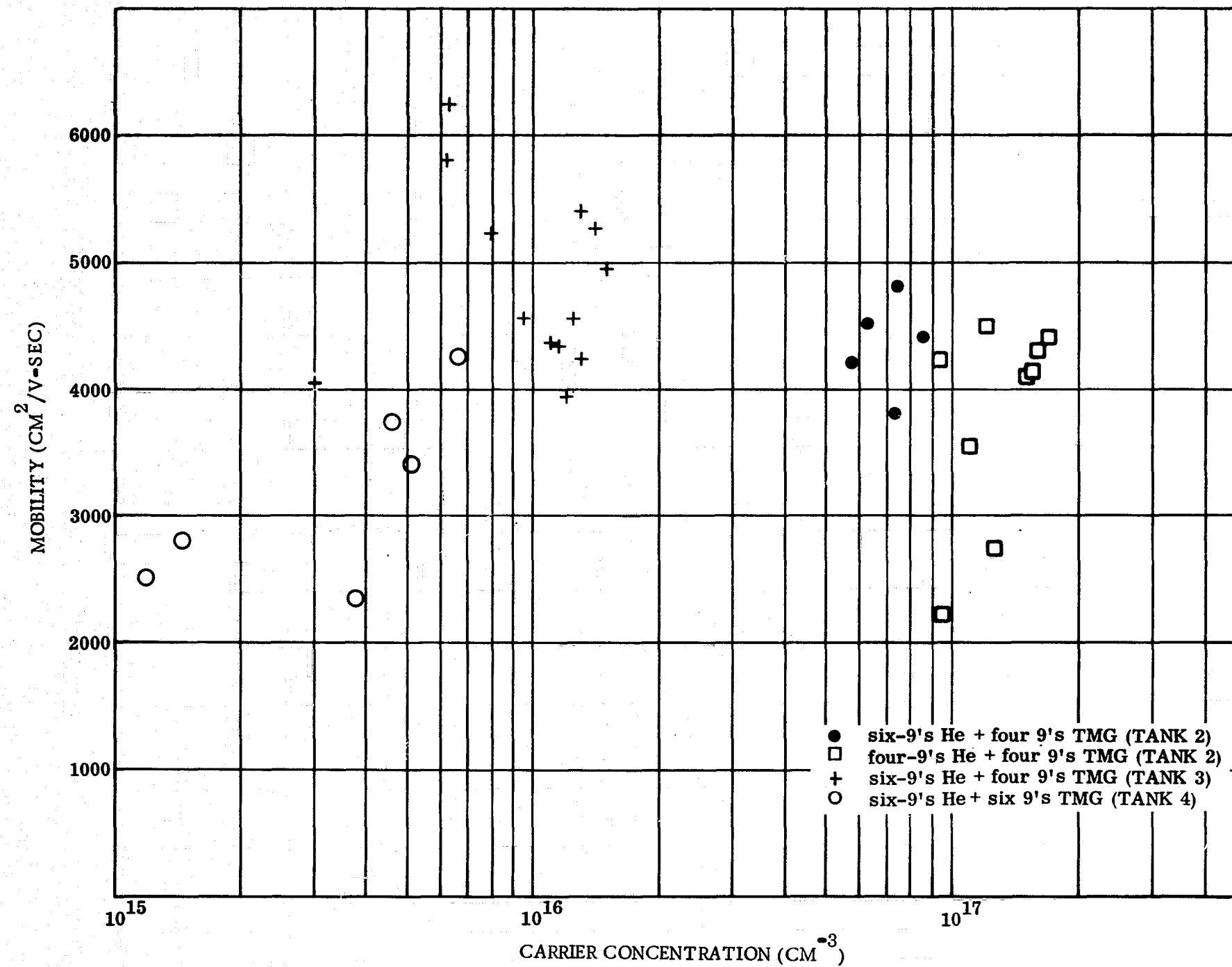(Thickness >10 μm)–H$_2$ Process

Figure 5. Mobility vs Carrier Concentration for GaAs/Aℓ$_2$O$_3$, Undoped Samples – He Process
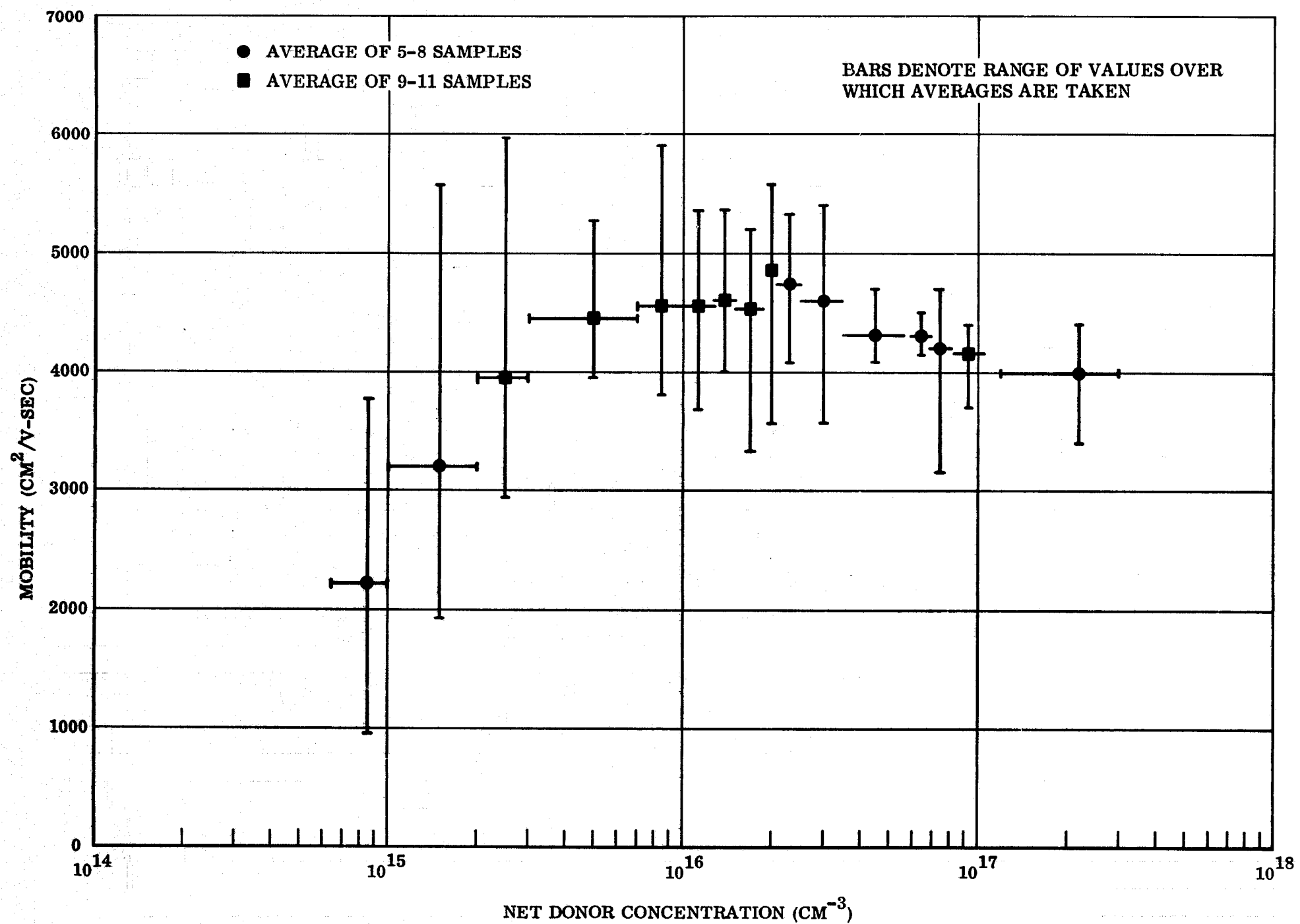
Figure 6. Mobility vs Carrier Concentration for GaAs/Aℓ_2O$_3$, Undoped Samples

The dominant impurity (or impurities) evident in thick undoped films grown by either the H_2 or the He process is a donor; since there is little change in the carrier concentration at 77 K from that at 300 K, it is apparent that the energy associated with this impurity is very small, the level probably being less than 0.005 ev from the conduction band. Measurements of the carrier concentration as a function of temperature over the temperature range from 63 to 300 K verify this conclusion and are shown in Figure 7. The carrier concentration is seen to decrease by less than 30 percent in this temperature range, indicating that the donor is still nearly completely ionized at 63 K. This sample was grown by the He process and is of reasonably good quality, as evidenced by a room temperature mobility of 5400 cm^2/V-sec and 77 K mobility of 12,500 cm^2/V-sec.

The only donor impurities having unambiguously established levels this shallow in GaAs are Se, Te, Si, Ge, Sn and probably S. Without knowing the exact preparation and handling techniques used in the production of the various quantities of TMG and AsH_3 used in this work, it is not possible to predict which impurities would be present; however, from the spectrographic analyses available on samples of TMG, it is known that Si is present as a major impurity (100-500 ppm) and hence would be one of the most likely possibilities.

Variation of properties with film thickness. − Detailed studies of thin samples have shown that undoped GaAs films grown on Al_2O_3 by the CVD method used in this program have always appeared to be p-type for the first few microns of growth. With subsequent growth the sample becomes n-type with a net donor concentration characteristic of the growth conditions and especially of the gases used for source materials. As will be discussed in more detail below, the thickness of the p-layer appears to be a function of the donor impurities in the reactant gases. If thick films grown from a particular set of reactant gases possess carrier concentrations $\sim 10^{17} cm^{-3}$, the p-layer may be less than 1 μm thick; however, p-layers as thick as 6-7 μm may be found if the donor impurities in the reactant gases are much lower, i.e., if thick films grown from the reactant gases have donor densities $\sim 10^{15} cm^{-3}$.

Once the film has converted to n-type the carrier concentration rises rapidly to the thick-film value. The mobility tends to continue to improve as the film becomes thicker, usually "saturating" by the time the film has grown to $\sim$15-20 μm. The electrical properties of a series of films grown at constant growth conditions with different thicknesses are shown in Table XII.

Since the values in Table XII are necessarily averages over the whole film, it appeared desirable to undertake profile measurements from which properties of the outer layers of a film could be deduced. Accordingly, a number of Hall bridge samples were reduced stepwise in thickness by polishing and etching techniques. Electrical measurements were carried out after the removal of each successive layer.

The results of measurements on one of these samples are shown in Figure 8. The mobilities and carrier concentrations are those measured after removal of the upper layer of the film, and are plotted versus the thickness of the remaining film. From these data were deduced the mobility of the removed layer, which is illustrated by the dashed curve in Figure 8. It can be seen that the outermost layers of the film possess significantly higher mobilities than are suggested by measurements of the whole film.

27
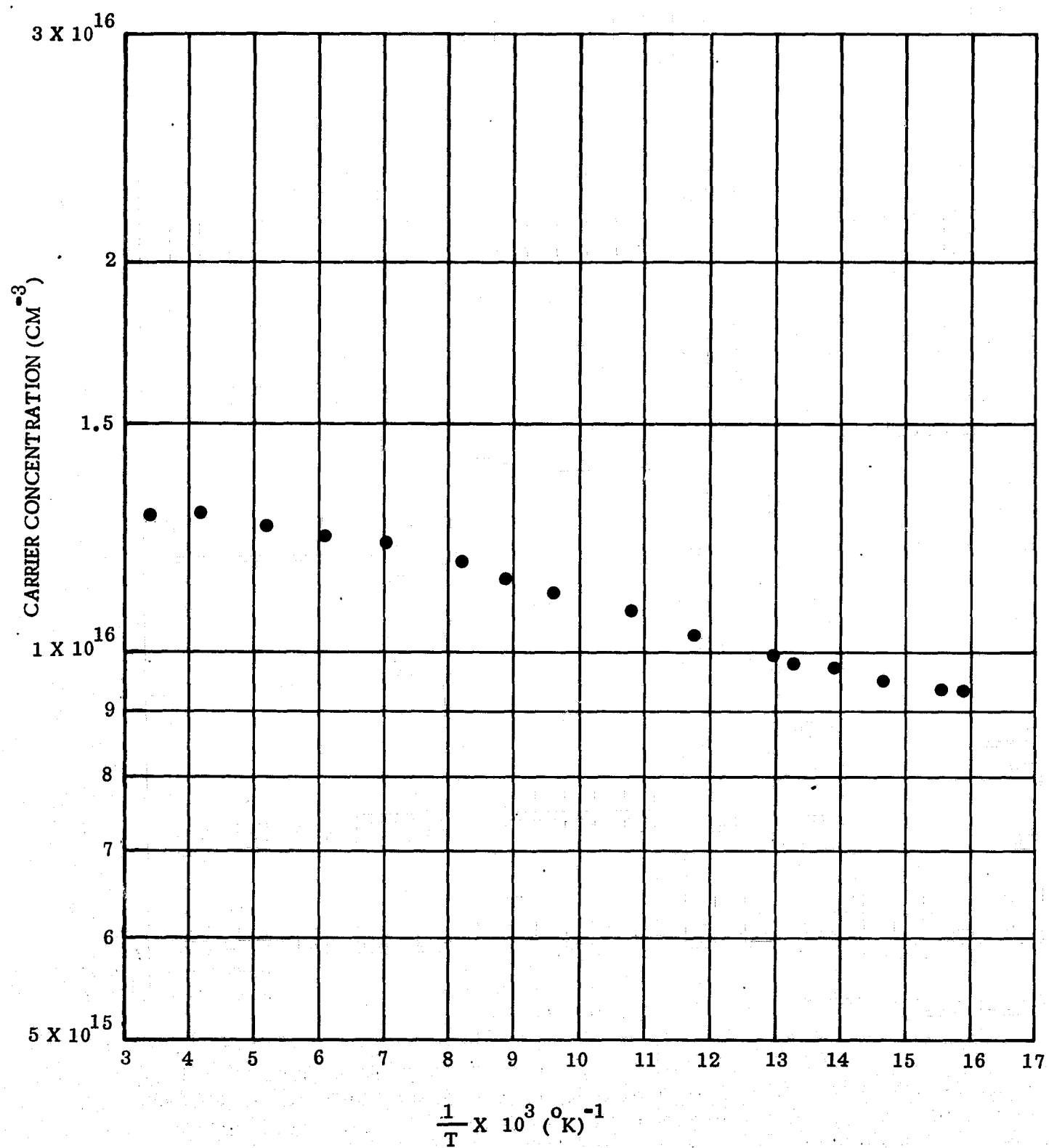
Figure 7. Variation of Carrier Concentration with Reciprocal Temperature
for an Undoped GaAs/Aℓ$_2$O$_3$ Film

TABLE XII

ELECTRICAL PROPERTIES OF EPITAXIAL (111)GaAs/(0001) Al_2O_3
AS A FUNCTION OF LAYER THICKNESS FOR A GIVEN
AsH_3-TMG RATIO (250-35-0)* at 675 C

Thickness (μm)	Resistivity (ohm-cm)	Carrier Concentration (cm^{-3})	Electron Mobility (cm^2/V-sec)
0.9	$\geq 10^4$	* *	(p-type)
2.9	4.3×10^3	* *	(n-type)
4.5	0.46	$\sim 8.0 \times 10^{15}$	1690
7.3	0.26	8.1×10^{15}	2950
8.6	0.14	1.2×10^{16}	3610
19.6	0.13	1.3×10^{16}	3630
24.4	0.11	1.3×10^{16}	4400

*See text p. 10 for significance of numbers.
** Not measurable

The capacitance-voltage characteristics of reverse-biased Schottky-barrier diodes formed on GaAs films have also been used to deduce the variation in carrier concentration with film thickness. Shown in Figure 9 are the results obtained with a lightly doped ($\sim 2 \times 10^{15}$cm^{-3}) ~ 26μm-thick GaAs/Al_2O_3 film which has been reduced in thickness in 3-5 μm steps, with diodes applied and measured after each step. The carrier concentration data for the first three steps change very little and are shown averaged in Figure 9. The vertical error bars indicate the estimated error due to diode area determination, and the horizontal error bars represent the range in depth for the individual data points over which the data has been averaged. The data after the third polish are plotted without averaging, because of the more rapid change in carrier concentration with depth.

Figure 8. Mobility and Carrier Concentration vs Depth for 19.3 μm-thick GaAs/Aℓ_2O$_3$, Undoped Sample

Figure 9. Carrier Concentration vs Depth Profile for 26.2 μm-
thick GaAs/Aℓ₂O₃ Undoped Sample
(from Capacitance-Voltage Measurements)

Properties of GaAs near the Al_2O_3 interface. - Considerable effort has been devoted to understanding the p-layer which appears to be present in all undoped films at the GaAs-Al_2O_3 interface. A large number of thick samples were beveled and stained by standard metallographic techniques to correlate the thickness of the p-layer with film properties and/or growth conditions. It was found that the thickness of the p-layer in a thick film depends most strongly on the net donor concentration in that film, and hence on the net donor impurity concentration in the reactant gases. The p-layer thickness (t), for films grown by the pre-AsH_3 technique, is shown plotted versus donor concentration (n) in Figure 10.

The behavior illustrated in this figure may be explained as follows: If it is assumed that the donor concentration in the film does not change with film thickness, and that there exists an acceptor concentration which decreases with distance from the substrate, then the thickness of the p-layer is determined by the distance at which the two exactly balance. For reactant gases which are low in donor impurities the balance condition therefore occurs farther from the interface than for gases high in donor impurity content. The plot of net donor concentration may then be interpreted as equivalent to a plot of acceptor concentration versus distance from the interface.

It can be seen from the figure, by extrapolation to zero thickness, that there is an apparent acceptor concentration at the interface of $\sim 10^{18}$ cm^{-3}. A plot of ln n versus ln t for the dashed curve in Figure 10 shows that n (and hence acceptor concentration) varies with distance from the interface as $1/t^2$. The dashed curve in Figure 10 is in fact a plot of $n = a/(t+b)^2$, where a and b are constants (equal to 4×10^8 cm^{-1} and 0.15×10^{-4} cm, respectively, when t has units of cm). However, the mechanism that would account for this type of variation of acceptor concentration with distance from the interface is not yet understood. Such a variation tends to rule out impurity diffusion via autodoping from the Al_2O_3 or from impurities present on the substrate surface at the initiation of growth.

The diffusion of impurities is also ruled out by observations of the p-layer thickness as a function of film thickness for films grown under identical growth conditions and gases. The properties of several films of different thicknesses are shown in Table XIII. The data indicate that the thickness of the p-layer apparently does not change during additional film growth at 675 C.

Contrary to what might be expected from the above discussion and from the data in Figure 10, the carrier concentrations measured in thin ($\sim 1\,\mu$m thick) undoped GaAs films are typically not on the order of 10^{16}-10^{17} cm^{-3}. The measured values are generally $\leq 10^{13}$ cm^{-3} with resistivities $\sim 10^4$ ohm-cm or greater. In order to explain this observation it must be assumed that there is self-compensation occurring in these thin samples, which implies the existence of at least one deep acceptor level.

With regard to the origin of the acceptor states near the GaAs/Al_2O_3 interface, a number of possibilities exist. These could include (1) defects, generated as a result of lattice mismatch, thermal contraction differences upon cooling from the growth temperature, and/or irregularities in the Al_2O_3 surface topology, and (2) acceptor impurities, either outdiffusing from the Al_2O_3 or present on the substrate
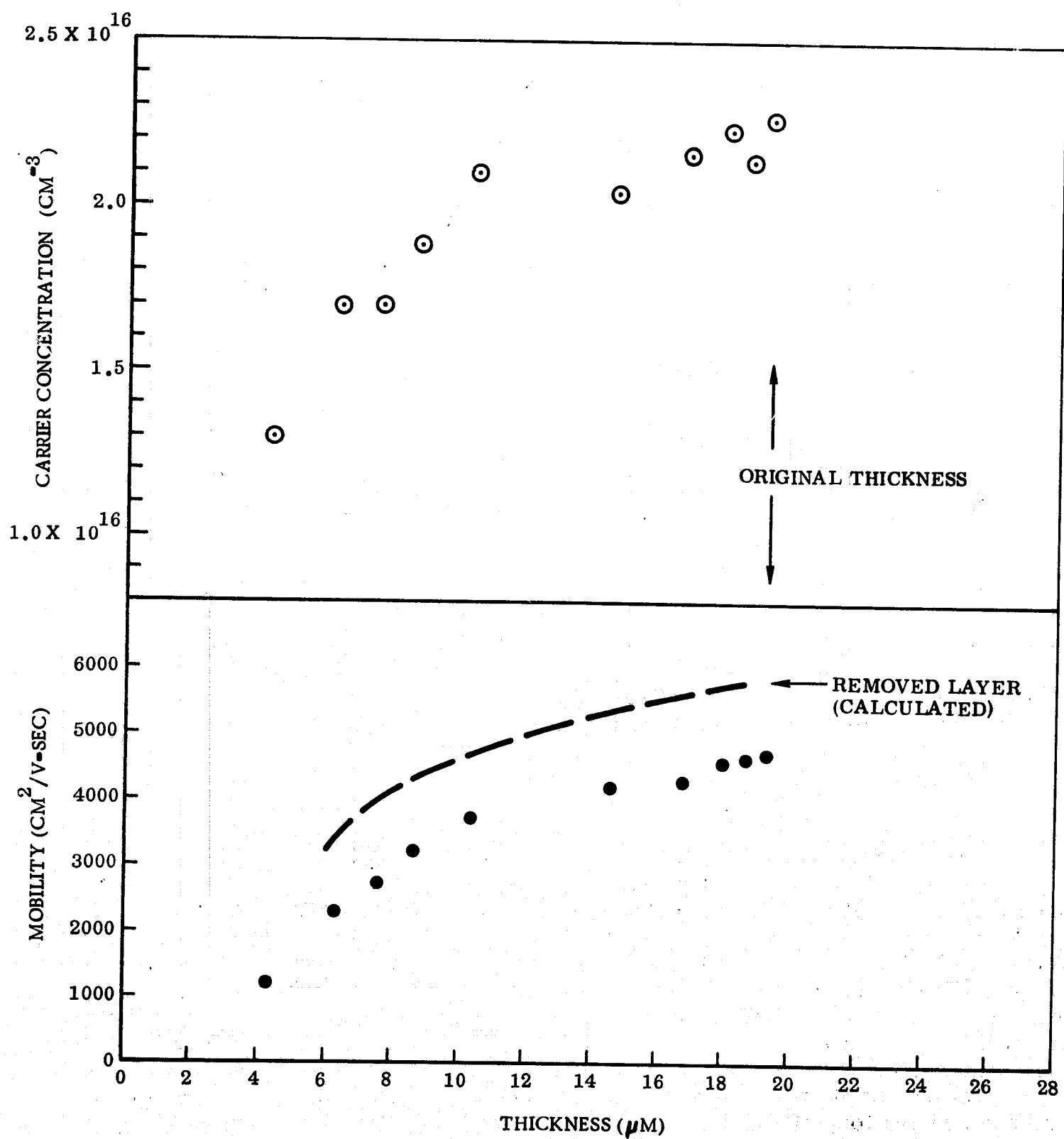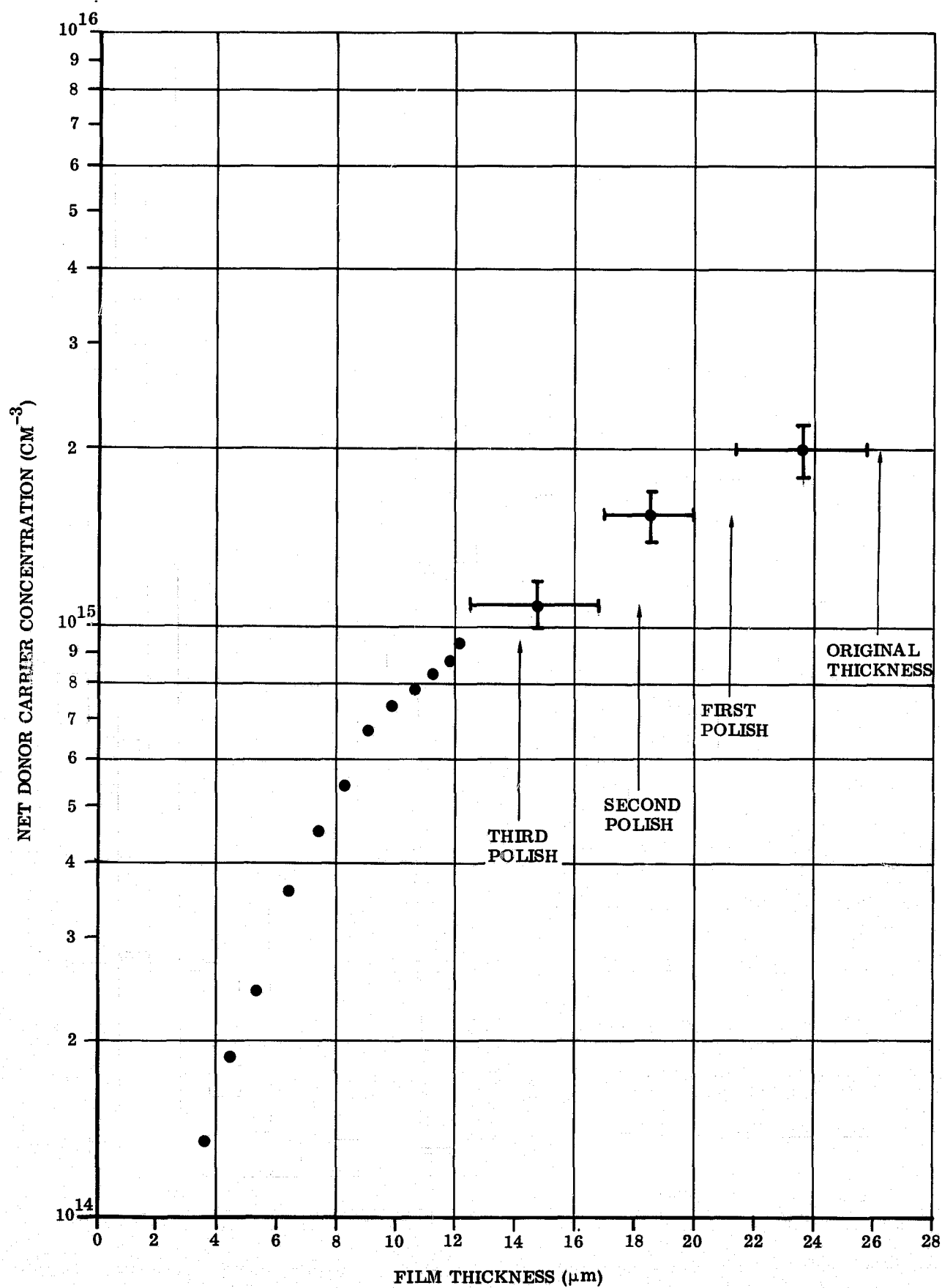
Figure 10. Carrier Concentration vs P-layer Thickness
for Undoped GaAs/Aℓ_2O$_3$ Films

33

TABLE XIII

ELECTRICAL PROPERTIES AND INTERFACE P-LAYER THICKNESS FOR SERIES
OF EPITAXIAL GaAs/(0001) Al_2O_3 FILMS GROWN AT
FLOWMETER SETTING OF 145-45* AT 675 C

Film Thickness (μm)	Resistivity (ohm-cm)	Carrier Concentration (cm^{-3})	Mobility (cm^2/V-sec)	P-Layer Thickness (μm)
1.4	10^4	p-type	--	1.4
5.0	11	5.5×10^{15}	105	2.9
8.4	0.33	1.2×10^{16}	1700	3.1
18.0	0.13	1.2×10^{16}	4000	2.9

*See text, p. 10, for significance of numbers

surface at the initiation of growth. The existence of defects is quite likely. The lattice mismatch for the (111) orientation of GaAs on (0001) Al_2O_3, based on room temperature lattice constants, amounts to approximately 17 percent. The stresses due to thermal contraction differences may be estimated from $\sigma \approx E(\alpha_s - \alpha_f) \Delta T$, where E is Young's modulus, $\sim 10^{12}$ dynes/cm^2 for GaAs, α_s and α_f are the coefficients of thermal expansion of the substrate and film, respectively, and ΔT is the temperature change. From measurements of the thermal expansion coefficients of GaAs (Ref 7) and Al_2O_3 (Ref 8) one can estimate the difference between thermal expansion coefficients to be $\sim 10^{-6}$/°C, yielding a stress $\sim 7 \times 10^8$ dynes/cm^2 in a film cooled from the growth temperature to room temperature. Although no data for the yield stress in GaAs appear to be available, the yield stress has been estimated (Ref 9) to be not more than 10^8 dynes/cm^2 at 800 C. Thus, one might expect that this yield stress will be exceeded in cooling a GaAs/Al_2O_3 film after growth at 700 C, with a consequent generation of defects near the interface as some of the stress is relieved.

Although it is difficult to estimate the effect of Al_2O_3 surface topology on the GaAs films, the influence of gross scratches on the electrical properties of the film can be quite pronounced. It has been observed that substrate scratches lead to regions of non-uniform growth which can result in high resistance barriers in thick n-type GaAs films on Al_2O_3.

Impurities cannot be completely ruled out as a source of acceptors in GaAs even though many of the results discussed above do not support this possibility, and the growth temperatures used do not encourage the diffusion of most impurities. Copper must be particularly suspect, since it can easily diffuse at growth temperatures in the neighborhood of 700 C and has been shown to be related to the p-type interface region sometimes observed in GaAs homoepitaxial growth (Ref 10). It is also possible that a high defect density in the GaAs at the Al_2O_3 interface would allow diffusion of impurities which normally would not diffuse in bulk GaAs at these temperatures.

34

During the later phase of the contract, attempts were made to produce thin
n-type layers by means of Se doping of films normally having a 5 μm-thick p-type
interface layer. Preliminary experiments showed it very difficult to achieve n-type
carrier concentrations below ~10^{17} cm^{-3} in ~1 μm-thick layers. Table XIV
tabulates the electrical properties of a number of thin Se-doped films. The data
indicate very low electron mobilities, probably the result of the defect scattering
and high degree of compensation in these thin layers. The inability to achieve low
n-type doping levels also suggests a self-compensating mechanism in these films,
as mentioned previously.

Early-stage growth characteristics. – The quality of an epitaxial film is strongly
dependent upon the growth process; therefore, investigation of the early stages of
growth under different growth parameters has been regarded as valuable for optimizing
the overall growth process. In situ recording of nucleation phenomena is not readily
achievable in chemical vapor deposition equipment; however, the technique of
"freezing" the growth at various stages and applying replica electron microscopy
and reflection electron diffraction (RED) to examine the results supplies some of
the same kind of information. The photomicrographs and RED patterns included
here indicate some of the nature of the heteroepitaxial growth process for (111)
GaAs on (0001) Aℓ_2O$_3$ (and probably on other insulating substrates which result in
(111) GaAs growth).

TABLE XIV

ELECTRICAL PROPERTIES OF Se-DOPED EPITAXIAL (111) GaAs/(0001) Aℓ_2O$_3$
FILMS

Growth Conditions* (AsH$_3$–TMG–H$_2$Se)	Pre-mix Time** (minutes)	Thickness (μm)	Resistivity (ohm-cm)	Carrier Concentration (cm^{-3})	Electron Mobility (cm^2/V-sec)
200–45–4	2	0.75	--	--	p-type
200–45–4	5	0.81	0.45	1.5×10^{17}	89
200–45–6	2	0.81	~12	Not measurable	Not measurable
200–45–6	5	0.76	0.25	5.4×10^{17}	46
200–45–8	2	0.80	~1	6.5×10^{17}	~10
200–45–16	5	0.71	0.023	1.7×10^{18}	160
200–45–40	5	3.5	0.0034	3.7×10^{18}	560

*See text, p. 10, for significance of numbers
**H$_2$Se flow time through reactor prior to admitting AsH$_3$–TMG mixture

The growth conditions used for many of these studies were dictated by observations previously made for thick films ($>20\,\mu$m) of GaAs grown on (0001) Al_2O_3, i.e., the highest mobilities which had been previously obtained ($>5000\ cm^2/$V-sec) were for films grown at about 675 C when the growth rate approached 0.8–1 μm per minute. Although the growth rate of the films for a given TMG concentration and given flow conditions did not change appreciably between 600–800 C, RED patterns of thick films (grown for approximately 30 min) supported the observation that film growth was better at 675 C than, for example, at 800 C, as evidenced by the strong Kikuchi lines and untwinned pattern shown in Figure 11. The effect of temperature on films grown for 10 seconds was also examined; films grown at 675 C, 700 C and 725 C were compared. The (110) RED patterns obtained from these growths are shown in Figure 12. They also suggest that better growth is obtained at 675 C than at 700 C or 725 C for the particular AsH_3:TMG ratio used.

In another experiment, GaAs/(0001)Al_2O_3 film formation was interrupted at different stages of development to study the growth process. Figures 13 and 14 show replicas of the films produced at 675 C by exposure to TMG-AsH_3 mixtures with AsH_3-TMG-dopant flowmeter settings of 250–45–0, respectively, for 1, 3, 5, 7, 10, 20, and 30 sec. At 1 sec (Figure 13), the Al_2O_3 surface seems to be almost covered by a host of individual medium-sized nuclei (about 0.15 μm across), many of which have sides that appear to be oriented in the same direction. The film surface is comparatively rough at this stage (average thickness of nucleus ~ 350A.) At 3 sec, the surface seems to have become quite smooth, but "islands" are evident, presumably openings of bare Al_2O_3. These openings appear to have filled in at the end of 5 sec, the surface remaining relatively smooth, but at 7 sec the surface has again become slightly roughened. The surface still appeared rough on a film grown for 10 sec (0.15μm thick) (Figure 14a), smoother after 20 sec of growth (0.3 μm thick) (Figure 14b), and finally appeared quite smooth after a film of GaAs was grown for 30 sec (0.45 μm thick) (Figure 14c).

The variation in the crystal quality of many of these thin films with changes in thickness and deposition parameters was also followed by RED (110) patterns. An examination of Figures 14 (a–c) indicates that films formed during the first 10 sec of growth (<2000A) possess varying degrees of twin structure; at 3000A (20 sec of growth), however, the pattern no longer displays the extra spots associated with twin structure.

Since twinning was apparent in GaAs films at a thickness of about 1500A or less, deposition conditions were sought which would provide 1500A films free from twinning.

The effects of different growth rates were examined at 675 C by increasing the TMG in several steps and attempting to reproduce film thicknesses of ~1500A. The RED results are shown in Figure 15. Figure 15b shows a lower "twin spot" density than Figure 15a, but the difference may be due to the sample in Figure 15b being thicker. Comparative structures were also obtained at settings of 200–70–0 for different film thicknesses. Figure 16 shows the RED patterns obtained for 5 sec, 10 sec, and 15 sec of growth. The twin spots seem to have disappeared in the RED pattern for the ~3150A film, as had been previously noted for films of this thickness.
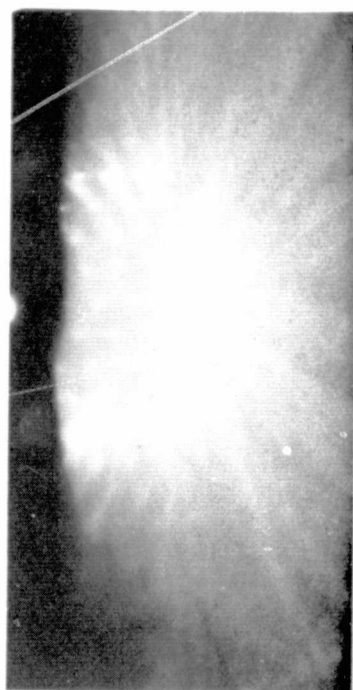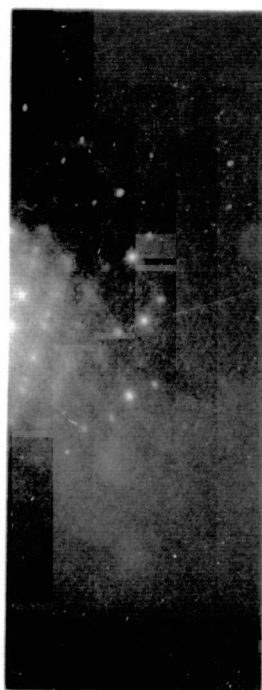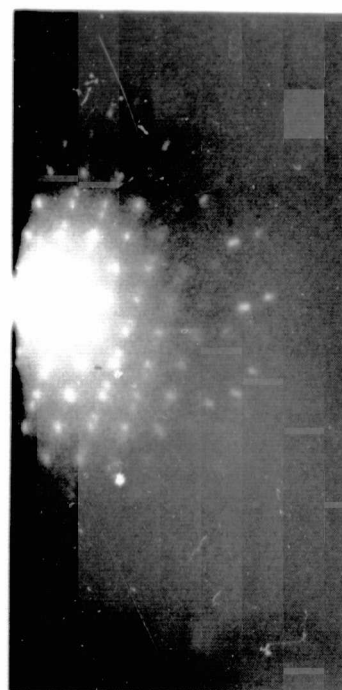
(a)   (b)   (c)

Figure 11. (110) RED Photographs of (111) Ga/As (0001) Al_2O$_3$
Films Grown for approximately 30 min at (a) 675 C, (b) 800 C, (c) 825 C
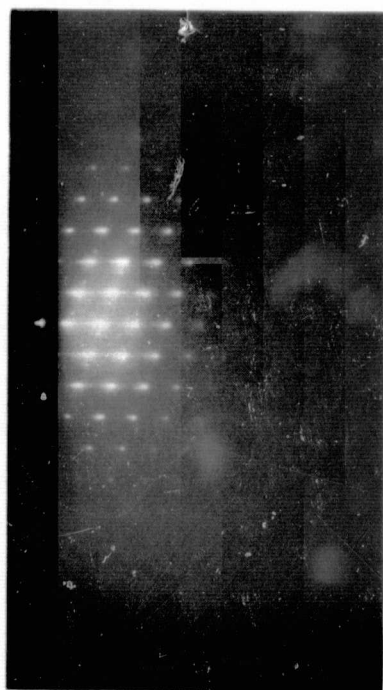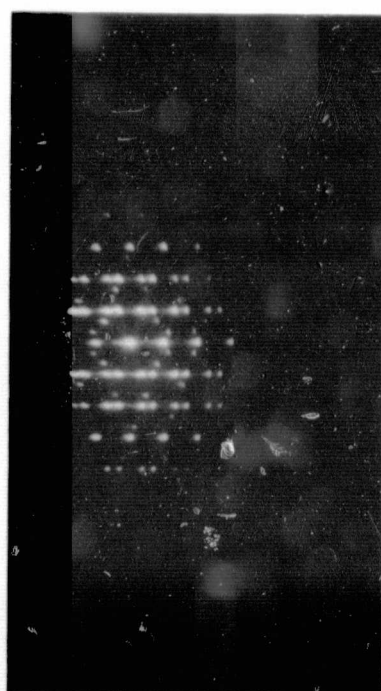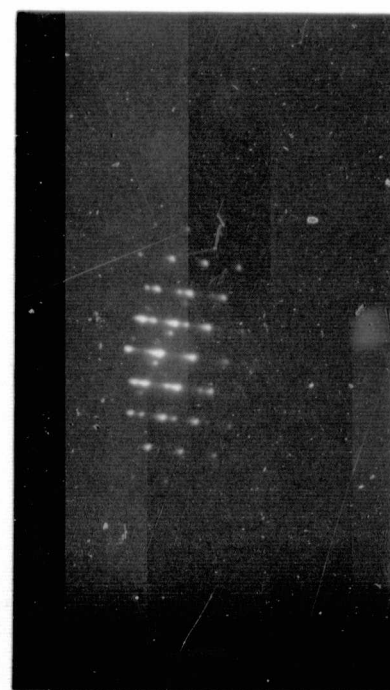
(a)   (b)   (c)

Figure 12. (110) RED Patterns for (111) GaAs/(0001) Al_2O$_3$ Films Grown
for 10 Sec at Reactant Gas Flow Meter Setting of 200-45-0 at
(a) 675 C, (b) 700 C, (c) 725 C
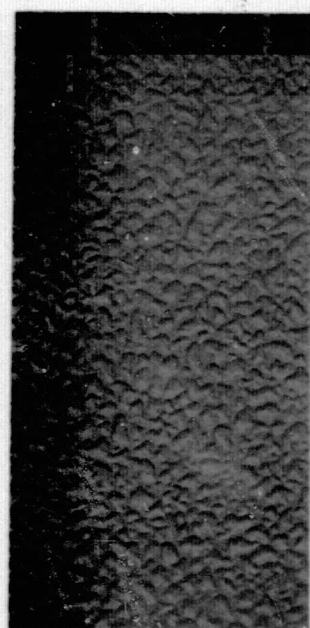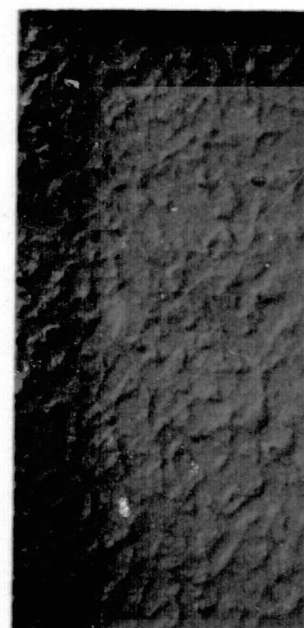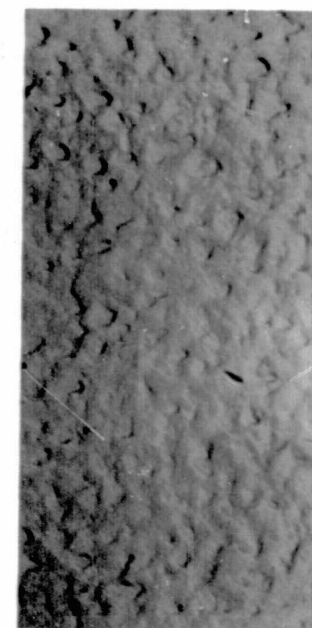
(a) (b) (c) (d)

Figure 13. Replicas for (111) GaAs/(0001) Al_2O$_3$ Films Grown at Setting of 250-45-0 at 675 C for
(a) 1 Sec, (b) 3 Sec, (c) 5 Sec, (d) 7 Sec   (All Replicas at 20,000X)
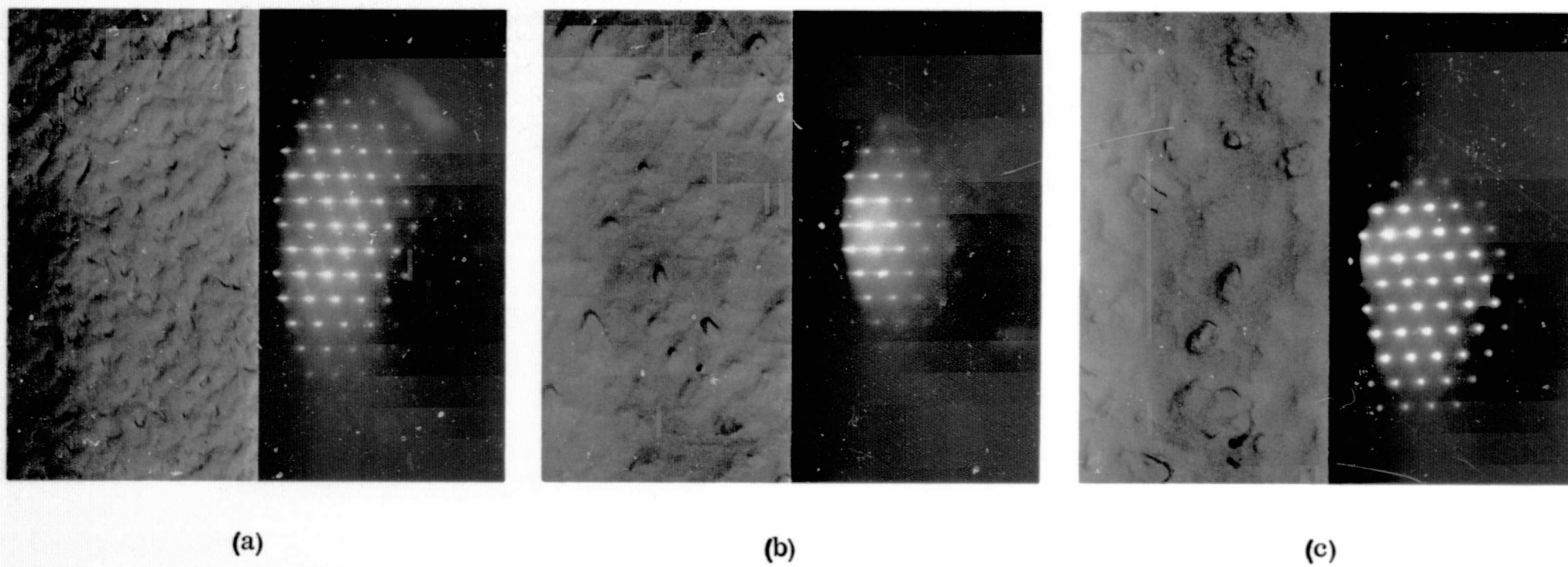
Figure 14. Replicas and (110) RED Patterns for (111) GaAs/(0001) Al_2O_3 Films Grown at 675 C at Setting of 200-45-0 for (a) 10 Sec, (b) 20 Sec, (c) 30 Sec (All Replicas at 20,000X)
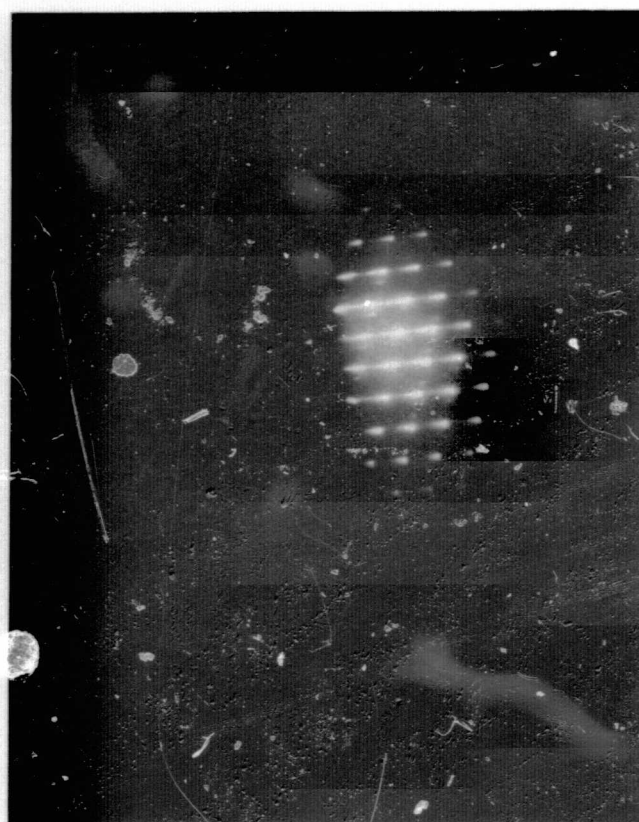
(a)
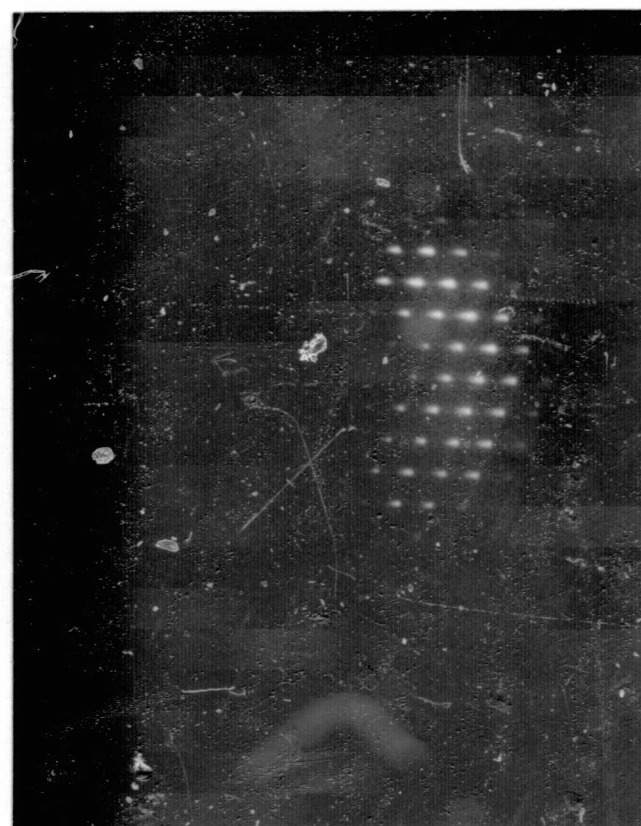
(b)

Figure 15. (110) RED Patterns for (111) GaAs/(0001) Aℓ_2O$_3$ Films Grown at 675 C for about 10 Sec at Reactant Gas Flowmeter Settings of (a) 200-60-0 (~1600Å) and (b) 200-70-0 (~2550Å)
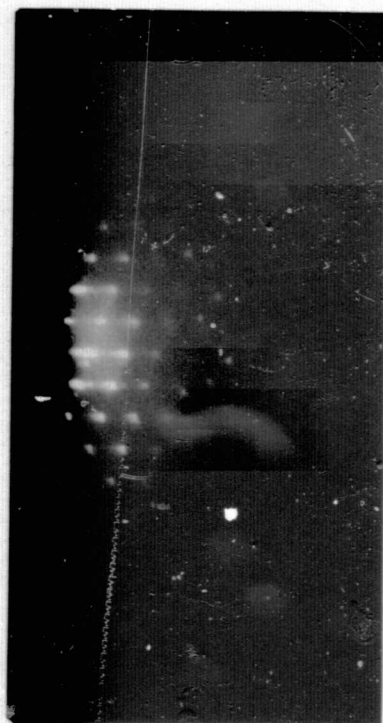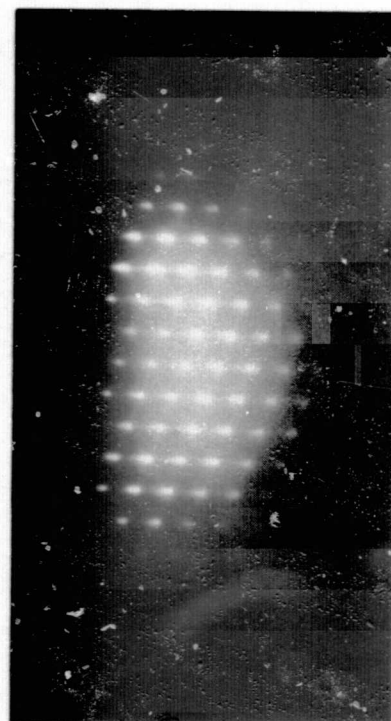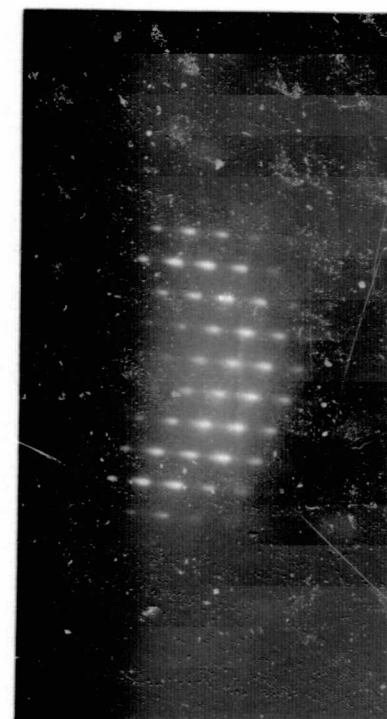
(a)   (b)   (c)

Figure 16. (110) RED Patterns for (111) GaAs/(0001) $A\ell_2O_3$ Films Grown at 675 C at Reactant Gas Flowmeter Setting of 200-70-0 for (a) 5 Sec (~1375 Å), (b) 10 Sec (~2550 Å), (c) 15 Sec (~3150 Å)

Replica electron microscopy and RED were also used for recording the effect of annealing on these very thin films. As shown in Figure 17, annealing a 1-sec film growth for 1 hour at 600 C and 675 C caused the coalescence of the GaAs islands to molten-like masses, which occasionally exhibited an "epitaxial" order. Annealing of a 3-sec-growth film (Figure 18) produced larger islands of GaAs, mostly joined in a random-like fashion. Annealing of a 3-sec growth made under poor growth conditions (deficient in AsH_3) yielded a structure which produced a RED pattern with multiple diffraction spots (Figure 19), indicative of the poor film quality.

RED patterns also showed the effect of using different AsH3-TMG ratios and post-annealing steps on the quality of growth formed after 1 sec at a TMG flowmeter setting of 45. In Figure 20 considerable differences can be observed in the patterns for AsH_3 flowmeter settings of 50 (a high density of strong extraneous spots), 150, 200, and 250 (weak twin spots present).

Although the $A\ell_2O_3$ surface appeared to be completely covered with GaAs after 5 sec (Figure 21) and 7 sec of growth (Figure 22), annealing at 600 C and 675 C revealed the presence of "islands" of bare $A\ell_2O_3$. The formation of islands was not attributed to volatilization of material at impurities on the surface but to coalescence, since most of the replicas appear to show that, once formed, only the number of islands changes, not the total amount of exposed $A\ell_2O_3$. No islands were observed after annealing a 10-sec growth of GaAs (0.15 μm thick) up to temperatures of 725 C (Figure 23). An anneal at 800 C in AsH_3 revealed the presence of a few islands of $A\ell_2O_3$, presumably formed by additional coalescence of the GaAs film resulting from the further annealing process (Figure 24). Although some changes in film topography were observed, the RED patterns revealed twin structures at the film surface. As already shown in Figure 14 (b, c), the twin structure is not evident in the RED patterns for the 20-sec and 30-sec growths. However, some variation in surface structure is apparent. Annealing a 30-sec growth at 725 C for 1 hour (Figure 25) produced a relatively smooth film, possessing a terraced, plateau-like structure. The RED pattern appeared to be better than that of the unannealed film and closely resembled that of bulk GaAs.

Figures 26 and 27 represent the results which were obtained when very dilute TMG-AsH3 mixtures were pyrolyzed for film growth. These were produced by stabilizing the growth conditions (flowmeter settings of 240-45-0) at 675 C, turning off the TMG for 15 sec, and diverting the H_2 carrier so that only residual TMG in the line was directed into the reactor for 1 sec (Figure 26) and 6 min (Figure 27). Figure 26 shows that the growth even at extreme gas dilutions can produce a multitude of very small uniformly-arranged nuclei ($\sim$200Å across) that almost cover the entire substrate surface.

If additional growth is essentially terminated and the temperature is maintained for several minutes, these nuclei may move and coalesce into relatively large (0.2 μm across) oriented triangular islands with pyramidal structures of the type shown in Figure 27. Several of the crystallites seen in this figure have coalesced and possess exterior shapes which suggest that twinned structures have formed. The RED patterns for these films do indicate the presence of twins in the GaAs and also reveal some reflections due to the substrate material.

(a)
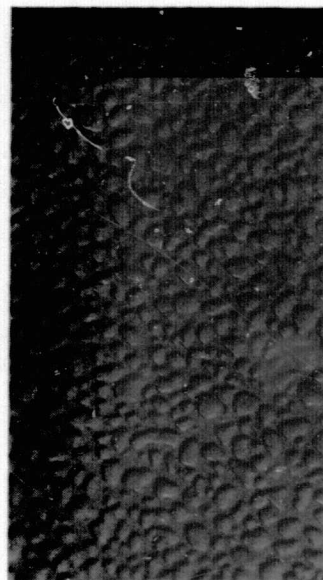
(b)
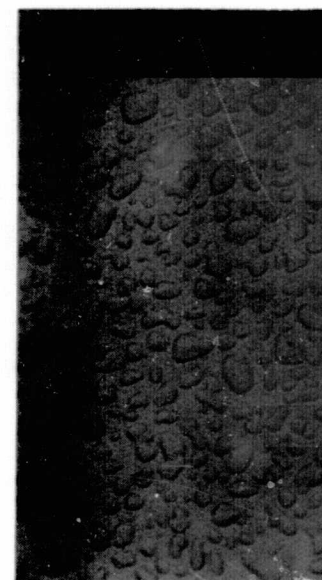
(c)

Figure 17. Replicas for (111) GaAs/(0001) Al_2O_3 Films Grown for 1 Sec at Setting of 250-45-0;
(a) as Grown, (b) after Annealing in AsH_3 for 1 Hr at 600 C, (c) after Annealing in
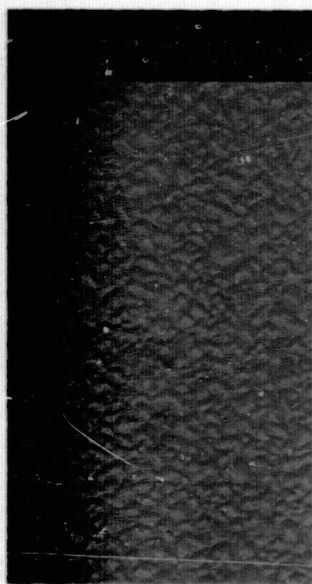AsH_3 for 1 Hr at 675 C (All Replicas at 20,000X)

44

Figure 18. Replicas and RED Patterns for a GaAs/(0001) $A\ell_2O_3$ Film Grown for 3 Seconds at Setting of 250-45-0; (a) as Grown, (b) after Annealing in AsH_3 for 1 Hr at 600 C, (c) after Annealing in AsH_3 for 1 Hr at 675 C (All Replicas at 20,000X)

Figure 19. Replicas and RED Patterns for a GaAs/(0001) $A\ell_2O_3$ Film Grown for 3 Seconds at Setting of 50-45-0; (a) as Grown, (b) after Annealing in AsH_3 for 1 Hr at 600 C, (c) after Annealing in AsH_3 for 1 Hr at 675 C (All Replicas at 20,000X)
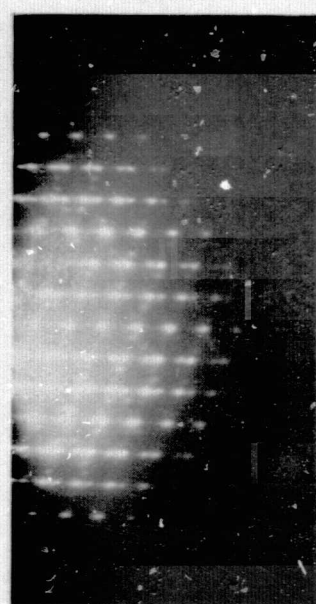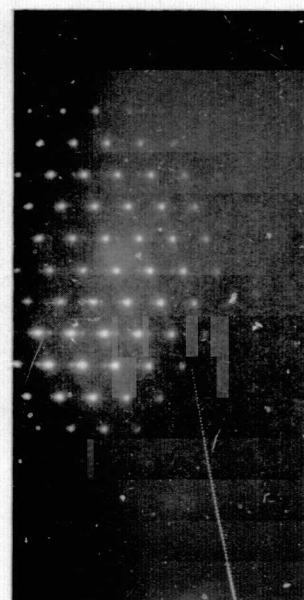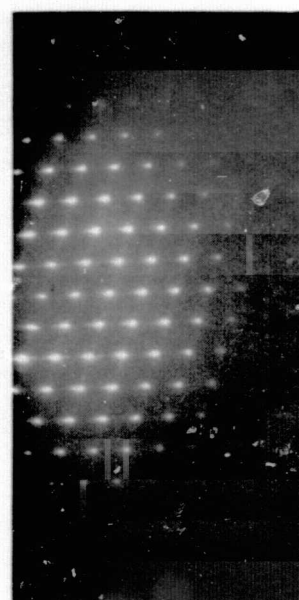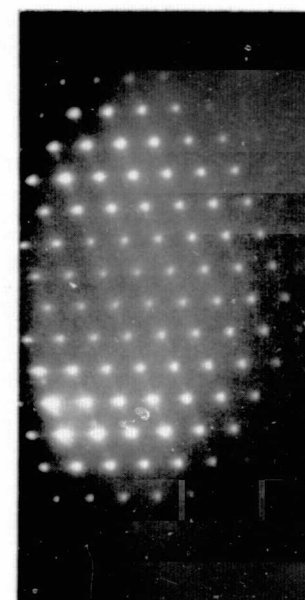
X = 50   X = 150   X = 200   X = 250

Figure 20. (110) RED Patterns for (111) GaAs/(0001) $A\ell_2O_3$ Films Grown at 675 C for 1 Sec for Different AsH_3 Settings and Annealed at 675 C for 1 Hr; (a) 50-45-0, (b) 150-45-0, (c) 200-45-0, (d) 250-45-0
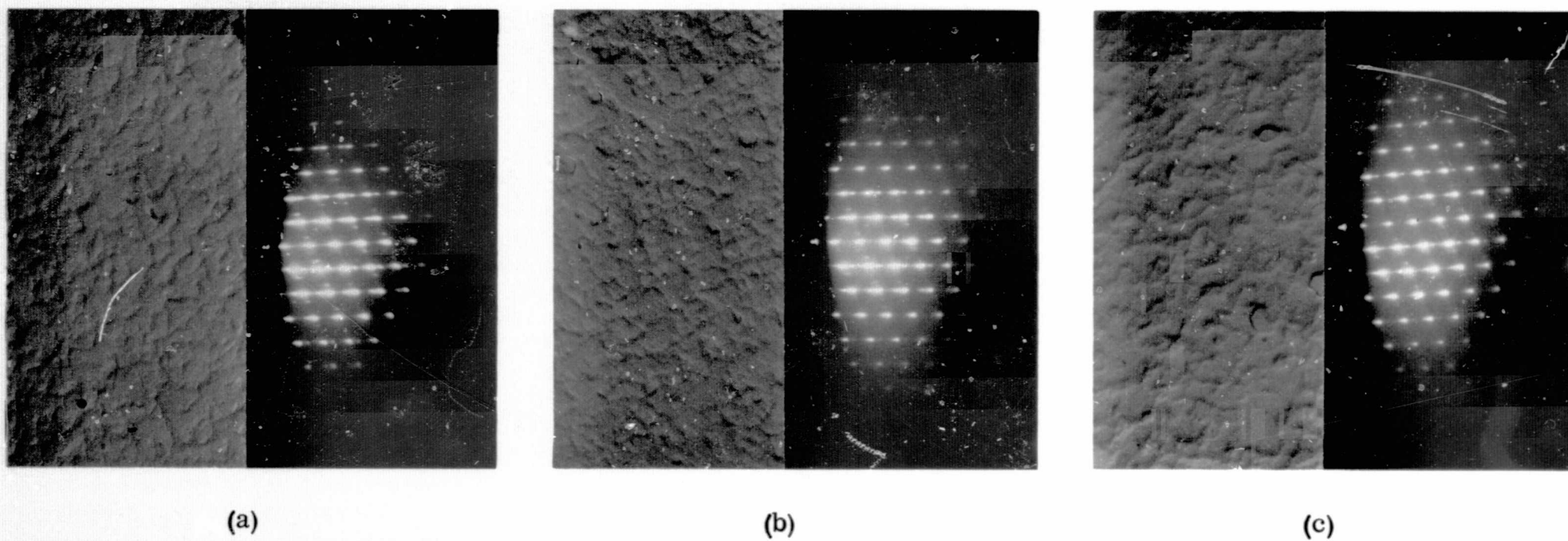
Figure 21. Replicas and (111) RED Patterns for (111) GaAs/(0001) Aℓ_2O$_3$ Films Grown for 5 Seconds at Setting of 250–45–0; (a) as Grown, (b) after Annealing in AsH$_3$ for 1 Hr at 600 C, (c) after Annealing in AsH$_3$ for 1 Hr at 675 C   (All Replicas at 20,000X)

(a)   (b)   (c)
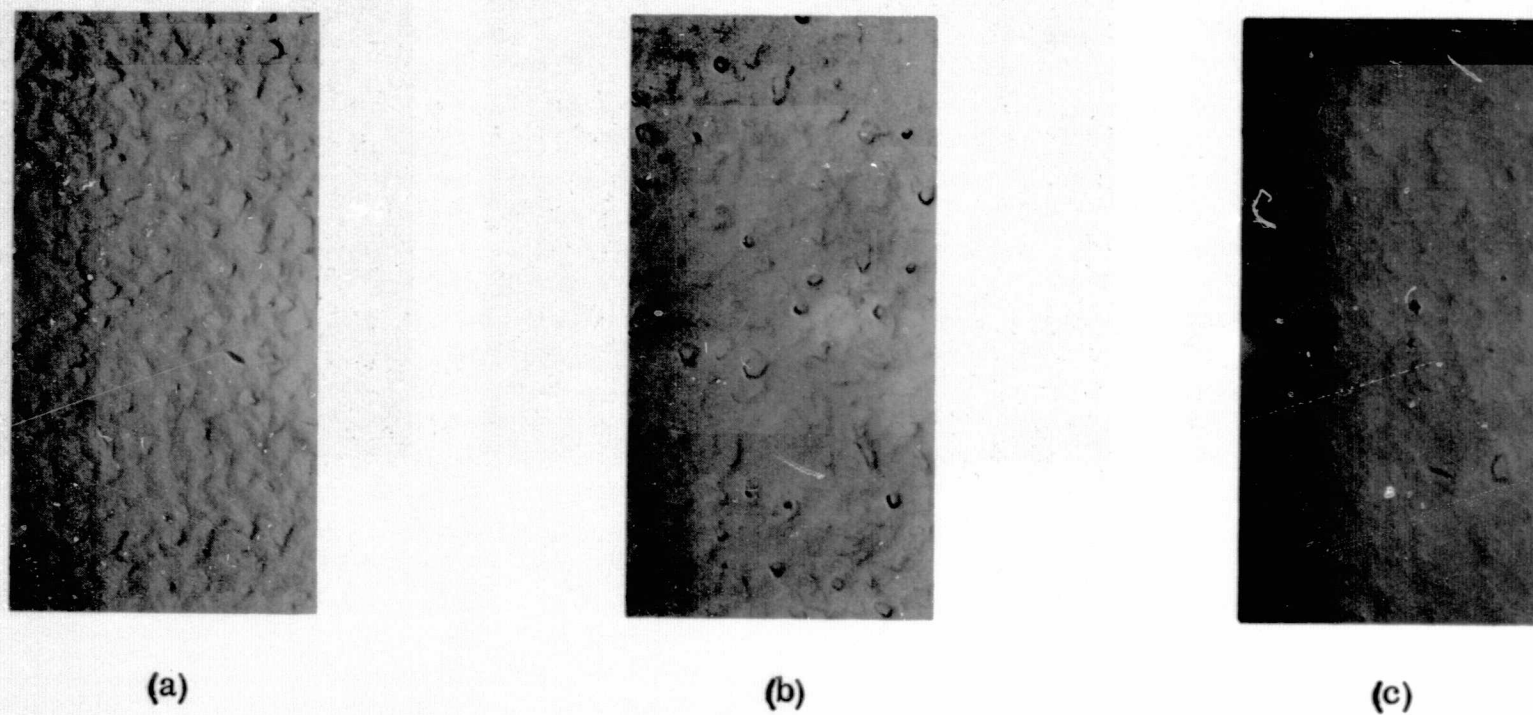
Figure 22.   Replicas for (111) GaAs/(0001) Al$_2$O$_3$ Films Grown for 7 Sec at Setting of 250-45-0; (a) as Grown,
(b) after Annealing in AsH$_3$ for 1 Hr at 600 C, (c) after Annealing in AsH$_3$ for 1 Hr at
675 C (All Replicas at 20,000X)

(a)   (b)   (c)   (d)
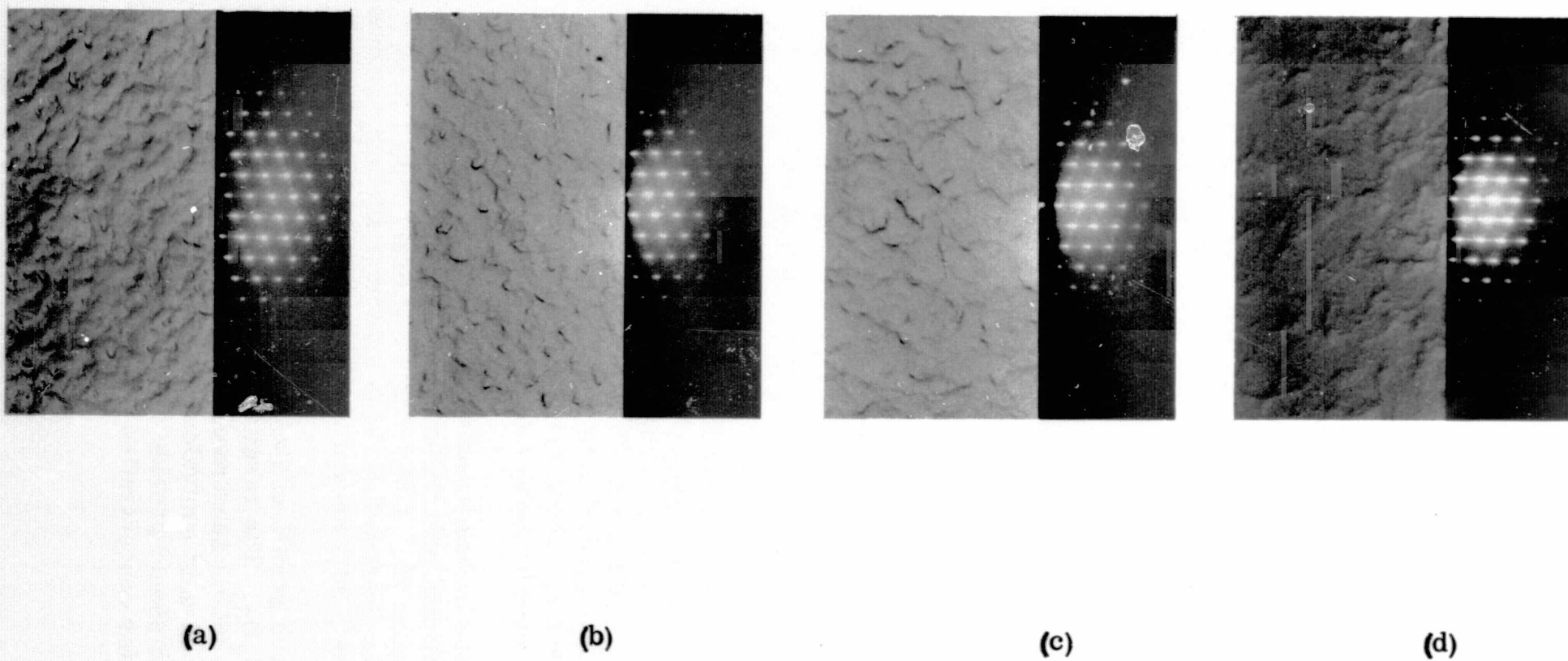
Figure 23. Replicas and (110) RED Patterns for (111) GaAs/(0001) Aℓ_2O3 Films Grown for 10 Sec at Setting of 250-45-0; (a) as Grown, (b) after Annealing in AsH$_3$ for 1 Hr at 600 C, (c) after Annealing in AsH$_3$ for 1 Hr at 675 C, (d) after Annealing in AsH$_3$ for 1 Hr at 725 C (All Replicas at 20,000)
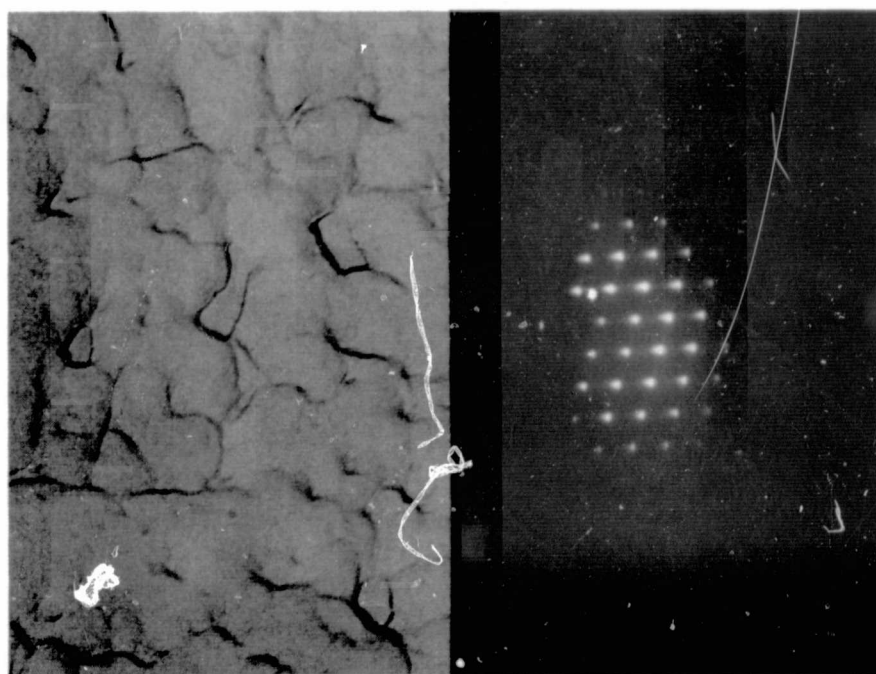
Figure 24. Replica and (110) RED Pattern for (111) GaAs/(0001) Al_2O_3 Film Grown
for 10 Sec at Reactant Gas Flowmeter Setting of 250-45-0 after Annealing
in AsH_3 for 1 Hour at 800 C

The early stages of the nucleation process were also compared on three
different orientations of Al_2O_3 which have induced growth of (111) GaAs, as deter-
mined by x-ray techniques. In Figure 28 the structures resulting from simultaneous
growth on (0001), (11$\bar{2}$3), and (10$\bar{1}$4) Al_2O_3 are shown. Based on the shape of the
GaAs islands, the degree of order is highest on the (0001) orientation and lowest on
the (10$\bar{1}$4) orientation. These results are in accord with the quality of thick films
which were evaluated by x-ray twin-density measurements.

Simultaneous nucleation-stage growth was also performed on substrates of
at least five additional orientations of Al_2O_3. Replicas of the overgrowths are
illustrated in Figure 29. A high degree of order with respect to island shape and
orientation can be observed on those substrate surfaces oriented 10 degrees and
20 degrees off the (0001) toward the (10$\bar{1}$4) plane of Al_2O_3.

Simultaneous growth of GaAs was then carried out on those two orientations
and on (0001) Al_2O_3. The resulting electrical properties are reported in Table XV.
The films on the (0001) substrate and on the one 10 degrees away from the (0001)
were found to be almost equivalent electrically; the substrate 20 degrees away from
the (0001), which should provide a (211)-oriented film of GaAs, produced an n-type
film with a carrier concentration $\sim 5 \times 10^{15}$ cm^{-3} and a low mobility.
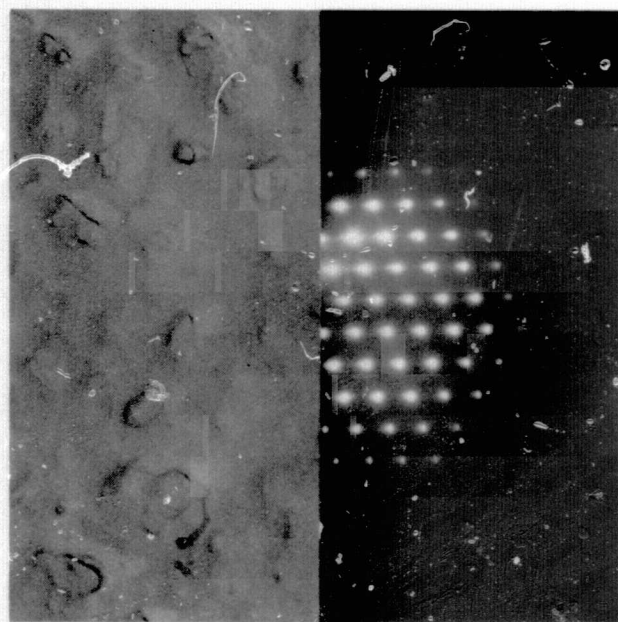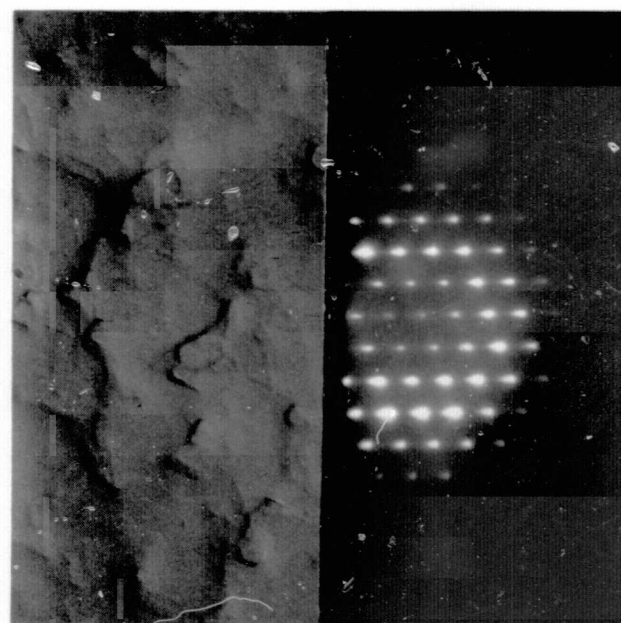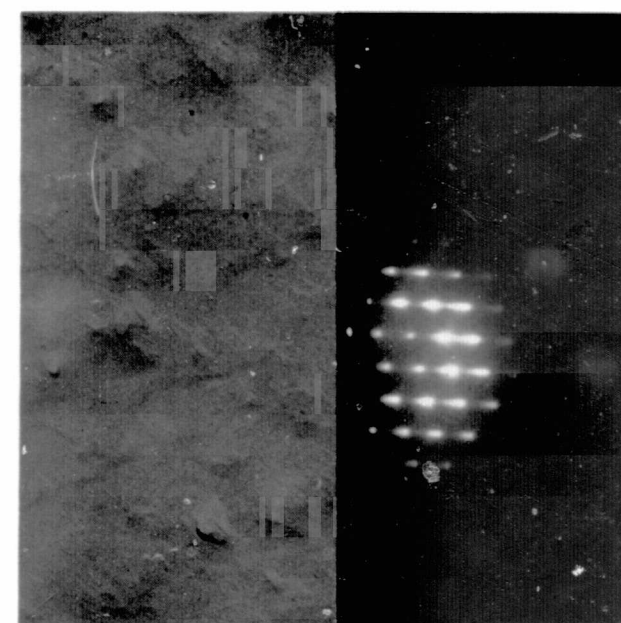
(a) (b) (c)

Figure 25. Replicas and (110) RED Patterns for (111) GaAs/(0001) Al_2O_3 Films Grown for 30 Sec at
Setting of 250-45-0; (a) as Grown, (b) after Annealing in AsH_3 for 1 Hr at 675 C,
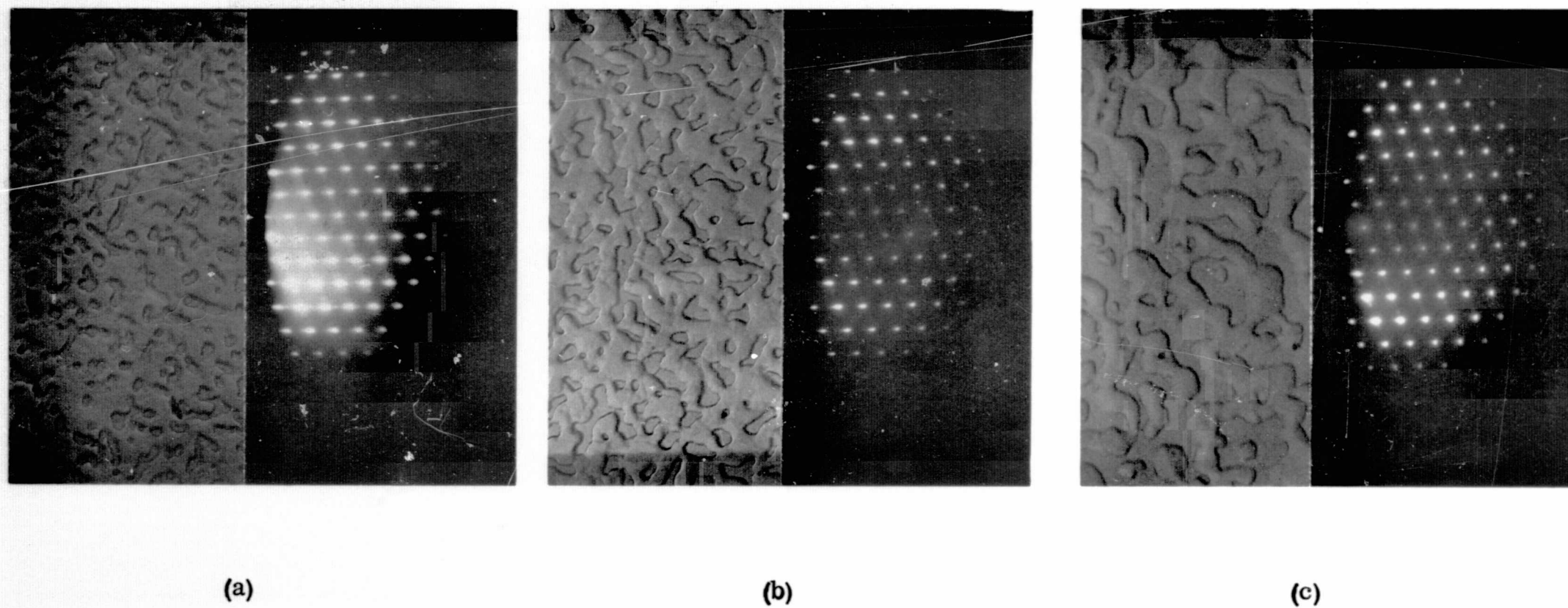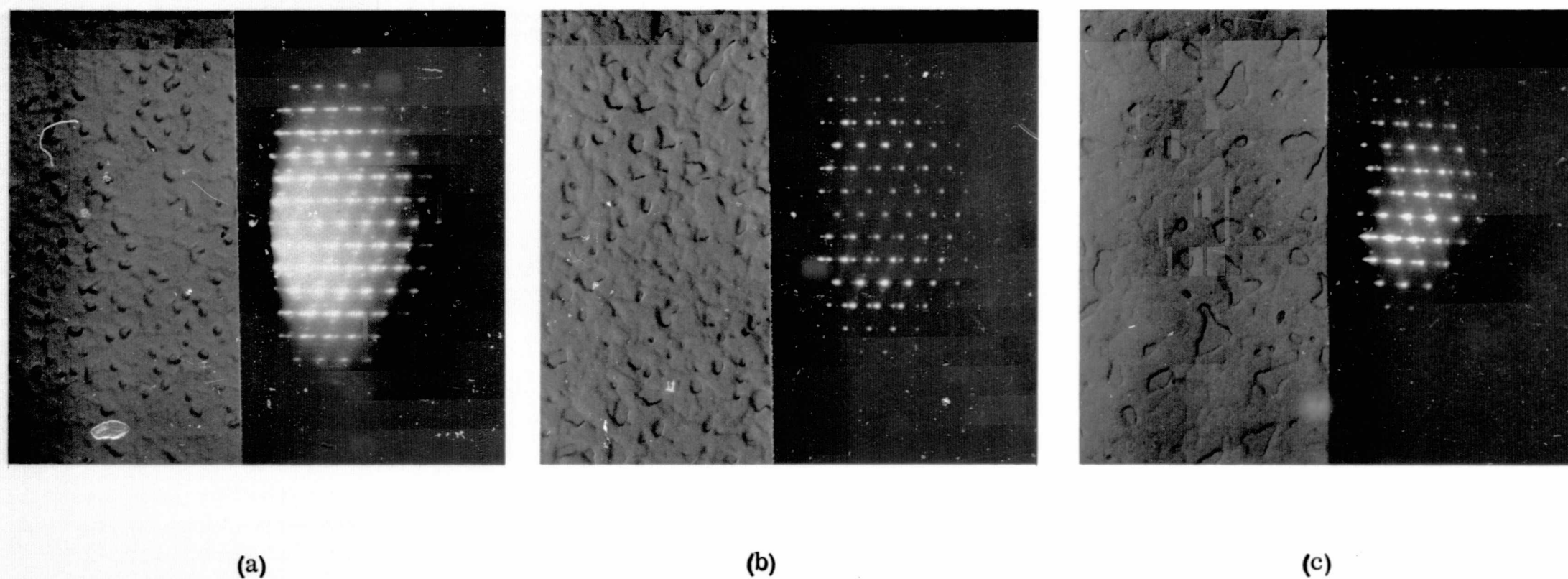(c) after Annealing in AsH_3 for 1 Hr at 725 C (All Replicas at 20,000X)
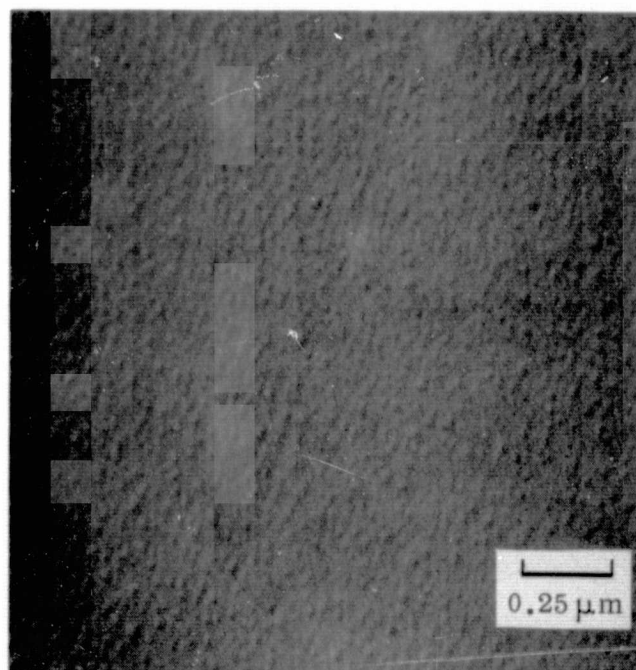
(a)
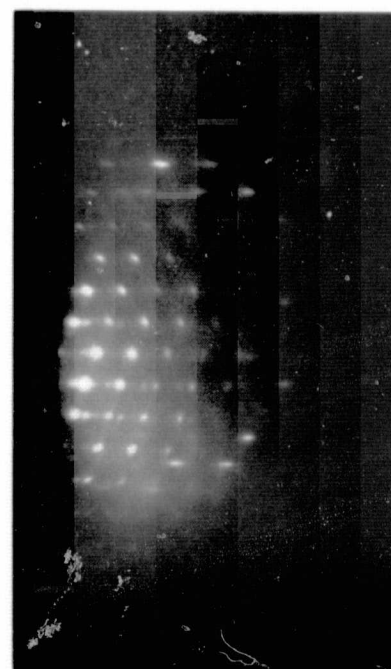
(b)

Figure 26. GaAs/(0001) Al$_2$O$_3$ Produced by Reaction of Residual TMG with AsH$_3$
for 1 Sec in an AsH$_3$-H$_2$ Atmosphere; (a) Surface Structure at Magnification
of 42,300X, (b) (110) Reflection Electron Diffraction Pattern
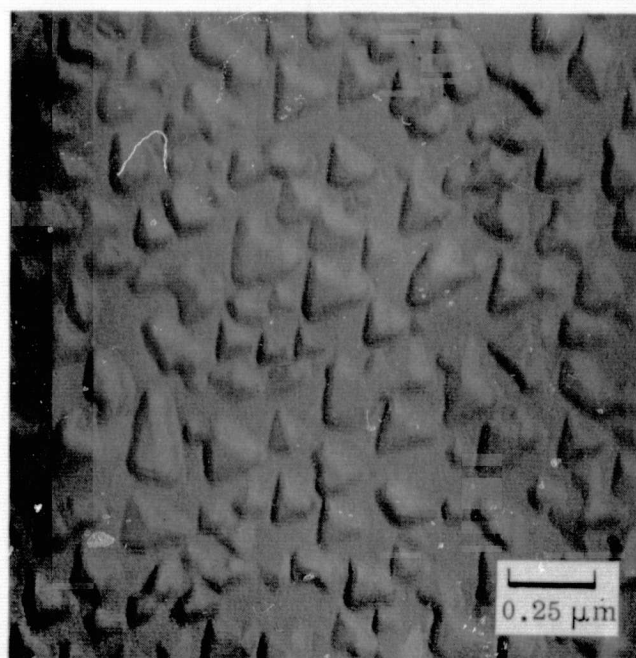
(a)
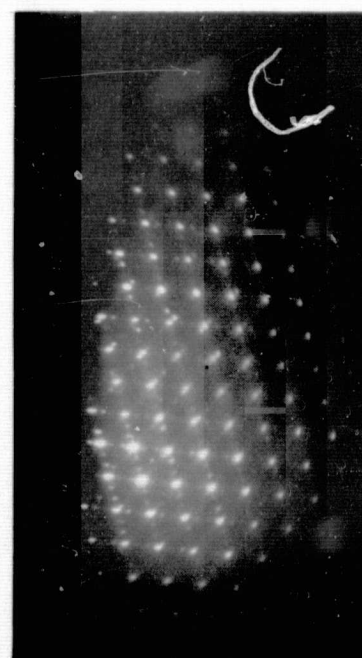
(b)

Figure 27. GaAs/(0001) Al$_2$O$_3$ Produced by Reaction of Residual TMG with AsH3
for 6 min in an AsH$_3$-H$_2$ Atmosphere; (a) Surface Structure at Magnification of
42,300X, (b) (110) Reflection Electron Diffraction Pattern

52
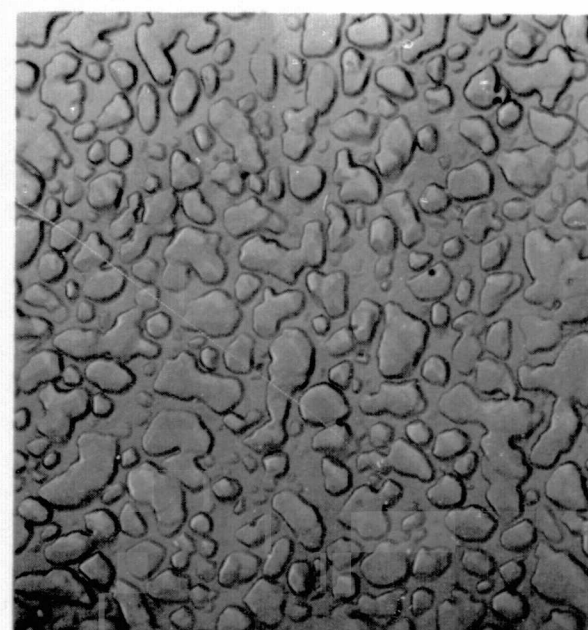
(a)   (b)   (c)

Figure 28.   (111) GaAs/Aℓ_2O$_3$ Produced by Reaction of Residual TMG with AsH$_3$ for 6 Min in AsH$_3$-H$_2$
Atmosphere; (a) (0001) Aℓ_2O$_3$, (b) (11$\bar{2}$3) Aℓ_2O$_3$, (c) (10$\bar{1}$4) Aℓ_2O$_3$ (All Replicas at 20,000X)

| 0.05 μm | 0.05 μm | 0.05 μm | 0.05 μm | 0.05 μm |
| (A) | (B) | (C) | (D) | (E) |
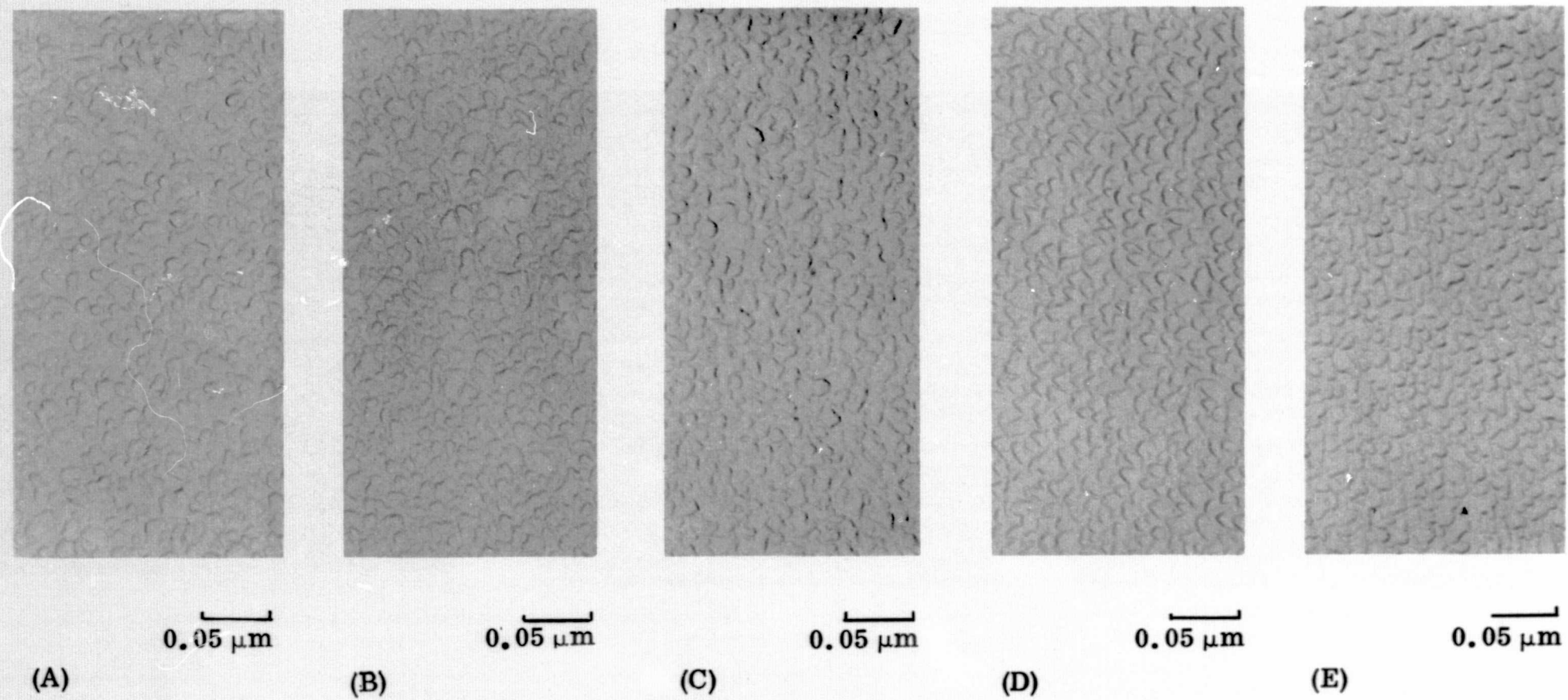
Figure 29. Replicas for GaAs/Aℓ_2O$_3$ Films Grown Simultaneously on (a) (11$\bar{2}$5), (b) (11$\bar{2}$6), (c) 5° from (11$\bar{2}$3) toward (10$\bar{1}$2), (d) 10° from (0001) toward (10$\bar{1}$4), (e) 20° from (0001) toward (10$\bar{1}$4) (All Replicas at 20,000X)

TABLE XV

EFFECT OF SUBSTRATE ORIENTATION ON THE ELECTRICAL PROPERTIES OF GaAs FILMS GROWN ON $A\ell_2O_3$

$A\ell_2O_3$ Orientation	Film Thickness (μm)	Resistivity (ohm–cm)	Carrier Concentration (cm^{-3})	Electron Mobility (cm^2/V–sec)
(0001)	18.8	0.049	2.7×10^{16}	4670
10° off (0001)	15.7	0.067	2.5×10^{16}	3790
20° off (0001)	17.8	9.70	5.1×10^{15}	127

Effects of heat treatment. – A series of annealing experiments on a group of three relatively thick GaAs/$A\ell_2O_3$ samples was carried out. The pertinent electrical data on the as–grown samples are shown in Figure 30. The samples were successively measured and annealed in a flowing H_2–AsH_3 mixture at various temperatures (shown as the abscissa in the figure) for one hour. The average mobility after the anneal at a given temperature is shown plotted as the ordinate at that temperature. It can be seen from the figure that the mobility of the Se–doped sample (#5–16B) changes very little with annealing up to 650 C. Similarly, the carrier concentration was found to decrease by only 13 percent. The undoped sample (#8–27B) experienced a continuing decrease in mobility which became very pronounced after the 550 C anneal. The carrier concentration at the same time dropped from ~1×10^{16} to 5×10^{15} cm^{-3}. After the 650 C anneal this sample converted to p–type with an acceptor carrier concentration of ~10^{16} cm^{-3} and a mobility of 290 cm^2/V–sec. The p–type sample for the same annealing sequence changed only slightly; the mobility increased from 140 to 230 cm^2/V–sec, and the carrier concentration decreased from 3×10^{16} to 2×10^{16} cm^{-3}.

Acceptor behavior in p–type films. – Measurements of the electrical properties were carried out as a function of temperature in an attempt to determine if the same acceptor is common to p–type heteroepitaxial GaAs produced by (1) annealing a thick undoped GaAs film at the growth temperature, and (2) lowering the AsH_3 flow rate during growth.

Measurements were first carried out over the temperature range 112–412K on a thick undoped GaAs/$A\ell_2O_3$ sample which was converted from n–type (n = 2.2x 10^{15} cm^{-3}, μ = 3400 cm^2/V–sec) to p–type (p = 6.3 x 10^{15} cm^{-3}, μ = 282 cm^2/V–sec) by annealing for one hour at the original growth temperature of 675 C. Such annealing is thought by some investigators to result in an increase in electrically–active Ga vacancies in GaAs. A plot of net acceptor concentration versus reciprocal temperature is shown in Figure 31. This carrier concentration data can be fitted to a model with one acceptor and a compensating donor species to within 2.5 percent over the whole temperature range. The energy level of the acceptor state responsible for the p–type behavior was found to be $\approx$0.15 ev. The number of donors remaining electrically active after annealing was 1.2 x 10^{15} cm^{-3}, or approximately 50 percent of those originally active. The number of active acceptors produced by the annealing was 10^{16} cm^{-3}.
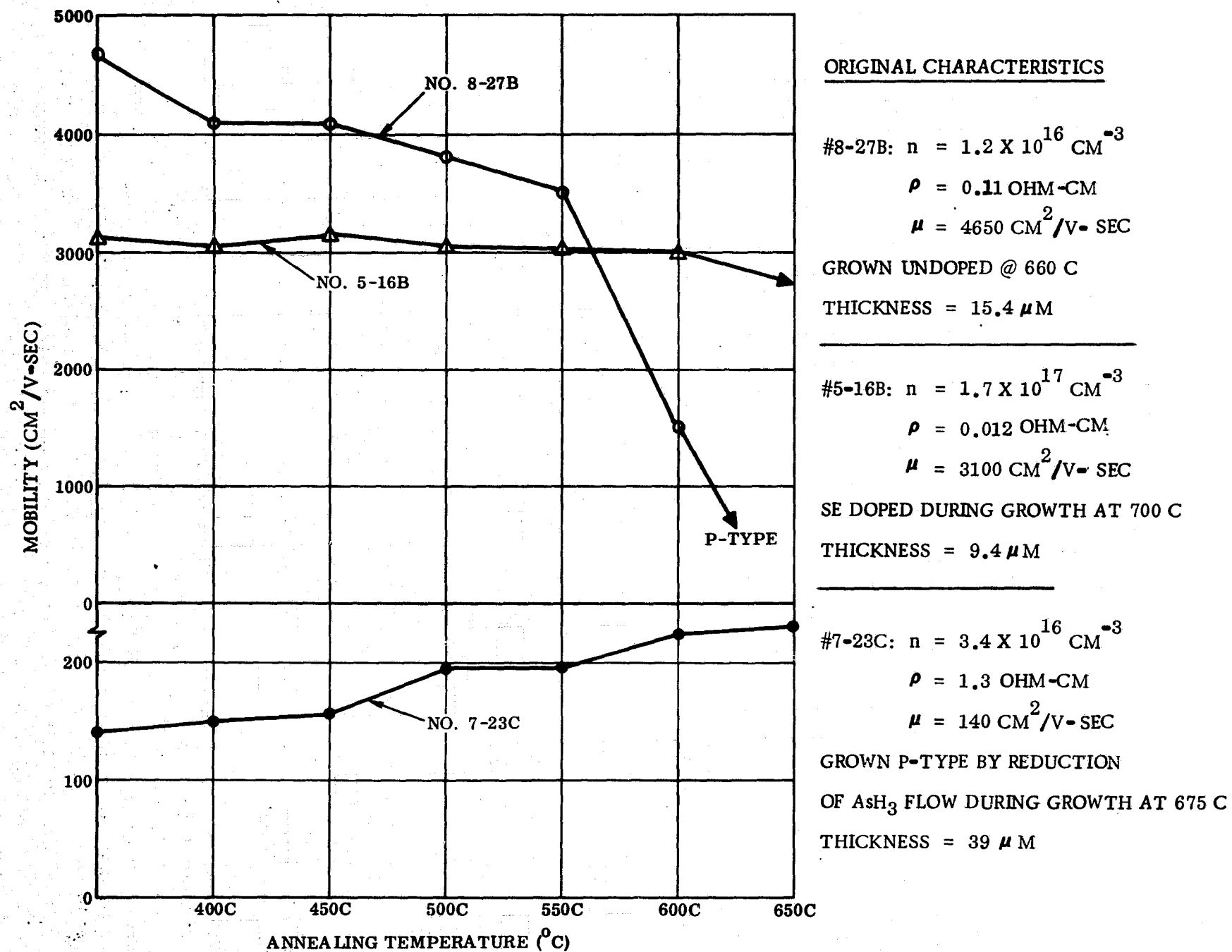
Figure 30. Effect of Annealing on the Mobility of Three GaAs/Al$_2$O$_3$ Films
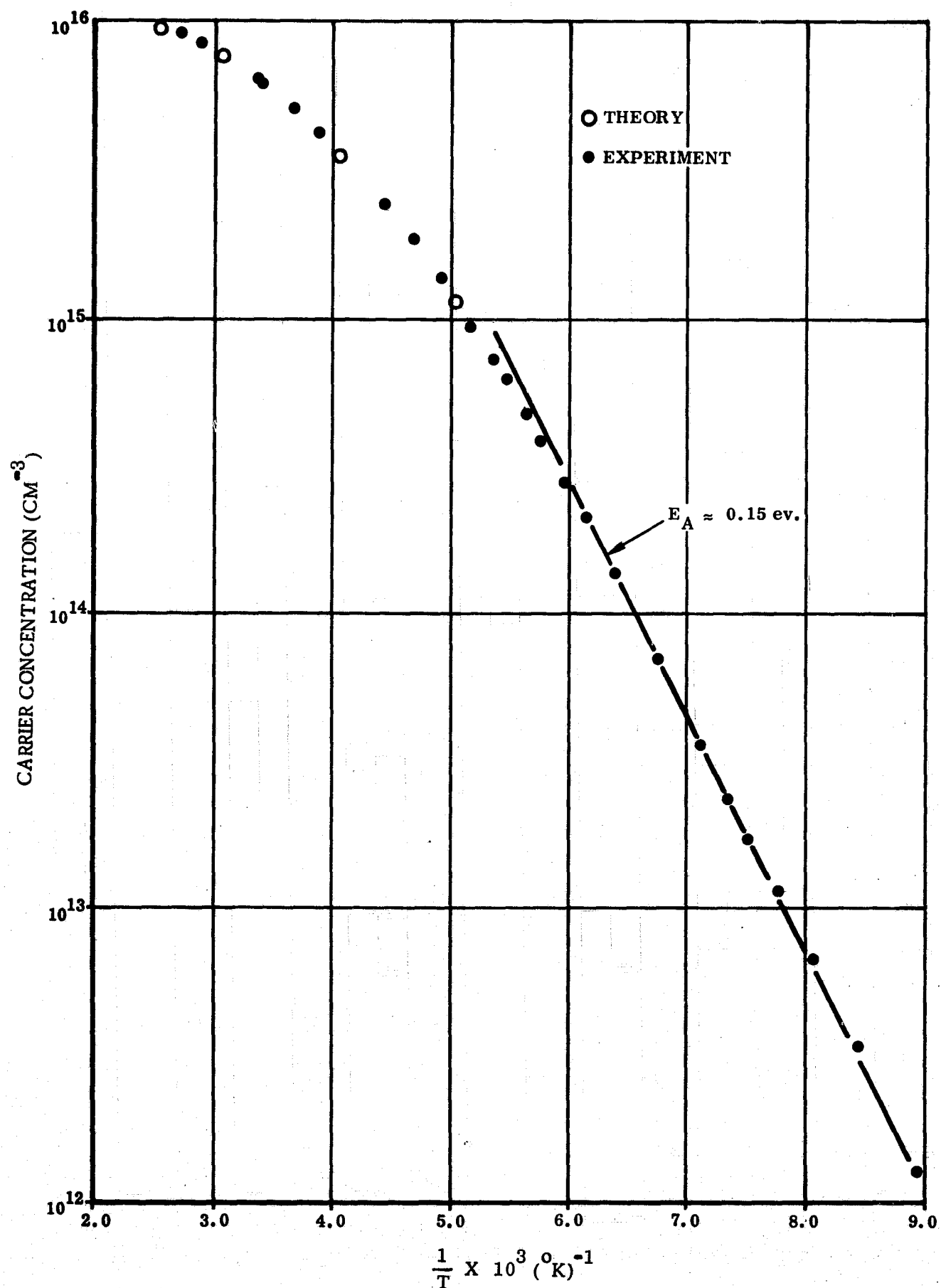
Figure 31. Carrier Concentration vs Reciprocal Temperature for P-Type GaAs/ (0001) Aℓ_2O$_3$ Film Produced by 675 C Anneal of Undoped N-Type Film

A sample grown with reduced AsH_3 flow was then measured over the temperature range ~63–390K. The results are shown in Figure 32, where net acceptor carrier concentration is plotted versus reciprocal temperature. The low temperature data indicate a much shallower level than before (≈ 0.015 ev) and also give evidence for a deep level, the energy of which cannot be ascertained from the present data. It is apparent that the acceptor responsible for the p-type behavior is different for the two cases. The conditions of growth suggest that this shallower level is a consequence of an As deficiency in the films.

"Gray-stage" characteristics. – A characteristics of the GaAs films that have been grown by the CVD process is the occurrence of a "gray stage" during the first few minutes of growth, in which the film is gray and dull in appearance. The length of time the film is in the gray stage is found to depend on the flow rates of the consistuent gases through the reactor. In general, higher than "normal" AsH_3 flow rates result in a longer gray stage; lower AsH_3 flow rates than "normal" (under conditions that provide thick n-type films) or increased carrier gas flow tends to shorten the gray stage. These results, together with the fact that a reactor of narrower design inhibits the gray stage, suggest that this behavior may be related to the flow patterns and turbulence of the gases passing through the reactor. Alternatively, the gray stage may be a consequence of the AsH_3-TMG ratio present in the reactor at any particular stage of growth. This intermediate gray stage is observed in both the H_2 and the He systems and appears to be a beneficial concomitant for the production of smooth, highly reflective surfaces on the GaAs layers.

Electrical measurements have shown that the gray stage is not related to the p-type layer discussed above and seems to have little effect on the overall electrical quality of thick films. A series of $GaAs/A\ell_2O_3$ films was grown (in H_2) in which various thicknesses of the gray stage growth were allowed to continue before the TMG-AsH_3 ratio was alerted to terminate the gray stage and effect reflective film growth. The gray stage growth was controlled for various lengths of time ranging from 1 to 20 minutes. The electrical parameters of this series of films are shown in Table XVI. Based on the average mobility values obtained, there does not appear to be a difference in quality among the films, suggesting that the gray appearance of the films during growth is not a primary factor in determining the electrical properties of the films.

From preliminary studies of the growth of GaAs on Cr-doped GaAs, it was found that the gray stage can also be induced in the homoepitaxial material and is thus not peculiar to growth on insulators.

Doping with diethylzinc. – Prior to the initiation of this contract some Zn-doped samples had been grown, and a set of conditions was established for the growth of films with a wide range of p-type carrier concentrations. During the contract period a new apparatus was constructed, and a study was begun to relate different growth parameters to the quality of the Zn-doped GaAs. Preliminary results indicating the effect of some of these variables are shown in Figure 33 in which hole concentration p is plotted versus H_2 flow rate over DEZ. The solid dots show the variation in p at 725 C. The crosses illustrate the variation in p at 700 C
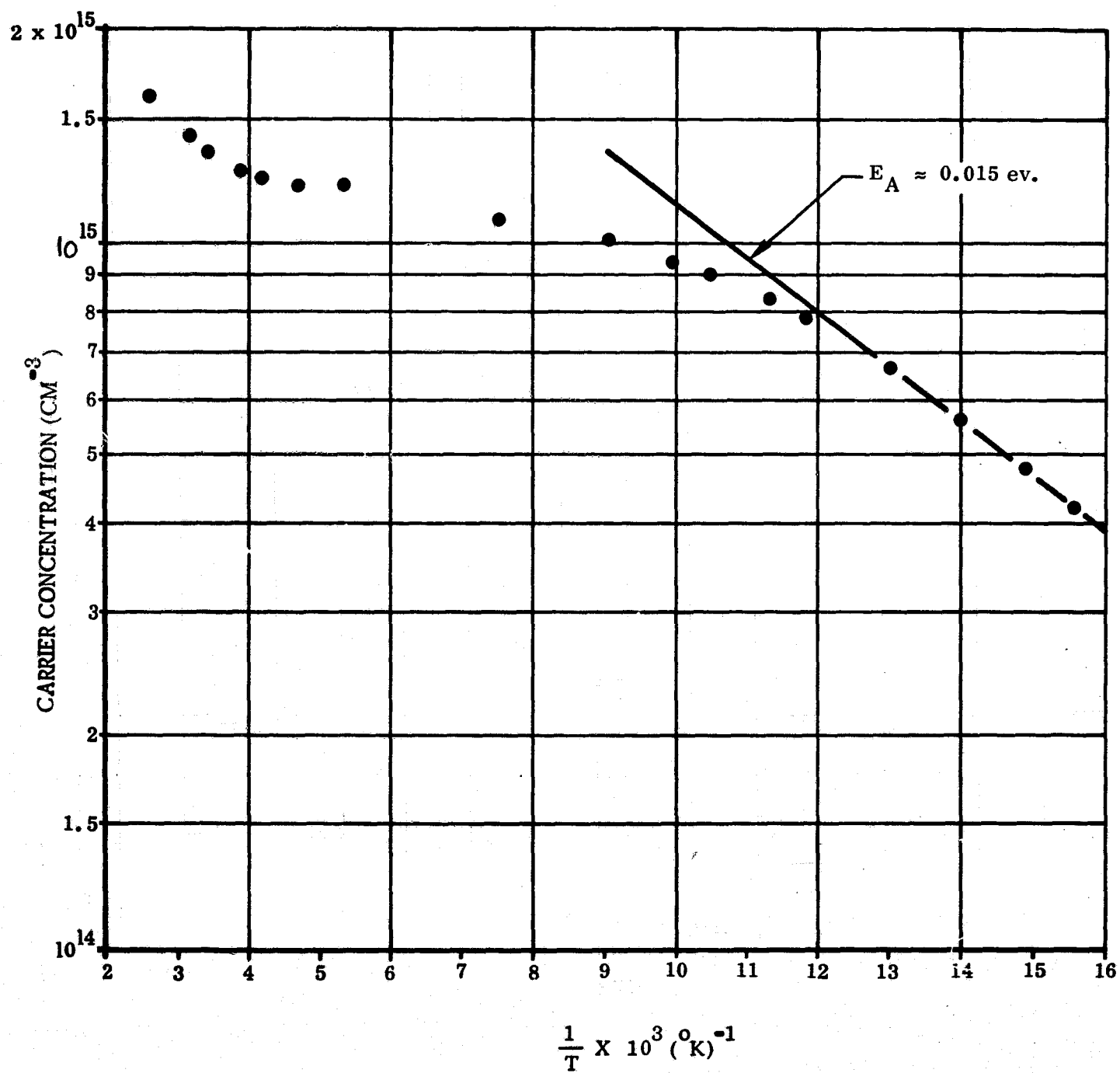
Figure 32. Carrier Concentration vs Reciprocal Temperature for P-Type GaAs/
(0001) Al_2O_3 Film Produced by Lowering AsH_3 Flow During Deposition

59

TABLE XVI

STUDY OF THE FORMATION AND EFFECT OF THE GRAY STAGE
AT 675C IN A H_2 ATMOSPHERE

Growth Conditions* (AsH_3-TMG-Dopant)	Time of Growth (min)	Thickness (μm)	Observations During Growth	Resistivity (ohm-cm)	Carrier Concentration (cm^{-3})	Electron Mobility (cm^2/V-sec)
250-45-0	31	28.0	Gray 1 min, then cleared	0.062	1.98×10^{16}	5070
300-45-0	20	19.0	Gray for 3-4 min	0.073	1.86×10^{16}	4620
300-45-0	22	21.7	Started to clear in 5 min	0.066	1.83×10^{16}	5140
325-45-0 (2 min) 370-45-0 (4 min) 210-45-0 (14 min)	20	19.2	Gray for 6 min	0.083	1.65×10^{16}	4560
325-45-0 (10 min) 210-45-0 (10 min)	20	20.8	Gray for 11 min	0.064	1.85×10^{16}	5250
300-45-0	22	22.6	Gray for 15 min	0.046	2.53×10^{16}	5350
300-45-0 (15 min) 210-45-0 (1-1/2 min) 190-45-0 (3-1/2 min)	20	18.9	Gray first 4 min, Clear 5-8 min total Gray 8-15 min total Clear 16-20 min total	0.064	2.05×10^{16}	4760
300-45-0	20	22.0	1/2 sample --gray and cleared near end of run	0.054	2.41×10^{16}	4800
			1/2 sample--gray entire run	0.099	1.47×10^{16}	4300

*See text, p.10 for significance of numbers
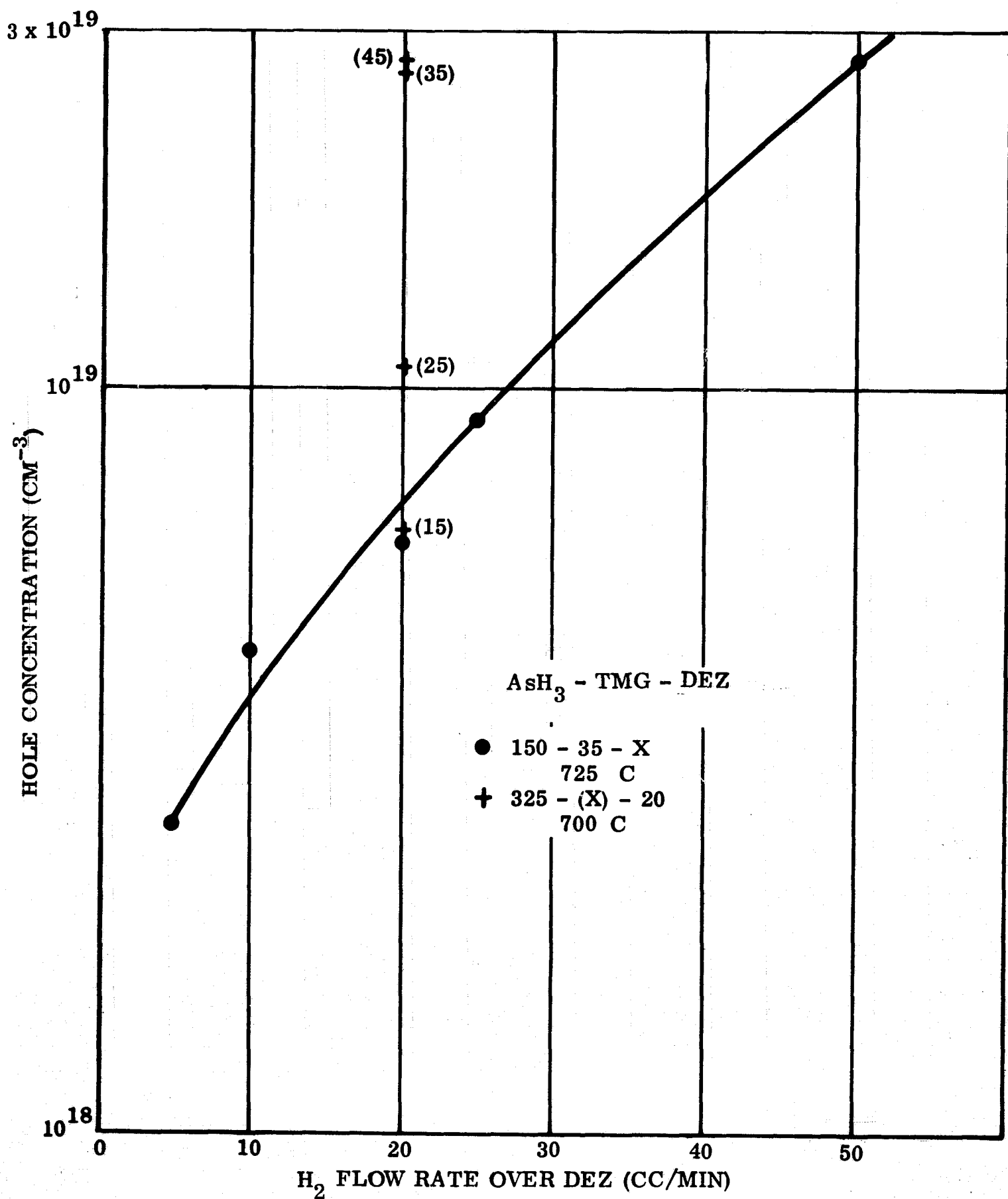
Figure 33. Hole Concentration in (111) GaAs Films Grown on (0001) Al_2O_3 as a Function of Diethylzinc (DEZ) and Trimethylgallium (TMG) Concentration

with a fixed Zn impurity concentration (i.e., constant flow rate of H_2 over DEZ) and a fixed AsH_3 flow rate, but with changes in TMG rate and hence in growth rate. In both cases the limits of doping have been $\sim 3 \times 10^{19}$ cm^{-3}. The p-type doping level is found to be quite dependent on the TMG concentration. The Hall mobilities of these p$^+$ films have been in the range from 50-100 cm^2/V-sec with corresponding resistivities ~ 0.003-0.01 ohm-cm.

Zn-doped GaAs studies were not pursued further during the period of this contract because of the award of a contract (USAMERDC, Ft. Belvoir, Va., Contract No. DAAK02-69-C-0333) devoted exclusively to the study of heavily Zn-doped GaAs films on insulating substrates. Reports of this Night Vision Laboratory contract have been distributed to NASA/ERC.

<u>Orientation relationships.</u> – X-ray diffraction and reflection electron diffraction techniques have been used to determine the crystallographic relationships between epitaxial GaAs and $A\ell_2O_3$, as was done in the Si-on-$A\ell_2O_3$ system (Ref 11). The $A\ell_2O_3$ substrate orientations studied are indicated in a portion of the $A\ell_2O_3$ stereographic projection shown in Figure 34. These orientations lie along seven zones:

A. $(0001) A\ell_2O_3 \rightarrow (10\bar{1}4)\ A\ell_2O_3$

B. $(10\bar{1}4) A\ell_2O_3 \rightarrow (01\bar{1}5)\ A\ell_2O_3$

C. $(10\bar{1}\bar{1}) A\ell_2O_3 \rightarrow (12\bar{3}2)\ A\ell_2O_3$

F. $(01\bar{1}2) A\ell_2O_3 \rightarrow (11\bar{2}3)\ A\ell_2O_3$

I. $(11\bar{2}0) A\ell_2O_3 \rightarrow (0001)\ A\ell_2O_3$

J. $(12\bar{3}\bar{2}) A\ell_2O_3 \rightarrow (01\bar{1}2)\ A\ell_2O_3$

K. $(10\bar{1}4) A\ell_2O_3 \rightarrow (11\bar{2}3)\ A\ell_2O_3$

The growth of the GaAs films on the above orientations was performed using primarily those deposition conditions which were known to be correct for GaAs growth on (0001) $A\ell_2O_3$. A change in temperature was sometimes required; some orientations appeared to grow better at 750 C than at 675 C.

The specific substrate orientations and the heteroepitaxial relationships found to date for the GaAs/$A\ell_2O_3$ system are summarized in Table XVII. X-ray diffraction intensity measurements to distinguish the reflections due to the predominant orientations (i.e., the "matrix") from those associated with the presence of twins were not made on zones A, B, C, F, I, and J in the earlier studies. However, distinction between the orientations of the matrix and those due to twinning has been made in the case of zone K.

Good deposits have been obtained on basal plane, i.e., (0001)-oriented, substrates, the relationships obtained are (111) GaAs $\|$ (0001) $A\ell_2O_3$ with [01$\bar{1}$] GaAs $\|$ [$\bar{1}2\bar{1}0$] $A\ell_2O_3$. On analyzing the $A\ell_2O_3$ planes A1 and A3 (see Figure 34) on the zone between the (0001) and the (10$\bar{1}$4) plane of $A\ell_2O_3$, the predominant orientation
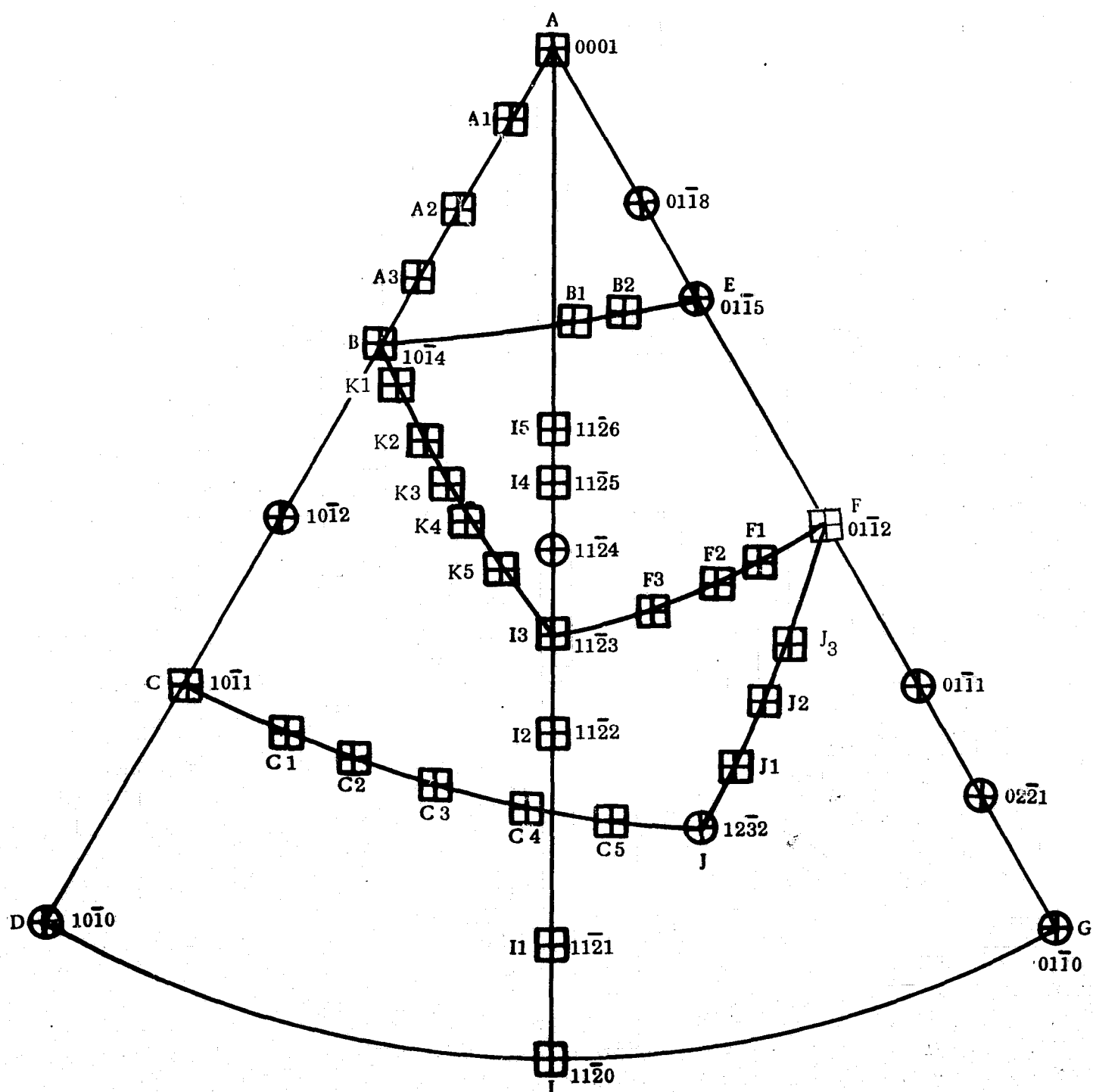
Figure 34. Portion of a Stereographic Projection of $A\ell_2O_3$. The Symbol ⊞ Indicates Orientations Reported in Table XVII

was found to be the (111) GaAs plane parallel to the (0001) face of the $A\ell_2O_3$ substrate. However, a (111) GaAs reflection was also found parallel to the $(10\bar{1}4)$ $A\ell_2O_3$ reflection. These two $\{111\}$ GaAs planes are twins. On A2, which is a substrate plane cut 19 degrees from the basal plane of $A\ell_2O_3$, the (111) plane of GaAs is not parallel to (0001) $A\ell_2O_3$ but tilted 5 degrees from it. Analysis of a deposit on $(10\bar{1}4)$ $A\ell_2O_3$ indicates the presence of (111) GaAs, but of poor quality.

Reflective deposits have been formed on two substrates (B1 and B2) that lie 18 and 25 degrees, respectively, from the $(10\bar{1}4)$ plane on the zone toward $(01\bar{1}5)$ $A\ell_2O_3$. On both substrates the following relations were detected: (111) GaAs // $(01\bar{1}2)$ and $(\bar{1}10)$ GaAs // $(01\bar{1}8)$ $A\ell_2O_3$. A weak (111) reflection was also found near the (0001) plane of $A\ell_2O_3$.

On substrates C1 to C5, cut along the zone between the $(10\bar{1}1)$ and the $(12\bar{3}2)$ planes of $A\ell_2O_3$, it was found that a pole representing (111) GaAs was consistently near the $(11\bar{2}3)$ $A\ell_2O_3$, despite the wide angular separation ($\sim$40 deg) of the five substrates (C1 to C5). However, the (111) GaAs plane was found to be tilted from the substrate, the amount of tilt increasing from 3 to 5 degrees as the substrate orientation approached the $(12\bar{3}2)$ plane of $A\ell_2O_3$. Analyses on C3 and C4 show that the pole representing the (111) GaAs lies about 5 degrees from the $(11\bar{2}3)$ pole of $A\ell_2O_3$. At the same time, the (111) twin plane of GaAs falls about 5 degrees from the $(11\bar{2}0)$ pole of $A\ell_2O_3$.

Along the zone between the (0001) and $(11\bar{2}0)$ planes of $A\ell_2O_3$, relatively reflective deposits of (111) GaAs were found almost parallel to the $(11\bar{2}3)$, $(11\bar{2}5)$, and $(11\bar{2}6)$ $A\ell_2O_3$ planes even though the $(11\bar{2}3)$ and $(11\bar{2}6)$ are only 18.9 degrees apart; an angle of only 5 degrees separates the $(11\bar{2}5)$ and $(11\bar{2}6)$ planes. Growths on $(11\bar{2}2)$ and $(11\bar{2}1)$ $A\ell_2O_3$ seem to be consistent with the twin relationships of (111) GaAs near $(11\bar{2}0)$ and $(11\bar{2}3)$ $A\ell_2O_3$.

An angle of only 26 degrees separates $(11\bar{2}3)$ $A\ell_2O_3$ and $(01\bar{1}2)$ $A\ell_2O_3$; yet, as indicated in Table XVII, three different modes of epitaxy have been seen along the zone joining these planes. It is not obvious why a substrate cut 9 degrees off the $(01\bar{1}2)$ produces (110) GaAs // $(01\bar{1}2)$ $A\ell_2O_3$ if it is used as the plane of deposition. The (110) GaAs growth is consistent, however, with the results found for the J1, J2 and J3 orientations, which are on the zone between $(12\bar{3}2)$ and $(01\bar{1}2)$ $A\ell_2O_3$ planes. It is clear that additional studies are required to help explain these observations and to distinguish between matrix and twin relationships.

The final zone investigated in this analysis was the zone between the $(10\bar{1}4)$ and $(11\bar{2}3)$ planes of $A\ell_2O_3$. On substrates cut along this zone, relatively reflective deposits were obtained on all the orientations except the $(10\bar{1}4)$. Poor films have been obtained consistently on this orientation, so poor in fact that it was virtually impossible to establish any crystallographic directional relationships. On analyzing the growth on the five $A\ell_2O_3$ planes, K1, K2, K3, K4, and K5 (see Figure 34), the predominant orientation found near K1 and K2 was (533) GaAs, consistent with (111) GaAs tilted approximately 2.5 degrees from $(10\bar{1}4)$ $A\ell_2O_3$ and $[00\bar{1}]$ GaAs // $[12\bar{1}0]$ $A\ell_2O_3$. (211) GaAs was found parallel to K3, 14 degrees from $(10\bar{1}4)$ $A\ell_2O_3$ with $\{111\}$ planes of GaAs titled 3 degrees from both the $(10\bar{1}4)$ and $(11\bar{2}3)$ planes of $A\ell_2O_3$. Intensity measurements could not distinguish the matrix from the twin.

64

TABLE XVII

CRYSTALLOGRAPHIC RELATIONSHIPS BETWEEN EPITAXIAL
GaAs AND Al_2O_3 SUBSTRATES FROM X-RAY DIFFRACTION STUDIES

Crystallographic Zone	Designation of Substrate Plane*	Orientation of Substrate Surface	Orientation Relationships	
			Planes	Directions
(0001) Al_2O_3	A	(0001)	(111) GaAs // (0001) Al_2O_3	$[01\bar{1}]$ GaAs // $[\bar{1}2\bar{1}0]$ Al_2O_3
to	A1	9° from (0001)	(111) GaAs // (0001) Al_2O_3 (111) GaAs // $(10\bar{1}4)$ Al_2O_3	$[01\bar{1}]$ GaAs // $[\bar{1}2\bar{1}0]$ Al_2O_3
$(10\bar{1}4)$ Al_2O_3	A2	19° from (0001)	(111) GaAs 5° from (0001) Al_2O_3 (111) GaAs 5° from $(10\bar{1}4)$ Al_2O_3	$[01\bar{1}]$ GaAs 5° from $[\bar{1}2\bar{1}0]$ Al_2O_3
$(38.2^{\circ}$ apart$)$	A3	26° from (0001)	(111) GaAs // (0001) Al_2O_3 (111) GaAs // $(10\bar{1}4)$ Al_2O_3	$[01\bar{1}]$ GaAs // $[\bar{1}2\bar{1}0]$ Al_2O_3
$(10\bar{1}4)$ Al_2O_3	B	$(10\bar{1}4)$	(111) GaAs // $(10\bar{1}4)$ Al_2O_3 of poor quality	--
to	B1	18° from $(10\bar{1}4)$	(111) GaAs // $(01\bar{1}2)$ Al_2O_3 (110) GaAs // $(01\bar{1}8)$ Al_2O_3	$[01\bar{1}]$ GaAs // $[2\bar{1}\bar{1}0]$ Al_2O_3
$(01\bar{1}5)$ Al_2O_3	B2	25° from $(10\bar{1}4)$	(111) GaAs // $(01\bar{1}2)$ Al_2O_3 (111) GaAs // $(01\bar{1}8)$ Al_2O_3	$[01\bar{1}]$ GaAs // $[2\bar{1}\bar{1}0]$ Al_2O_3
$(34.0^{\circ}$ apart$)$				

*See substrate orientations in stereographic projection in Figure 34.

TABLE XVII (CONTINUED)

Crystallographic Zone	Designation of Substrate Plane*	Orientation of Substrate Surface	Orientation Relationships	
			Planes	Directions
$(10\bar{1}1)$ Al_2O_3	C	$(10\bar{1}1)$	(111) GaAs // $(10\bar{1}1)$ Al_2O_3	$[01\bar{1}]$ GaAs // $[0\bar{1}11]$ Al_2O_3
to	C1	9.5^o from $(10\bar{1}1)$	(111) GaAs 3° from $(11\bar{2}3)$ Al_2O_3	$[01\bar{1}]$ GaAs // $[0\bar{1}11]$ Al_2O_3
$(12\bar{3}2)$ Al_2O_3	C2	11.5^o from $(10\bar{1}1)$	(111) GaAs 3° from $(11\bar{2}3)$ Al_2O_3	$[01\bar{1}]$ GaAs // $[0\bar{1}11]$ Al_2O_3
	C3	20° from $(10\bar{1}1)$	(111) GaAs 5° from $(11\bar{2}3)$ Al_2O_3	$[01\bar{1}]$ GaAs 6° from $[1\bar{1}00]$ Al_2O_3
	C4	25.5^o from $(10\bar{1}1)$	(111) GaAs 5° from $(11\bar{2}3)$ Al_2O_3	$[01\bar{1}]$ GaAs // $[1\bar{1}00]$ Al_2O_3
	C5	34.5^o from $(10\bar{1}1)$	(111) GaAs 5° from $(11\bar{2}3)$ Al_2O_3	$[01\bar{1}]$ GaAs // $[1\bar{1}00]$ Al_2O_3
$(01\bar{1}2)$ Al_2O_3	F	$(01\bar{1}2)$	(111) GaAs // $(01\bar{1}2)$ Al_2O_3	$[01\bar{1}]$ GaAs // $[\bar{2}201]$ Al_2O_3
to	F1	9° from $(01\bar{1}2)$	(110) GaAs // $(01\bar{1}2)$ Al_2O_3	$[01\bar{1}]$ GaAs // $[0\bar{1}11]$ Al_2O_3
$(11\bar{2}3)$ Al_2O_3	F2	16° from $(01\bar{1}2)$	(111) GaAs 8° from $(11\bar{2}3)$ Al_2O_3	$[01\bar{1}]$ GaAs // $[0\bar{1}11]$ Al_2O_3
	F3	20° from $(01\bar{1}2)$	(111) GaAs 7.5^o from $(11\bar{2}3)$ Al_2O_3	$[01\bar{1}]$ GaAs // $[0\bar{1}11]$ Al_2O_3
$(26^o$ apart)				

*See substrate orientations in stereographic projection in Figure 34.

TABLE XVII (CONTINUED)

Crystallographic Zone	Designation of Substrate Plane*	Orientation of Substrate Surface	Orientation Relationships	
			Planes	Directions
$(11\bar{2}0)$ Al_2O_3	I	$(11\bar{2}0)$	(111) GaAs 5° from (1120) to $(11\bar{2}3)$ Al_2O_3	$[01\bar{1}]$ GaAs // $[1\bar{1}00]$ Al_2O_3
to	I1	10.39^o from $(11\bar{2}0)$; $(11\bar{2}1)$	(111) GaAs 10° from $(11\bar{2}0)$ toward $(11\bar{2}3)$ Al_2O_3	$[01\bar{1}]$ GaAs // $[1\bar{1}00]$ Al_2O_3
(0001) Al_2O_3 $(90^o$ apart)	I2	20.1^o from $(11\bar{2}0)$; $(11\bar{2}2)$	(311) GaAs // $(11\bar{2}2)$ Al_2O_3, (111) GaAs // $(11\bar{2}3)$ Al_2O_3	$[01\bar{1}]$ GaAs // $[1\bar{1}00]$ Al_2O_3
	I3	28.8^o from $(11\bar{2}0)$; $(11\bar{2}3)$	(111) GaAs // $(11\bar{2}3)$ Al_2O_3	$[01\bar{1}]$ GaAs // $[1\bar{1}00]$ Al_2O_3
	I4	42.5^o from $(11\bar{2}0)$; $(11\bar{2}5)$	(111) GaAs // $(11\bar{2}5)$ Al_2O_3	$[01\bar{1}]$ GaAs // $[1\bar{1}00]$ Al_2O_3
	I5	47.7^o from $(11\bar{2}0)$; $(11\bar{2}6)$	(111) GaAs // $(11\bar{2}6)$ Al_2O_3 (211) GaAs 2° from $(10\bar{1}4)$ Al_2O_3	$[01\bar{1}]$ GaAs // $[1\bar{1}00]$ Al_2O_3
$(12\bar{3}2)$	J1	5° from $(12\bar{3}2)$	(110) GaAs // $(01\bar{1}2)$ Al_2O_3	$[01\bar{1}]$ GaAs // $[20\bar{2}1]$ Al_2O_3
to	J2	10° from $(12\bar{3}2)$	(110) GaAs // $(01\bar{1}2)$ Al_2O_3	$[01\bar{1}]$ GaAs // $[20\bar{2}1]$ Al_2O_3
$(01\bar{1}2)$ $(25.7^o$ apart)	J3	14° from $(12\bar{3}2)$	(110) GaAs // $(01\bar{1}2)$ Al_2O_3	$[01\bar{1}]$ GaAs // $[20\bar{2}1]$ Al_2O_3

*See substrate orientations in stereographic projection in Figure 34.

67

TABLE XVII (CONTINUED)

Crystallographic Zone	Designation of Substrate Plane*	Orientation of Substrate Surface	Orientation Relationships	
			Planes	Directions
$(10\bar{1}4)$ $A\ell_2O_3$ to $(11\bar{2}3)$ $A\ell_2O_3$ $(32^O$ apart)	K1	3° from $(10\bar{1}4)$	(111) GaAs 2.5^O from $(10\bar{1}4)$ $A\ell_2O_3$	$[01\bar{1}]$ GaAs // $[\bar{1}2\bar{1}0]$ $A\ell_2O_3$
	K2	10° from $(10\bar{1}4)$	(111) GaAs 2.5^O from $(10\bar{1}4)$ $A\ell_2O_3$	$[01\bar{1}]$ GaAs // $[\bar{1}2\bar{1}0]$ $A\ell_2O_3$
	K3	14° from $(10\bar{1}4)$	(111) GaAs 3° from $(10\bar{1}4)$ $A\ell_2O_3$ (111) GaAs 3° from $(11\bar{2}3)$ $A\ell_2O_3$	$[01\bar{1}]$ GaAs 8° from $[\bar{1}2\bar{1}0]$ $A\ell_2O_3$
	K4	17° from $(10\bar{1}4)$	(111) GaAs // $(11\bar{2}3)$ $A\ell_2O_3$	$[01\bar{1}]$ GaAs // $[\bar{1}2\bar{1}0]$ $A\ell_2O_3$
	K5	25° from $(10\bar{1}4)$	(111) GaAs 5° from $(11\bar{2}3)$ $A\ell_2O_3$ toward the $(12\bar{3}2)$	$[01\bar{1}]$ GaAs 6° from $[\bar{1}2\bar{1}0]$ $A\ell_2O_3$

*See substrate orientations in sterographic projection in Figure 34.

On K4 (17 degrees from $(10\bar{1}4)$ $A\ell_2O_3$) and K5 (25 degrees from $(10\bar{1}4)$ $A\ell_2O_3$), the (322) plane of GaAs was found essentially parallel to these orientations. For K4, (111) GaAs coincided with $(11\bar{2}3)$ $A\ell_2O_3$, but was tilted 5 degrees from $(11\bar{2}3)$ $A\ell_2O_3$ when the substrate was K5.

The data indicate a high degree of twinning present in GaAs films formed along this zone of $A\ell_2O_3$. K3 was the midpoint of the structure, controlling (211) GaAs growth, with twinning occurring across the plane. The $\{111\}$ matrix seemed to be identified with the $A\ell_2O_3$ substrate plane closest to either the $(10\bar{1}4)$ or $(11\bar{2}3)$ planes of $A\ell_2O_3$.

These zonal studies have indicated that GaAs growth on $A\ell_2O_3$ can be quite complex, with twinning being the rule rather than the exception. As in the Si-on-$A\ell_2O_3$ (SOS) system (Ref 11), it appears that those $A\ell_2O_3$ planes that possess a high degree of symmetry are most susceptible to the growth of GaAs with an orientation of a low index plane. The dominant growth at the major intersection is $\{111\}$. $\{110\}$ occurs on the $(01\bar{1}2)$ when the substrate plane is about 9 degrees from the $(01\bar{1}2)$, but $\{111\}$ is found when the substrate plane is the $(01\bar{1}2)$.

The data indicate that orientation differences do exist in the SOS and GaAs-on-$A\ell_2O_3$ systems, despite their similar lattice parameters and cubic-type structures. In SOS, bonding seemed to be explained by a filling-in of $A\ell$ ion sites and bonding to the oxygens. In GaAs-on-$A\ell_2O_3$, it may be that bonding occurs via an As bridge to the $A\ell$ ions. These differences seem consistent with the fact that a high temperature H_2 treatment of $A\ell_2O_3$ produces a surface incompatible with GaAs growth but better for SOS film growth.

Because of the high degree of twinning present in most of the GaAs films it becomes exceedingly difficult in this system to separate the various modes of epitaxy by full-circle goniometer measurement. As has been observed in films grown on (0001) $A\ell_2O_3$, films free of twinning may be obtained when the proper growth parameters are chosen, and better film growth might be expected on other orientations with additional parameter studies. Such studies do not seem required at this time because of the high quality of the films grown on the basal plane of $A\ell_2O_3$. However, further studies would be warranted if it were important to establish an $A\ell_2O_3$ orientation which controlled (100) growth and a better (110) growth of GaAs on $A\ell_2O_3$.

GaAs on spinel. - The high defect structure possessed by commercial-type Verneuil spinel is readily revealed by the epitaxial growth of GaAs, as shown in Figure 35. However, good quality (111) Czochralski spinel has been a good substrate for GaAs growth; simultaneous growth on (111) $MgA\ell_2O_4$ and (0001) $A\ell_2O_3$ has produced epitaxial films of equivalent high quality. The apparent advantage to the use of spinel as a substrate lies in its cubic structure, thereby making it a possible insulating substrate for the growth of practically any orientation of the zinc-blende materials, represented in this case by GaAs.

Early $GaAs/A\ell_2O_3$ orientation studies had not established a substrate orientation for (100) GaAs growth; consequently, a boule of commercially available Czochralski spinel was oriented to the (100), sliced into wafers, and mechanically polished. (100) GaAs was grown on the wafers, but good growth was not reproducible. X-ray topography (see Figure 36) revealed strain in the crystal and optical microscopy showed scratches on the surface. Additional polishing to remove the scratches was performed at Autonetics, but only partial success was achieved, as revealed by the GaAs overgrowth. The reflectivity of the (100) $GaAs/(100)$ $MgA\ell_2O_4$ composite is shown in Figure 37; the surface structure is shown in Figure 38. The epitaxy indicates that variations in quality exist within the substrate.

Single-crystal growth of GaAs was later achieved on (110)-oriented spinel at temperatures as low as 625C. Surface structural characteristics and x-ray and reflection electron diffraction evaluations (Figure 39) of the films on spinel have shown (100) GaAs growth (rather than (110) GaAs overgrowth, which might have been expected) parallel to the (110) spinel substrate surface. Matching of atom positions in the two lattices suggests a better match between the two (110) planes than between (100) GaAs and ($1\bot0$) spinel.

Although the electrical quality of the films on spinel has been inconsistent, with most films exhibiting extremely high resistivities, it is significant that some good quality (100) GaAs films have been obtained. The electrical properties of two of these films are shown in Table XVIII, together with the properties of films grown simultaneously on $A\ell_2O_3$.

TABLE XVIII

ELECTRICAL PROPERTIES OF GaAs FILMS GROWN SIMULTANEOUSLY
ON (110) SPINEL AND (0001) $A\ell_2O_3$ AT 650-675C

Substrate	Film Thickness (μm)	Resistivity (ohm-cm)	Carrier Concentration (cm^{-3})	Electron Mobility (cm^2/V-sec)
(110) spinel	20.9	0.135	1.1×10^{16}	4200
(111) $A\ell_2O_3$	22.0	0.057	2.5×10^{16}	4400
(110) spinel	18.8	0.375	5.6×10^{15}	2960
(111) $A\ell_2O_3$	19.8	0.051	2.6×10^{16}	4700
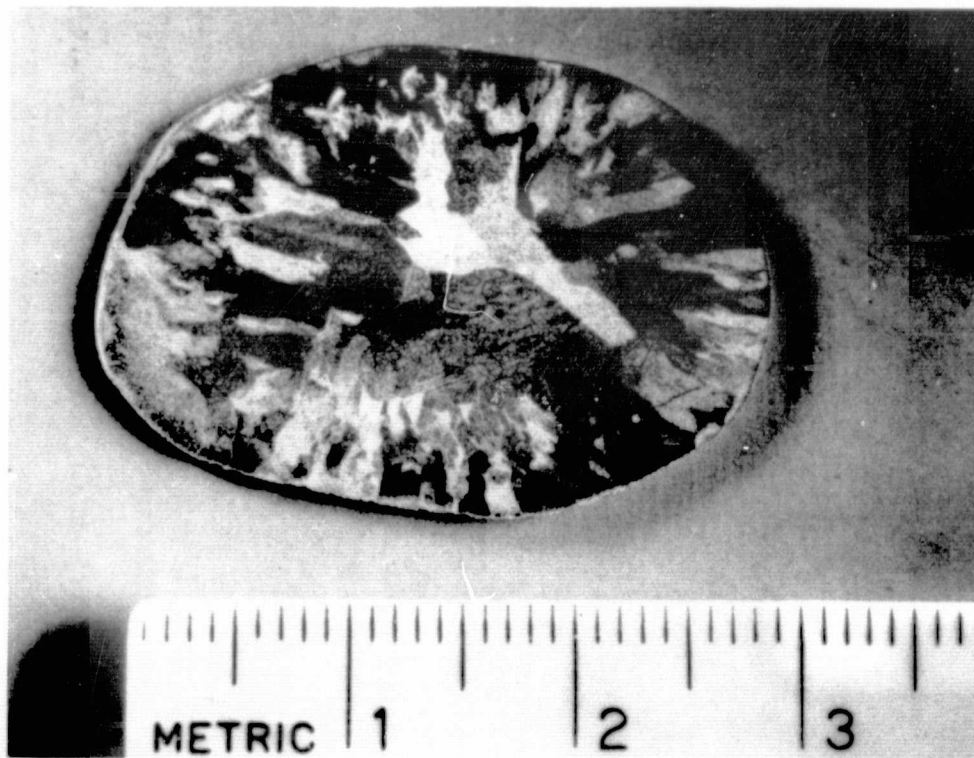
Figure 35. The Effect of Grain Boundaries in Verneuil
Spinel on the Growth of GaAs
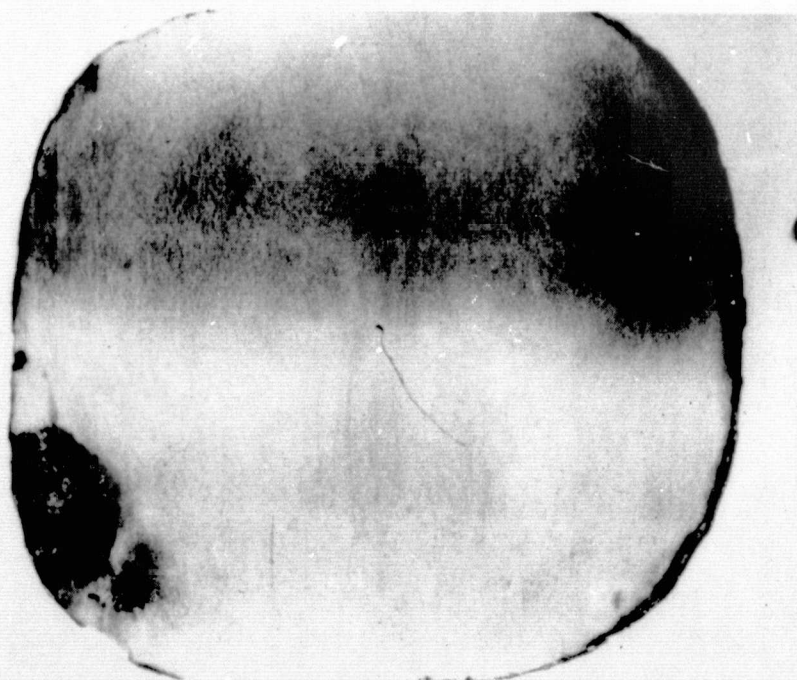
Figure 36. A Lang X-Ray Topograph of (100) Czochralski Spinel Revealing Strained
Areas (Dark Portions) in the Crystal (about 0.5 in. Square)

71
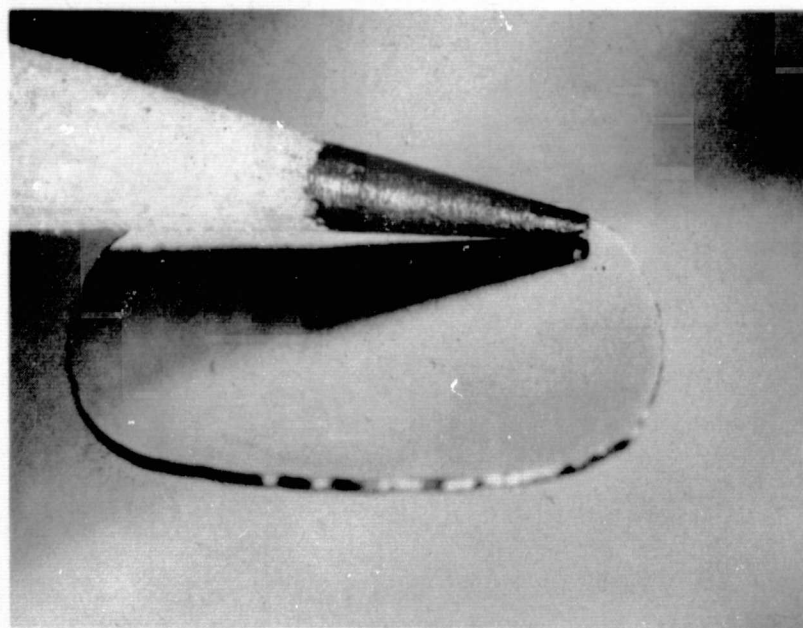
Figure 37.   Reflectivity of (100) GaAs Growth on a 0.5-inch-
wide (100) Spinel Substrate

50 μm

Figure 38.   Surface Structure of (100) GaAs Growth on (100) Spinel

(A)

(B)

(C)

Figure 39. (100) GaAs on (110) Spinel Showing a) Surface Structure, b) Laue Pattern of Composite, c) (110) RED Pattern

73

The electrical properties of GaAs grown on spinel were found to be very sensitive to substrate surface preparation. All films grown on (110) substrates polished by outside vendors have been of inferior quality. The improved electrical and crystallographic quality of the recent GaAs films grown on (110) spinel has been a direct consequence of new substrate polishing techniques developed in Autonetics metallography laboratories.

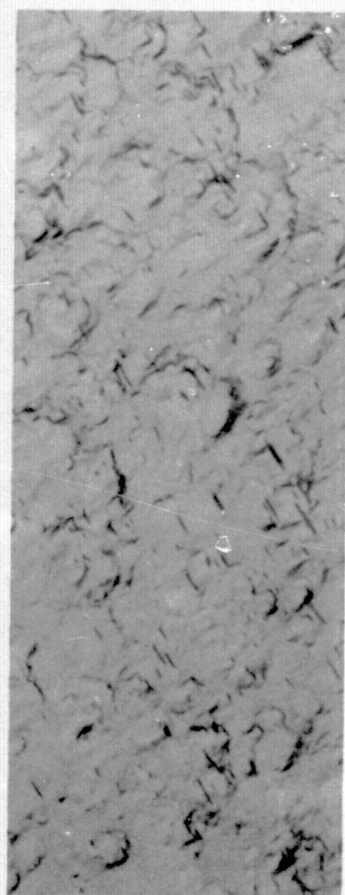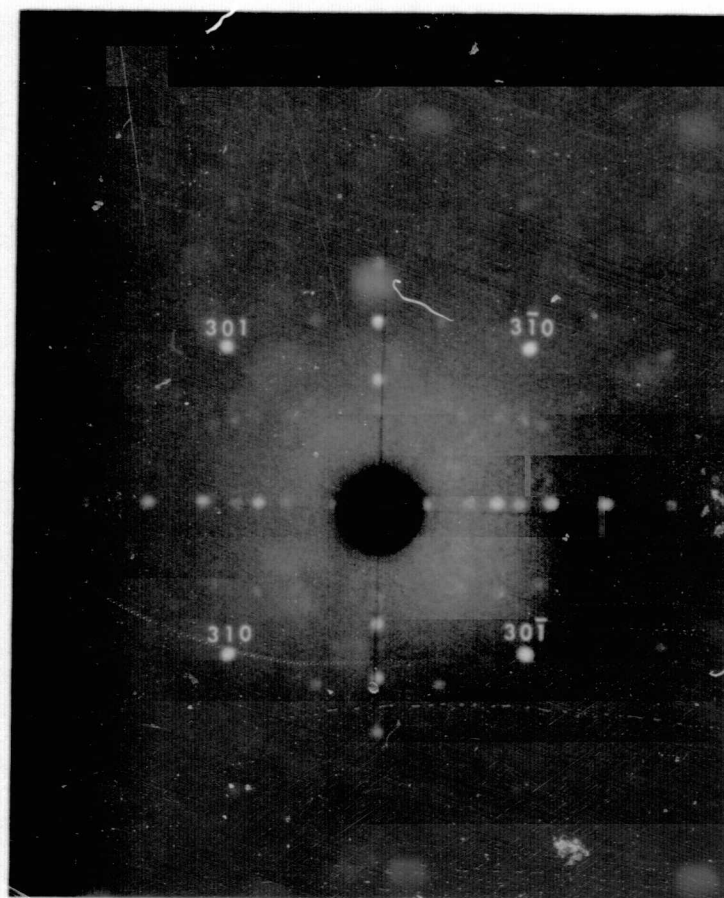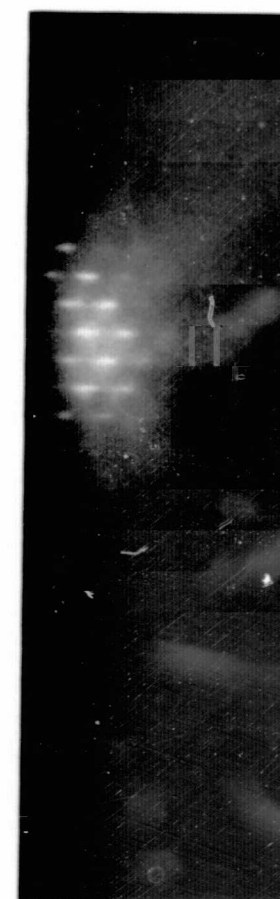Effects of substrate properties on film properties. - X-ray rocking-curve measurements have been carried out on several of the GaAs/$A\ell_2O_3$ samples previously identified as having good electrical properties and crystal structure. The results indicated a considerable range of line broadening, with the samples that exhibited lower twin densities and higher mobilities also giving the narrowest rocking-curve widths, i.e., displaying the smallest distribution of misoriented regions about the primary orientation direction. Usually no microtwins were detected in the GaAs films on (0001) $A\ell_2O_3$ when mirrorlike films were obtained. (See previous section on orientation relationships.)

An interesting condidtion was noted when large grains were present in the larger slices of Verneuil $A\ell_2O_3$, as illustrated in Figure 40. The film (Figure 40a) replicated the structure in the $A\ell_2O_3$, shown as observed between crossed polaroids in Figure 40b. X-ray evaluation showed the large grain to be about 1.5 deg off the basal plane. The poor quality film growth in this part of the deposit may have been related to a high degree of strain or defect structure in this region, formed in the crystal during its cooling from temperatures of about 2000C to room temperature, rather than to misorientation; high quality films have been grown on other substrates as much as 4 deg off the (0001) plane.

Heating the pedestal and the $A\ell_2O_3$ substrate in an atmosphere of H_2 to temperatures above the growth temperature (up to 825C) prior to GaAs deposition was explored as an in situ cleaning technique. Such heating should help to outgas the SiC-covered C pedestal and make the early GaAs growth stages more uniform and lower in uncontrolled contamination. Electrical data indicated that films equivalent electrically to those grown without the heat treatment could be prepared in this way. In addition, this cleaning step resulted in fewer localized contaminated spots on the film surface. These spots, or regions of nonreflective GaAs, are sometimes found on the GaAs/$A\ell_2O_3$ films and are thought to be related to contamination of the substrate surface.

Studies were also carried out using gas phase etching at high temperatures as a means of improving the $A\ell_2O_3$ surface prior to growth. In the past, these steps had resulted in surfaces that were not compatible with good GaAs epitaxial growth. However, new procedures permitted a recovery of the $A\ell_2O_3$ surface for GaAs growth. It now appears feasible to remove any polycrystalline $A\ell_2O_3$ which might be left after mechanical polishing of the surface and to expose a single-crystal $A\ell_2O_3$ surface for epitaxial growth. However, the etching reveals the presence of defects in the $A\ell_2O_3$ crystal, as shown in Figure 41.

Layered and device structures. - During the latter part of the contract, more effort was directed toward the techniques of fabrication and the electrical characterization of simple divice structures. This work is summarized below.

Doping profiles in n/n$^+$ structures. - The impurity profiles in a series of n/n$^+$ - GaAs/(0001) $A\ell_2O_3$ films were evaluated from Schottky-barrier diode

74
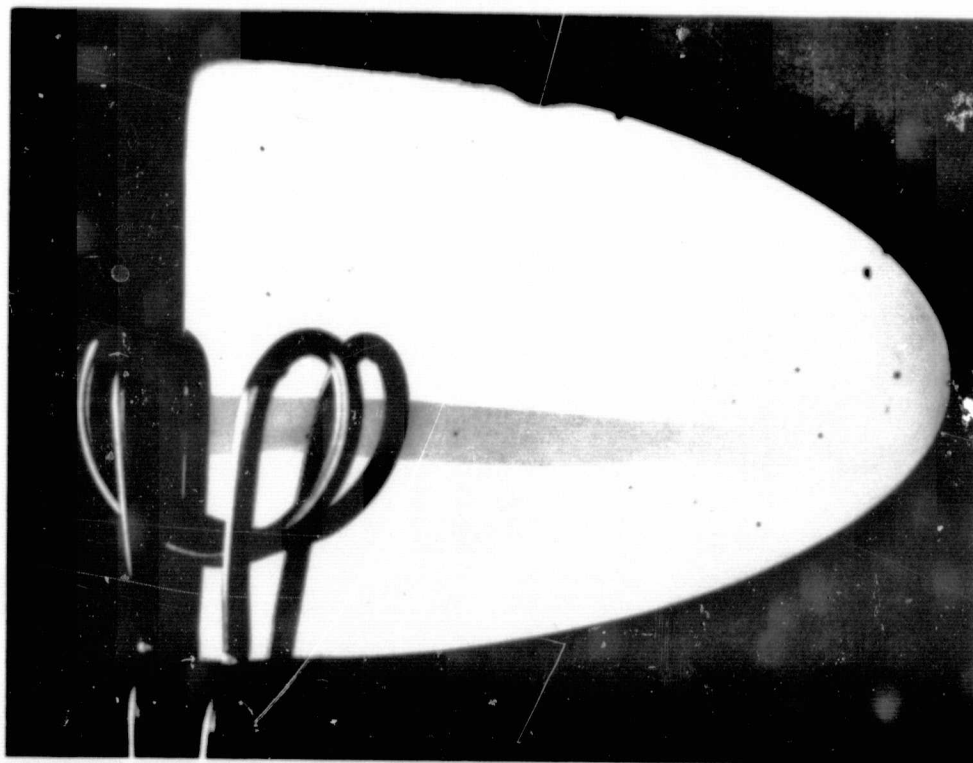
(a)

Figure 40. (0001) Al_2O_3 (a) with GaAs Film, (b) without Film, as Seen between Crossed Polaroids

(A)

110 μm

(B)
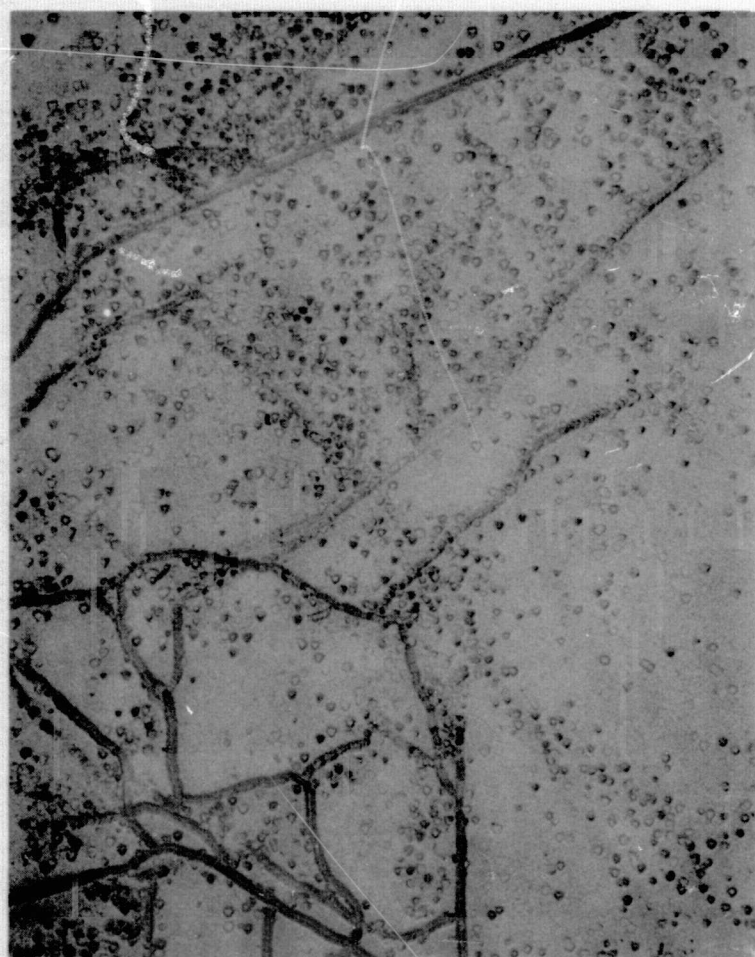
100 μm

Figure 41. Defects in Al_2O_3 Revealed by Gas Phase Etching in a) (0001) Verneuil Al_2O_3, b) (0001) Czochralski Al_2O_3

measurements. The results were deduced from measurements of capacitance versus reverse-bias voltage for barriers formed by the evaporation of $A\ell$ dots on the surface of the n-layer. Two of these structures were formed by deposition of an n-layer following evacuation of the reactor after growth of the n^+ layer, and two were formed by deposition after flushing the reactor with H_2 gas for 10 and 20 minutes, respectively, after the n^+ growth.

The doping profiles for n-layers of ~0.9 μm thickness are shown in Figure 42. The results indicate that a flatter doping profile results in those n-layers that were formed after evacuation of the reactor. The simple purges, however, appeared to result in a lower net donor concentration in the n-layer.

Characteristics of p-n junctions. - The characteristics of reverse-bias voltage versus current have been examined on several p-n junctions, formed by the growth of an n-layer on (0001) $A\ell_2O_3$ followed by a p-layer produced by the technique of lowering the AsH_3 flow rate through the reactor. Mesas were then etched in the epitaxial layer to form junctions ~10^{-4} cm^2 in area. The measurements were carried out on films having n-layer donor concentrations of ~10^{15} and 10^{16} cm^{-3}.

The results are shown in Figure 43. Two junctions (with n ~10^{16} cm^{-3}) are seen to have rather "soft" reverse characteristics with low breakdown voltages. The junction formed on a more lightly doped layer, however, exhibits good reverse characteristics and dc behavior similar to that of an IMPATT diode structure ($n^+/n/p^+$) formed in bulk Si in this laboratory; the Si device had previously been operated as a cw X-band oscillator.

Twelve p^+ GaAs/nGaAs/$A\ell_2O_3$ samples were prepared to evaluate the effects of donor concentration in the n-layer on the electrical behavior of the p-n junctions. Various undoped n-type films were selected for the study, with net carrier concentrations ranging from ~10^{15} to ~8×10^{16} cm^{-3}. For most of the carrier concentrations chosen, one sample was polished prior to the deposition of the p^+ layer and one was used in the "as grown" condition. Diodes with ~5×10^{-4} cm^2 area were formed in each layer after the vacuum deposition of a Au-Ge ohmic contact onto the p^+ layer.

Capacitance-versus-voltage (reverse) data were taken to determine the carrier concentrations at the junction. The results indicated little difference between the electrical properties of junctions that were formed on the as-grown GaAs film. Although the reverse characteristics tend to show a "soft" breakdown in many cases, a ℓn V_B -vs- ℓn n (V_B = breakdown voltage, n = carrier concentration) plot shown in Figure 44 falls along a line very nearly parallel to the theoretical breakdown voltage-vs-carrier concentration curve for GaAs, although displaced slightly toward lower voltages from the theoretical curve. (The lengths of the lines in the figure indicate the range of values observed for a number of diodes on the same wafer.)

More detailed electrical measurements at low current levels with bias voltages 0.1 volt were then carried out on this same group of p^+GaAs/nGaAs/$A\ell_2O_3$ samples. Reverse current densities ranged from ~4×10^{-9} amps cm^{-2} to ~4×10^{-6} amps cm^{-2} at 0.1 volt bias voltage for the junctions examined. The results of these measurements are shown in Figure 45. There appears to be no apparent
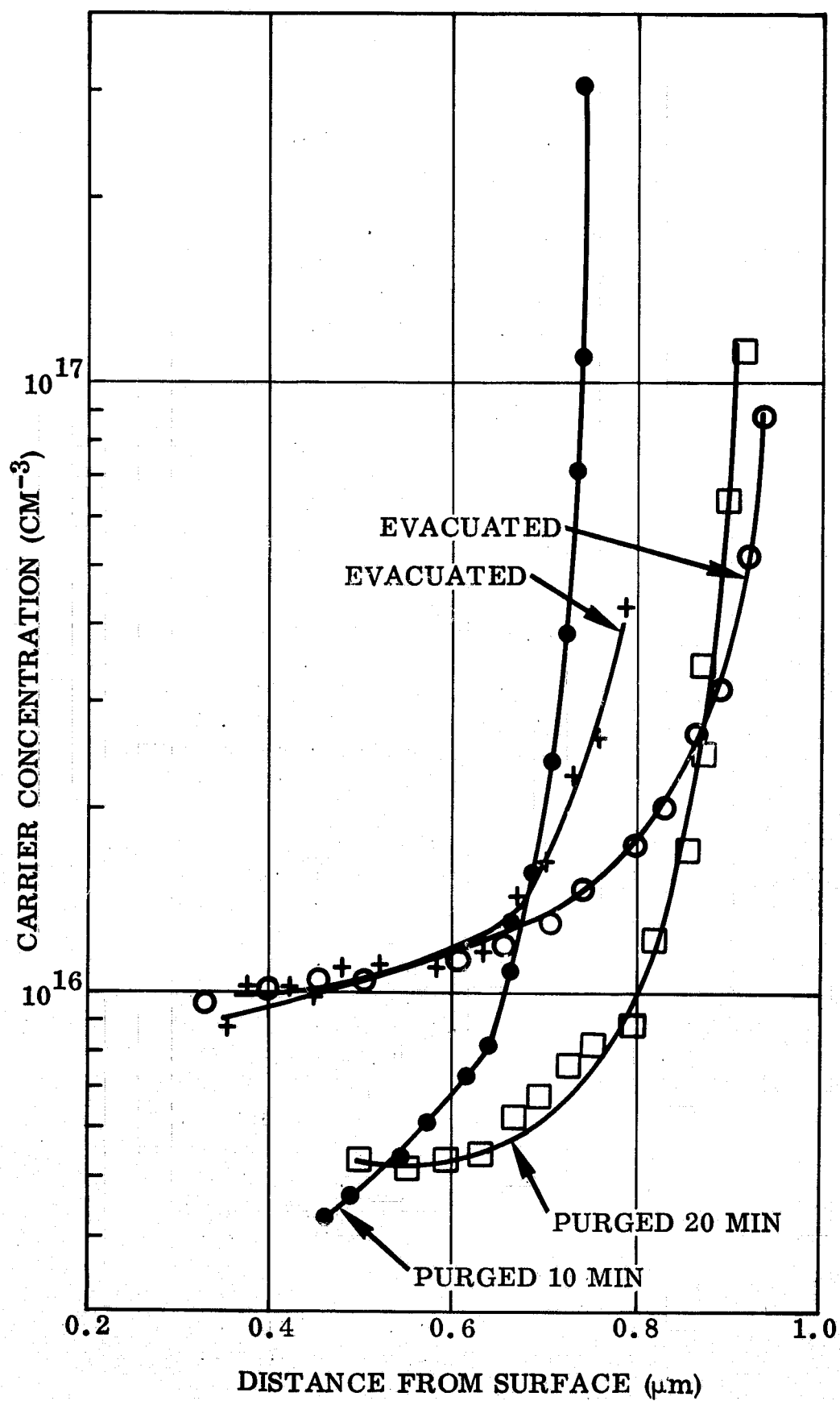
Figure 42. Comparison of the Effect of Purging vs Evacuation after N+
Growth on the Impurity Profile in Four 0.9 μm-thick N-layers
Grown on N+ GaAs/ (0001) Aℓ₂O₃
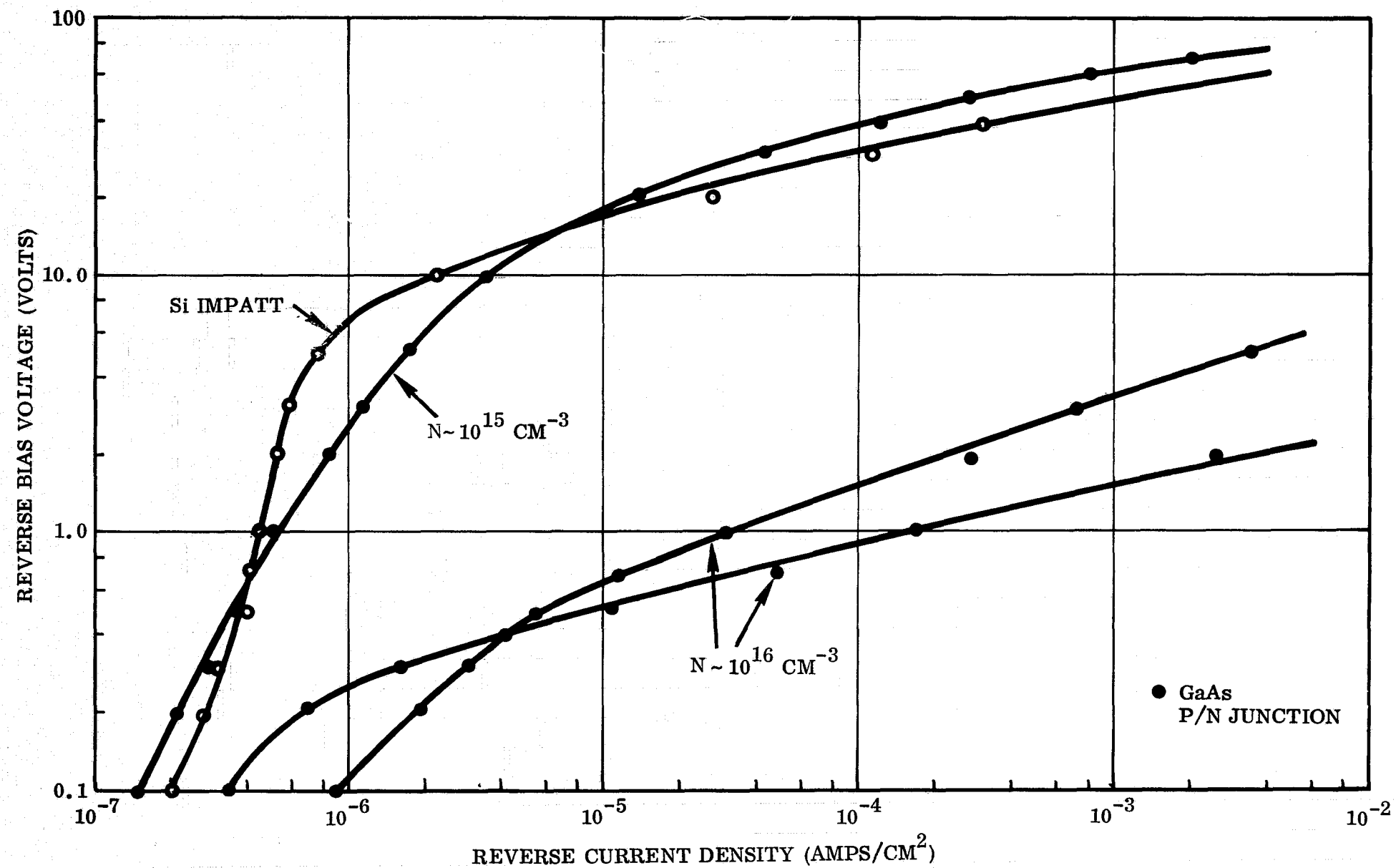
Figure 43. Reverse Bias Voltage Versus Current Density for Three P/N Junctions Formed in GaAs/ (0001) Aℓ$_2$O$_3$
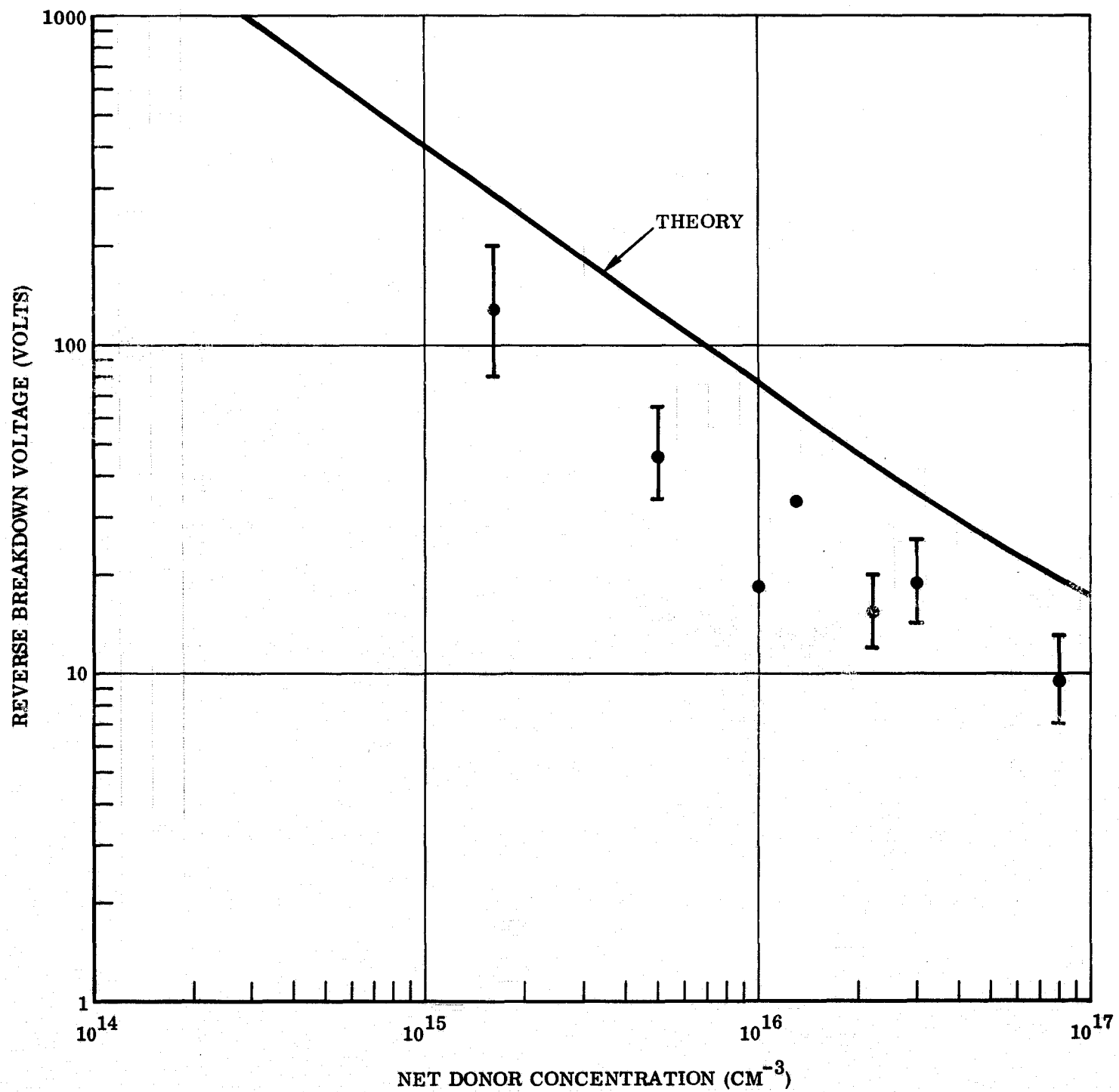
Figure 44. Reverse Voltage Breakdown vs Donor Carrier Concentration for
P+/N Junctions Formed in GaAs/Aℓ₂O₃ (Bars Denote Range of
Breakdown Voltage Observed in Several Junctions)
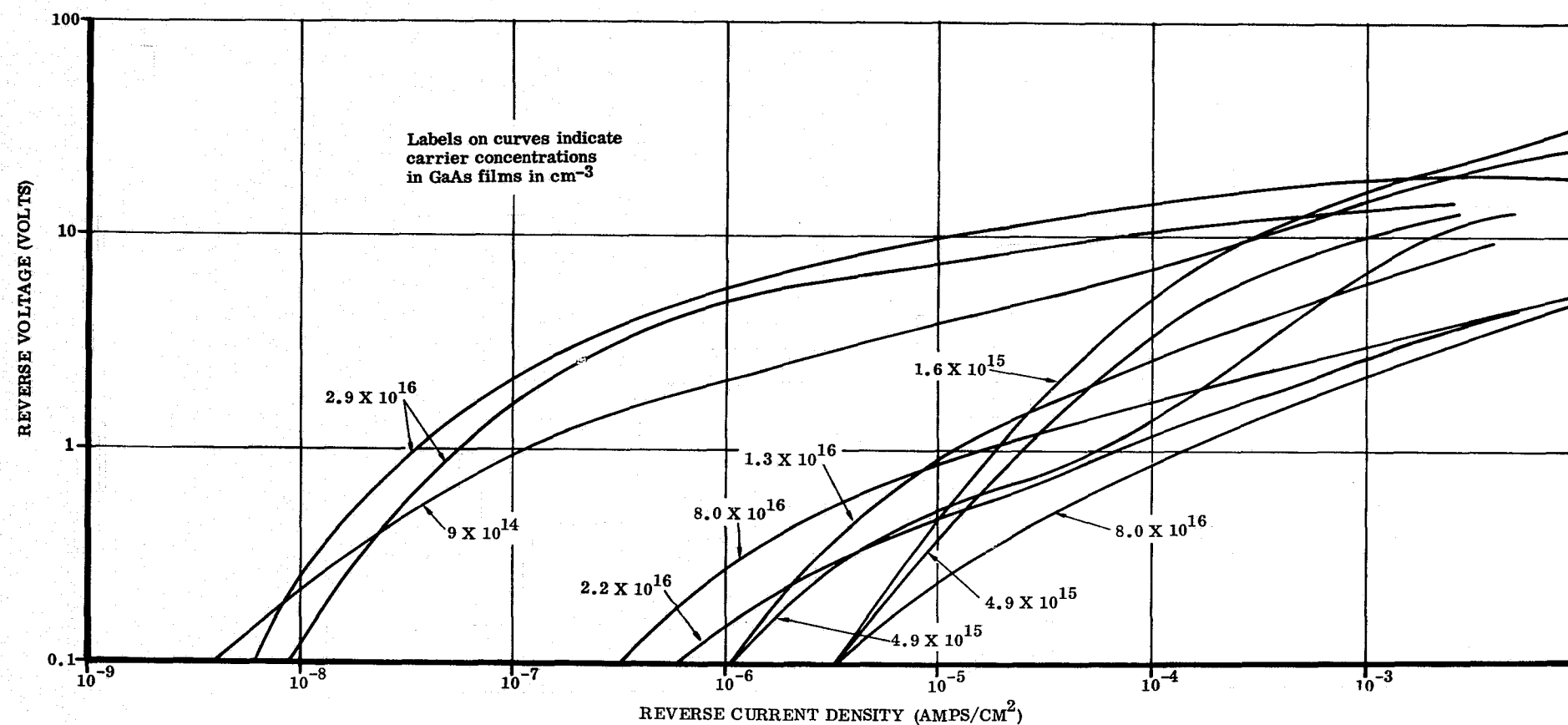
Figure 45. Reverse Bias Voltage vs Reverse Current Density for P+/N
Junctions Formed in GaAs/Aℓ_2O$_3$

correlation between reverse current at low bias voltages (i.e., leakage current) and carrier concentration. Optical examination of the surface characteristics of the junctions suggests that the lower leakage currents may be associated with a smoother GaAs surface; however, further verification of this point is required.

Measurements of reverse current versus voltage were also carried out as a function of temperature from 20 to 300 C for one of the diodes having low leakage current. The variation of reverse current with temperature (for a constant bias voltage of 1.0 volt) is shown in Figure 46. The solid and open circles represent two distinct heating cycles and indicate good reversibility for the reverse current characteristics. The temperature variation suggests that at the lower temperatures generation current, which is proportional to $e^{-Eg/2kT}$ dominates. The more rapid increase in current at higher temperatures suggests the presence of an additional component due to diffusion current, proportional to $e^{-Eg/kT}$.

The forward current-voltage characteristics were also examined on the same p-n junction used for the temperature measurements. The current is found to obey an exponential law of the form $I_f \propto e^{-qV/2kT}$ at low voltages (see Figure 47), indicating the dominance of recombination current, while at higher voltages the current varies as $I_f \propto e^{-qV/1.4\,kT}$. The latter suggests that diffusion current and recombination current are comparable in this region.

Tunnel diode fabrication. - Experiments to verify feasibility of formation of good quality tunnel diodes utilizing heteroepitaxial GaAs/Al$_2$O$_3$ have been carried out during the last three months of the contract period. Heavily Zn-doped (p$^+$) epitaxial layers with a wide range of thicknesses were processed to form vertical-junction tunnel diodes by the dot-alloy technique. Some of the results of this work are as follows:

(a) Alloying temperatures of ~400C are sufficient to ensure wetting of the p$^+$ GaAs surface with AuGe, AuSn, and SnS alloys; cooling rates of 200 deg C in 3-5 sec provide proper recrystallization of the regrowth region.

(b) The thermal mass of the sample is not a factor in obtaining optimum tunneling characteristics.

(c) A necessary condition for maximum peak-to-valley current ratios is complete penetration of the metal alloy through to the GaAs-Al$_2$O$_3$ interface.

(d) Tunnel diode characteristics appear to be a function of GaAs thickness; optimum results to date have been achieved for layer thicknesses ~2-3µm.

(e) Peak-to-valley current ratios as high as 9:1 have been achieved using the eutectic alloy AuGe (80:20). A typical I-V characteristic for one of these tunnel diodes is shown in Figure 48.

Two back-to-back tunneling devices were prepared for high frequency evaluation. These units were cleaved to small size and mounted on the flat end-surfaces of 0.050-in. diameter copper rods, for insertion in existing microwave test fixtures. Results with a specially fabricated oscillator test circuit in a microstrip circuit configuration showed that the device exhibited oscillations at a fundamental frequency of 100 MHz.
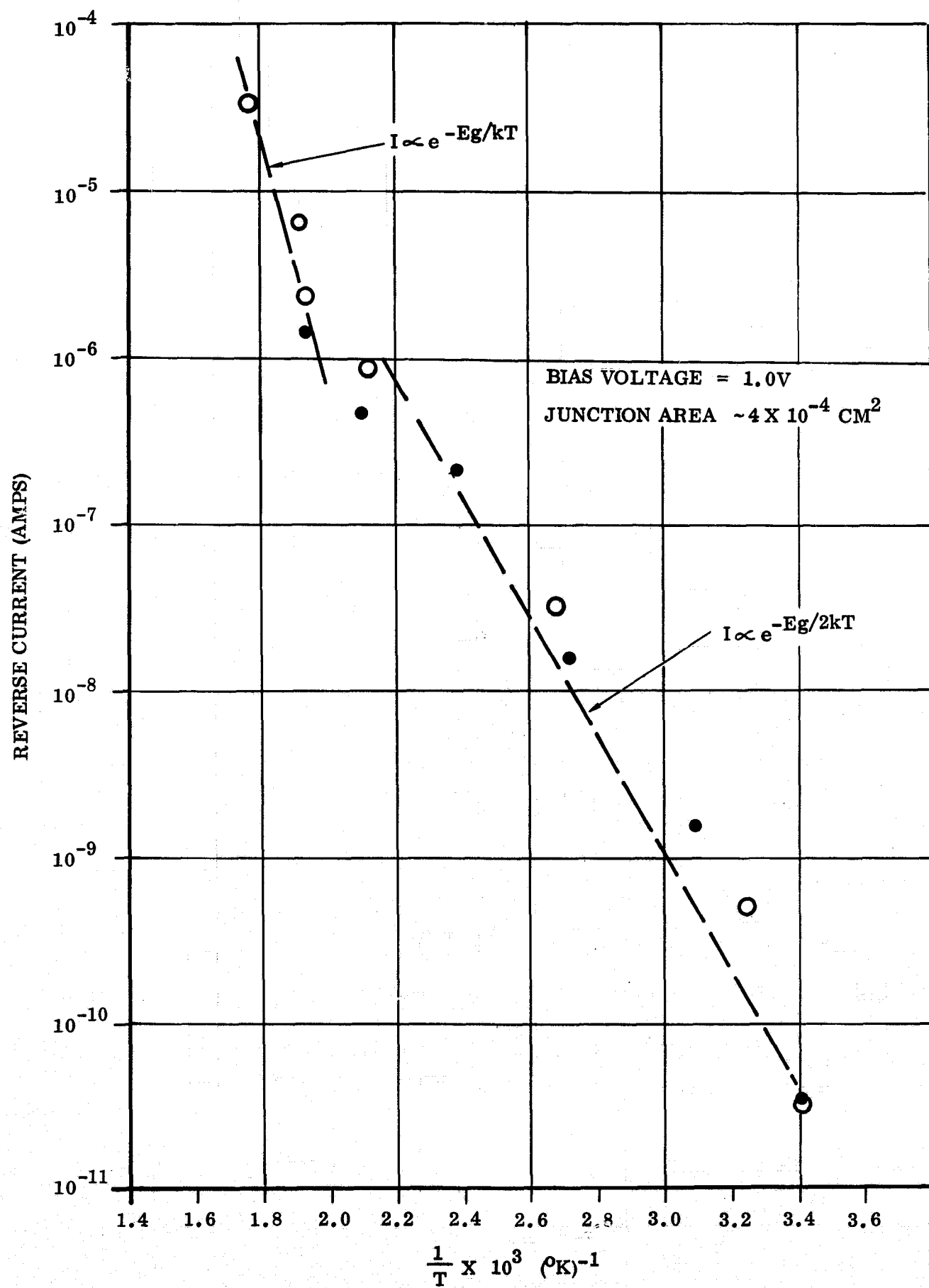
Figure 46. Reverse Current vs Reciprocal Temperature for a
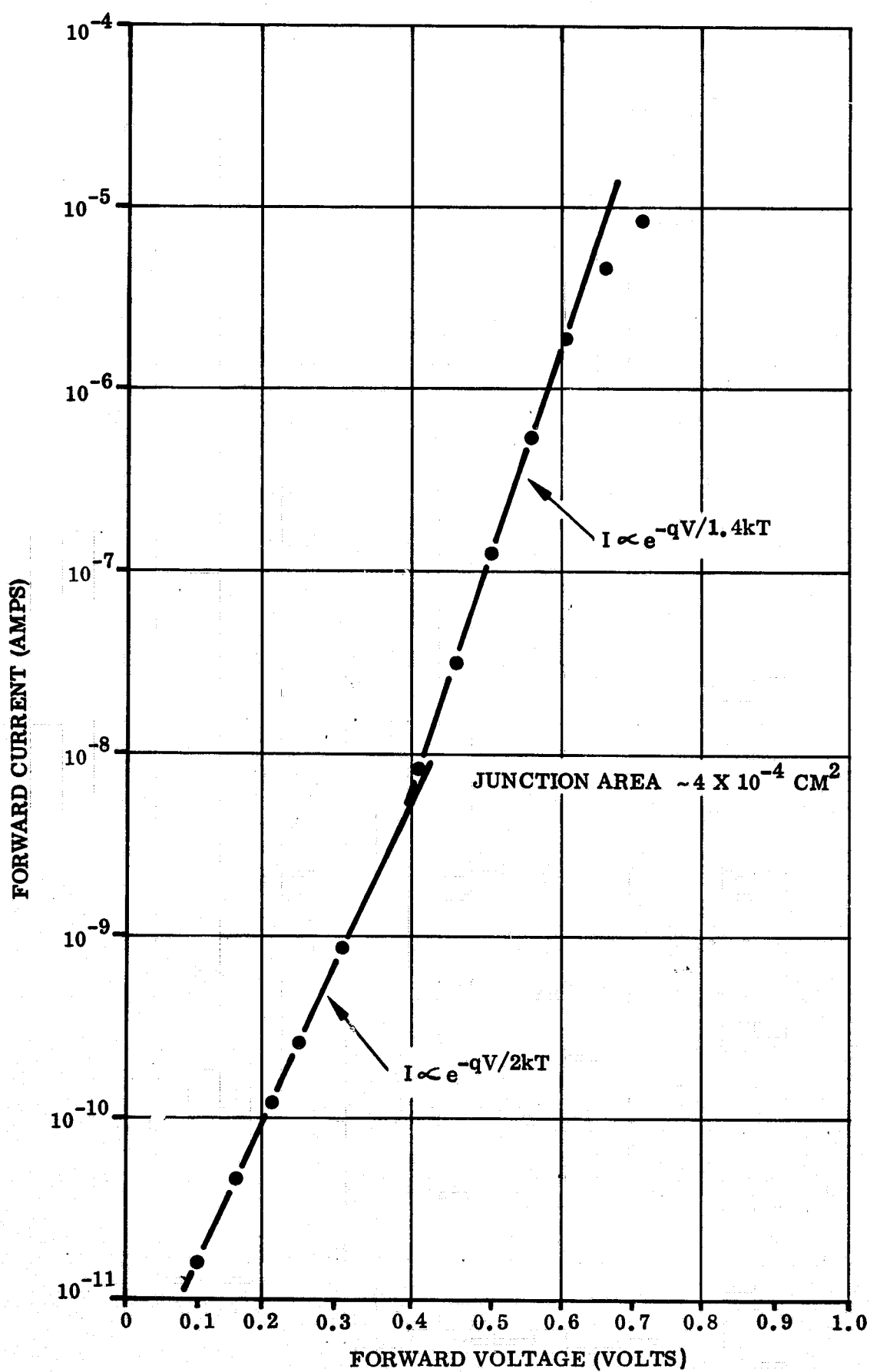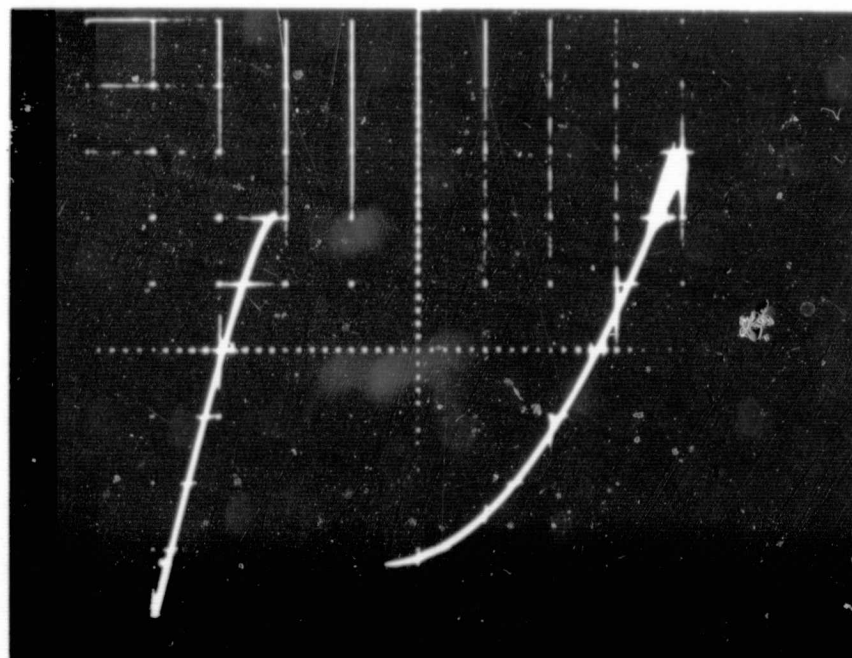P+/N Junction Formed in GaAs/Aℓ_2O$_3$

83

Figure 47. Forward Current vs Voltage for a P+/N Junction
Formed in GaAs/Aℓ_2O$_3$

10 ma/div

0.2 V/div

Figure 48. I-V Characteristic of Tunnel Diode in P+ (111) GaAs/Al_2O_3.
Peak-to-Valley Ratio 8.7:1

A second oscillator was constructed in order to determine the optimum circuit operating parameters for the device. Measurements of the tunnel diode peak current, valley current, peak voltage and valley voltage were made in order to determine the theoretical maximum power obtainable from the device. These measurements yielded a maximum available oscillator power of 245 μwatts; in practice, it is found that between 30 and 50% of this theoretical power can be obtained at the output port of a tunnel diode oscillator.

This second microstrip circuit had a natural unloaded design frequency of 185 MHz. Two frequencies of operation were obtained in this circuit configuration by changing the resistive and reactive loading. One output occurred at 80 MHz and a second mode at 180 MHz. When the capacitive end loading of the tuning stub is taken into account, the value of frequency observed on the spectrum analyzer for the second and higher mode of operation is very close to the unloaded frequency of the circuit.

An approximate calculation of the resistive cutoff frequency of the devices yielded a value of f_{ro} = 600 MHz. This is in reasonable agreement with observations of the upper frequencies produced by spurious responses and harmonics. Sporadic responses from this diode have been seen on the spectrum analyzer at frequencies up to 500 MHz.

Field-effect transistor fabrication. - Several attempts have been made to fabricate a p-n junction gate field-effect transistor. Although these attempts were less than successful in terms of a finished functioning device, the steps

85

taken are outlined below since the device fabrication technology has now been established.

Originally, samples of $nGaAs/p^+GaAs/A\ell_2O_3$ were processed; a p^+ layer ~4-5 μm thick was specified, with an n layer of 1-2 μm thickness and net carrier concentration ~10^{15}-10^{17}cm^{-3}. The FET structural design was selected such that the nGaAs channel thickness could be reduced between source and drain by masking and etching techniques subsequent to mounting the separated units on headers. Source-drain separation was ~2 mils, with contact length ~40 mils.

The fabrication process is summarized as follows: arrays of 32x60 sq. mil mesas were formed by etching the nGaAs layer; SiO_2 was sputtered overall (~3000Å), and four windows 5x40 sq. mil etched into the oxide; AuGeNi was vacuum-deposited overall and alloyed in a H_2 atmosphere to form low-resistance ohmic contacts for source and drain on the nGaAs surface and two gate contacts on the exposed p^+ GaAs sublayer. The nGaAs surface between source and drain was exposed by the photolithographic process; the units were then separated into 80x80 sq. mil dice and mounted on headers; Au wire leads were bonded to source, drain, and gate contact regions. Figure 49 shows the FET device structure.

Electrical tests revealed that, for two samples that met the material parameter specifications, the alloyed source and drain ohmic contacts penetrated the nGaAs layer resulting in a shorted $n-p^+$ interface.

The nGaAs layer thickness for a second set of samples was increased from 1-2μm to 3-4μm to avoid the alloy penetration which had produced the shorted $n-p^+$ interface. Gate reverse-breakdown voltages exceeding 10 volts indicated that the nGaAs layer electron concentration was ≤10^{17}cm^{-3}. Families of field-effect characteristics observed on the curvetracer did not exhibit pinch-off due to depletion of the nGaAs channel. Apparently the post-etching process to reduce the channel thickness was not totally effective in increasing the channel transconductance. Enough information was obtained from this device structure to indicate that a thin nGaAs layer and minimum p-n junction gate area must be maintained if low-voltage pinch-off and high transconductance are to be obtained.

A new FET structural design was then generated such that the source and drain ohmic contacts to the nGaAs channel layer would be formed by an additional n^+-GaAs layer (~1μm thick); the p-n junction gate area was decreased to ~20% of the former value to reduce gate capacitance. The nGaAs channel layer thickness was again made ~1-2μm, as in the initial samples, since no difficulty with ohmic contact alloy penetration of the channel layer was anticipated for this design.

However, electrical measurements revealed that the expected p-n junction gate reverse-breakdown voltages (≥10 volts) were not achieved. Two sets of these FET devices were selected for electrical parameter evaluation; however, both exhibited reverse breakdown voltages less than 2 volts, which resulted in minimal channel conductance modulation.
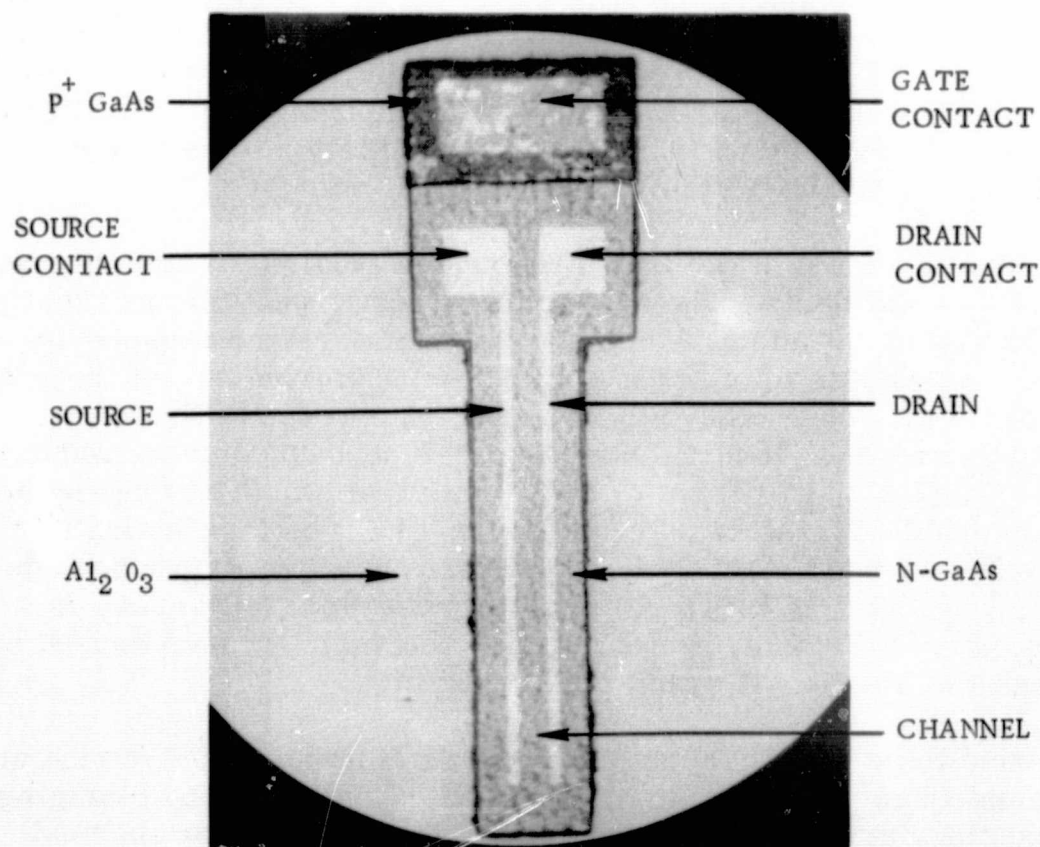
Figure 49.   FET Device Structure Formed in GaAs/$A\ell_2O_3$

Si on $A\ell_2O_3$ - In accordance with Item 9 of the Statement of Work of Modification #1 of this contract, Autonetics submitted during the first nine-month period a total of 40 samples of epitaxial Si on $A\ell_2O_3$.   Included were films grown with the (111), (100), and (110) orientation with thickness ranging from 1400Å to 1.1 μm, as requested by the Technical Monitor.

In order to prepare these films, a completely new deposition system was utilized in a laboratory area removed from that used for GaAs studies.   This system utilized Si deposition techniques previously developed at Autonetics.   Control of the (110) Si growth would not have been feasible had not previous orientation studies been carried out (Ref. 11).

Substrate Surface Properties

Auger electron spectroscopy and low-energy electron diffraction (LEED) were used at the North American Rockwell Corporation (NR) Science Center to examine the effects of various cleaning treatments of the (0001) surface of α -$A\ell_2O_3$.   Stimulation for this work was provided by the observation that the quality of GaAs epitaxial growth on such surfaces is strongly dependent on surface treatment, among other factors. Two-dimensional structural changes caused by such treatments are reflected in the LEED pattern.   Associated compositional changes, including impurities, should be detectable with Auger electron spectroscopy.

Two groups of samples were examined.   The first group was subjected to various cleaning treatments and annealed at high temperatures in a H_2 atmosphere in the CVD

reactor and then exposed to atmospheric conditions for about a week prior to insertion into the LEED system. The samples of this group were backed with 2000Å of vacuum-deposited Ta; heating in the LEED system was then accomplished by passing current through the Ta coating. To minimize atmospheric contamination, the second group of samples was not Ta backed, was placed in acetone immediately after surface treatment, and was not removed until just prior to the LEED examination.

Three substrates a, b, and c of the first group were studied. These had been subjected to the following treatments in H_2: a-30 min at 700C; b-30 min at 1200C; c-30 min at 1200C followed by 60 min at 900C. Because of severe atmospheric contamination, it was not possible to observe a LEED pattern from any of these specimens without in situ heating. Auger analysis revealed copious quantities of C on the surface, in addition to O_2 and $A\ell$. Heating sample a to 725C caused some reduction in C and the appearance of a (1 x 1) LEED pattern, indicative of a bulk arrangement of surface atoms. Considerable diffuse background in the LEED pattern indicated that the surface was not well-ordered. After heating at about 900C the Auger peak due to C nearly disappeared, and a (4 x 4) LEED pattern was observed. However, in attempting to heat the sample to higher temperatures, thermal stresses caused by the heating current through the Ta deposit cracked the specimen.

Sample b was found to be heavily contaminated with C and cracked during an initial thermal treatment in vacuum. Sample c was heated indirectly by clamping it to a Ta strip and passing current through the strip. Because of poor thermal contact, however, the substrate could not be heated above about 800C. This treatment resulted in some reduction of a heavy initial deposit of C and the appearance of a diffuse (1 x 1) pattern.

Two samples of the second group were studied. One was cleaned in acetone and then heated at 1300C for 60 min; the other was processed by placing it in hot HF-HNO_3 solution for 10 min. Both were stored in acetone until studied. A slightly diffuse (1 x 1) pattern was observed from both of these samples immediately after insertion into vacuum. Auger analysis revealed very little C, indicating that acetone was quite effective in preventing environmental contamination. Heating the samples to a maximum attainable temperature of about 1000C caused some improvement in the (1 x 1) pattern as well as near removal of the Auger peak due to C.

The results of these exploratory studies suggest that the surface condition as determined by LEED and Auger spectroscopy is not strongly dependent on various cleaning procedures used. Since the GaAs epitaxial studies show a definite dependence on high-temperature treatment of the surface, structural or chemical changes must occur that are not revealed by LEED and Auger spectroscopy. Alternatively it is possible that any changes caused by surface treatment are masked by the effect of exposing the sample to the atmosphere and acetone.

Reaction Mechanisms

The use of the metal-organics for semiconductor film formation was not without concern for the possibility of major C contamination. Graham et al (Ref 12) reported that the pyrolysis of TMG at 520C in an argon carrier gas produced a metallic-looking film containing 8.0% C. Plust (Ref 13) described the production of Ga of semiconductor purity by photolysis of TEG, but Graham obtained gray-black solids containing metallic Ga using Plust's process.

To prevent the possible formation of nonvolatile carbonaceous side-products, two steps were initially taken in the work of this contract: (a) the use of H_2 as the carrier gas to suppress and/or tie up any free radicals that may be assumed to be involved in the mechanism for the pyrolysis of TMG; and (b) the use of the Group V hydride(s) in excess over the stoichiometric amount required to react with a given amount of TMG, as represented, for example, by reaction [1] for the formation of GaAs:

$$(CH_3)_3Ga + AsH_3 \xrightarrow{\Delta} GaAs + 3CH_4. \qquad [1]$$

The AsH_3 (or other group V hydride) in excess probably reacts with the TMG before it has a chance to pyrolyze, thus avoiding the formation of undesirable products. It also provides an As atmosphere to help prevent dissociation at elevated temperatures. The relatively low temperatures used for GaAs formation also apparently prevent C from being a major contaminant in the GaAs films. If C were present as a minor contaminant, it would most probably be due to impure starting materials or improper handling in the deposition apparatus.
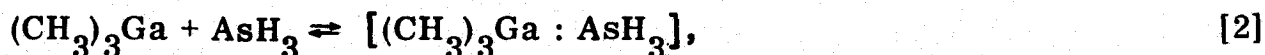
Harrison and Tompkins (Ref 14) performed an experiment in which TMG and AsH_3 were mixed at room temperature in 1:1 molecular proportions in the vapor state for 18 hr and then heated to about 200C. This produced a red film which was postulated to be stoichiometric GaAs. Unfortunately, the experiment was not evaluated sufficiently. If the rate of formation and quantity of methane had been measured, one would have more confidence in the study of the stoichiometry of reaction [1]. There may have also been a reaction between AsH_3 and a gray film which Harrison and Tompkins reported had formed on the walls of the tube at room temperature. This film may have been a reaction product between TMG and Pyrex, which has been previously observed (Ref 15).

At the time that studies of reactions between the metal-organics and the hydrides were initiated for use in preparation of compound semiconductors it was expected that reaction [1] was the predominant reaction. Knowledge of the prior investigation of Harrison and Tompkins at low pressures came later.
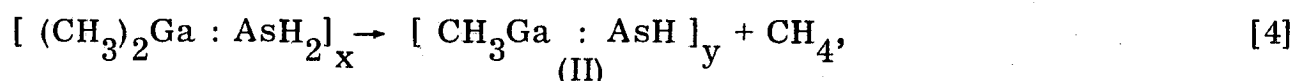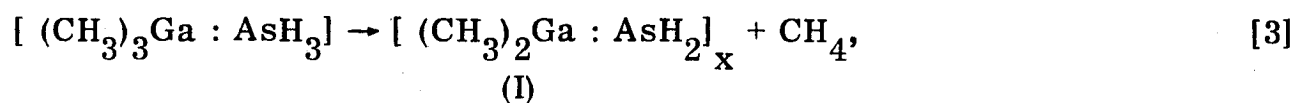
Reaction [1] would also be expected to occur equally well with an inert carrier gas. Therefore, starting with the second quarter of this program, He was examined as a carrier gas in the CVD process.

GaAs was formed successfully from TMG and AsH_3 in essentially an inert atmosphere (neglecting the H_2 formed from the decomposition of excess AsH_3). This lends further evidence to the view that the primary reaction is as indicated in reaction [1] above. By keeping the AsH_3 in excess, pyrolysis of TMG to form nonvolatile carbonaceous-Ga products in the inert atmosphere does not take place.

Slight differences are in evidence between the H_2 - and He-carrier studies, in that intermediate reaction products are more clearly visible in the reactor as a volatile greenish-black powder when He is used as the carrier gas. This could be an undecomposed polymeric product formed from an unstable TMG-AsH_3 addition compound,

$$(CH_3)_3Ga + AsH_3 \rightleftharpoons [(CH_3)_3Ga : AsH_3], \qquad [2]$$

followed by stepwise release of CH_4, as in [3] and/or [4],

$$[(CH_3)_3Ga : AsH_3] \rightarrow [(CH_3)_2Ga : AsH_2]_x + CH_4, \qquad [3]$$
$$\text{(I)}$$

$$[(CH_3)_2Ga : AsH_2]_x \rightarrow [CH_3Ga : AsH]_y + CH_4, \qquad [4]$$
$$\text{(II)}$$

with the formation of GaAs as the end product (reaction [1]). Compounds I and/or II in equations [3] and [4] may not be stable in a H_2 atmosphere.
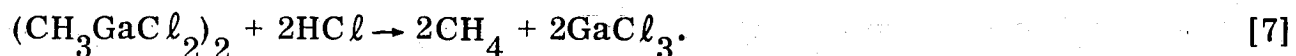
A few experiments were also performed using $AsC\ell_3$ and TMG as the reacting materials. Epitaxy was not achieved on the insulators, and this approach was soon discarded. It may be that the reaction is complicated by the formation of $HC\ell$, produced by the reduction of $AsC\ell_3$ by H_2:

$$2AsC\ell_3 + 3H_2 = 1/2As_4 + 6HC\ell. \qquad [5]$$

Further reaction by TMG with $HC\ell$ could produce the compound methyl gallium dichloride in the first stage of the reaction (Ref 16):

$$2(CH_3)_3Ga + 4HC\ell \rightarrow (CH_3GaC\ell_2)_2 + 4CH_4, \qquad [6]$$
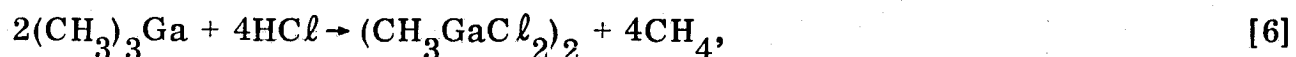
followed by complete dealkylation

$$(CH_3GaC\ell_2)_2 + 2HC\ell \rightarrow 2CH_4 + 2GaC\ell_3. \qquad [7]$$

$HC\ell$ could also obstruct epitaxy if the growth rate of the depositing film is less than its etching rate by the $HC\ell$.

CONCLUSIONS

These studies have demonstrated that GaAs films possessing device-quality properties can be produced on both sapphire ($A\ell_2O_3$) and spinel ($MgA\ell_2O_4$). Thick (>15 μm) undoped GaAs films with room temperature mobilities between 5000 and 6000 cm^2/V-sec for carrier concentrations in the range from ~ 10^{15} to ~ 10^{17} cm^{-3} have been grown by the trimethylgallium (TMG)-arsine (AsH_3) process in the temperature range 650-700 C. These studies have shown that by manipulation of the relative AsH_3-TMG concentrations it is possible to control to some extent the carrier concentration, resistivity, and even conductivity type of the resultant films, thus making the formation of multilayered structures of differing conductivity type a relatively simple task for device formation.

Nucleation and early-stage growth studies have revealed some details of the mechanisms of film formation and have corroborated orientation relationship investigations that tend to indicate (0001) $A\ell_2O_3$ as the preferred sapphire substrate for (111) GaAs growth.

Preliminary studies using stoichiometric spinel as substrates have shown that essentially equivalent GaAs films can also be grown on (111) and (110) spinel. From the observed growth of (100) GaAs on (110) spinel and from the GaAs/$A\ell_2O_3$ orientation studies, it is concluded that the factors which influence heteroepitaxial growth of GaAs are probably different from those in the heteroepitaxial Si system.

Vertical-junction tunnel diodes, uniquely suited to the GaAs-insulator composite, have been fabricated. These diodes, formed in p^+ GaAs/$A\ell_2O_3$, have operated in a 100 MHz oscillator.

It is anticipated that the CVD growth process utilized in these investigations will permit new degrees of freedom and new concepts of device design in situations in which insulators are used as substrates, and will find widespread application in other hetero- and homo-epitaxial systems.

REFERENCES

1. Tietjen, J. J. and Amick, J. A., J. Electrochem. Soc. 113, 724 (1966).

2. Knight, J. R., Effer, D., and Evans, P. R., Solid State Electron. 8, 178 (1965).

3. Zanowick, R. L., J. Electrochem. Soc. 114, 146C (1967).

4. Manasevit, H. M., and Simpson, W. I., J. Electrochem. Soc. 115, 66C (1968).

5. Manasevit, H. M., Appl. Phys. Letters 12, 156 (1968).

6. Jolly, W. L., Anderson, L. B., and Beltrami, R. T., J. Amer. Chem. Soc. 79, 2443 (1957).

7. Feder, R., and Light, T., J. Appl. Phys. 39, 4870 (1968).

8. Am. Inst. of Phys. Handbook, McGraw-Hill Book Co., New York (1963), p. 4-72.

9. Black, J., and Lublin, P., J. Appl. Phys. 35, 2462 (1964).

10. Reid, F. J., and Robinson, L. B., Proc. of the Int. Sym. on Gallium Arsenide, edited by C. I. Pederson, Oct. 1968, Dallas, Paper No. 10, p. 59.

11. Manasevit, H. M., Nolder, R. L., and Moudy, L. A., Trans. TMS-AIME 242, 465 (1968).

12. Graham, W. A., and Gatti, A. R., A. D. Little, Inc., Cambridge, Mass., Final Report, Contract AF19(604)-4975, 31 Dec. 1960.

13. Plust, H. G., U. S. Pat. 2,898,278; August 4, 1959.

14. Harrison, B., and Tompkins, E. H., Inorg. Chem. 1, 951 (1962).

15. Manasevit, H. M., PhD Thesis, "Study of Reactions of Silyl Bases with Selected Lewis Acids," p. 44, Illinois Institute of Technology, Chicago, Ill., June 1959.

16. Coates, G. E., "Organo-Metallic Compounds," 2nd Ed., John Wiley & Sons, Inc., New York (1960), p. 151.

APPENDIX A. NEW TECHNOLOGY

The substitution of an inert carrier gas, namely He, for H_2 in the TMG-AsH$_3$
process for GaAs deposition has provided GaAs films with mobilities equivalent to
and in some cases greater than those for films formed in a H_2 atmosphere. The higher
perfection may possibly be related to the nonreducing atmosphere provided by He
and to the consequent absence of certain impurities which might, when H_2 is used,
be incorporated into the film by reduction reactions. These effects are recorded on
pages 1, 5, 7, 10, 18, 20, 23, 27, 89, and 90.

After a diligent review of the work performed under this contract, no new
innovation, discovery, improvement or invention, other than the above, was made.